DIVERGENT BEAM ULTRASOUND COMPUTED TOMOGRAPHY FOR DIFFERENTIAL THERMOGRAPHY

BY

MICHAEL JOHN HANEY

S.B., Massachusetts Institute of Technology, 1977
S.B., Massachusetts Institute of Technology, 1977
M.S., University of Illinois, 1981

THESIS

Submitted in partial fulfillment of the requirements
for the degree of Doctor of Philosophy in Electrical Engineering
in the Graduate College of the
University of Illinois at Urbana-Champaign, 1985

Urbana, Illinois

UNIVERSITY OF ILLINOIS AT URBANA-CHAMPAIGN

THE GRADUATE COLLEGE

OCTOBER 1985

WE HEREBY RECOMMEND THAT THE THESIS BY

MICHAEL JOHN HANEY

ENTITLED DIVERGENT BEAM ULTRASOUND COMPUTED TOMOGRAPHY FOR DIFFERENTIAL THERMOGRAPHY

BE ACCEPTED IN PARTIAL FULFILLMENT OF THE REQUIREMENTS FOR THE DEGREE OF DOCTOR OF PHILOSOPHY

William D. O'Brien, Jr.
Director of Thesis Research

Timothy N. Erick
Head of Department

Committee on Final Examination†

William D. O'Brien, Jr.
Chairperson

Lon A. Frizzell

W. Kenneth Jenkins

† Required for doctor's degree but not for master's.

O-517

DIVERGENT BEAM ULTRASOUND COMPUTED TOMOGRAPHY FOR DIFFERENTIAL THERMOGRAPHY

Michael John Haney, Ph.D.
Department of Electrical Engineering
University of Illinois at Urbana-Champaign, 1985
William D. O'Brien, Jr., Ph.D., Advisor

The applications of divergent beam ultrasound computed tomography for noninvasively estimating temperature change in biological tissue, were examined. This study was prompted by the recognition that both ultrasound speed of propagation and frequency dependent attenuation (two physical properties measurable by ultrasound tomography) are temperature sensitive. Speed generally increases with temperature, and attenuation coefficient generally decreases with temperature, for nonfatty tissue.

Compilations of available literature data for thermal dependencies in biological media were created. Polynomial models applied to the available literature data suggested that a linear temperature dependence is a reasonable model over the temperature range of 10 to 40^{o}C for most tissues. The more sophisticated models studied did not provide substantially better results. However, the limited amount of data and the high degree of variability in the data suggested that more study is needed.

A study of the variance introduced and propagated by the ultrasound computed tomography data acquisition and image reconstruction showed that the noise introduced by computation was small compared to the noise propagated by the computation. If not

for physical difficulties in the available equipment, images of speed and attenuation coefficient could have been reconstructed with a variance of 1 part in 10^3. Temperature changes of 5.5^oC could then be estimated with a standard deviation on the order of 0.5^oC.

Interpolated modeling for algebraic reconstruction was examined, but did not demonstrate itself to be economically justifed over conventional algebraic reconstruction.

The principle conclusion of this work was that the constraining factor in temperature estimation was the variance in the available literature data. Additional data, with better variance, are required.

ACKNOWLEDGEMENTS

I would like to most gratefully thank my advisor, Professor William D. O'Brien, for pointing me toward this project, for providing insight and encouragement (and funding), and for his unlimited patience in this entire matter. I would also like to most gratefully thank Professor Richard M. Brown, for his continued confidence in me, and for helping me feel guilty enough to finally finish.

I gratefully acknowledge the assistance of Mary Yen and Dianne Steiger in the experimental aspects of this work, and the assistance of Bob Cicone, Wanda Elliott, Kay Carnes, Billy McNeill, and Joe Cobb in the technical aspects.

Finally, I would like to thank my family and friends, for their understanding and encouragement, without which I would never have completed this work.

TABLE OF CONTENTS

CHAPTER 1

INTRODUCTION

Temperature measurement in the human body has several dimensions of medical significance. Gross but localized body temperature, as measured with a conventional thermometer, provides a simple monitor of patient state, and can signal danger of infection or potential enzyme failure that can arise from prolonged and/or high fever. Spatially more refined measurements, such as those provided by infrared surface thermography, can assist in localizing and diagnosing highly vascularized tumor masses. For hyperthermia treatment (whether as an isolated therapy, or combined with radiation, chemotherapy, or controlled drug release), a specific elevated temperature distribution is desired. If the heating modality does not produce sufficiently high temperatures at the desired points, the treatment may not be effective. If the heating exceeds the desired temperature, needless healthy tissue damage may arise. Thus, accurate three-dimensional temperature measurement is important.

Unfortunately, most conventional temperature measurement techniques are invasive. Thermometers and thermistors require a path into the tissue in order to make a measurement beneath the

surface. Thermocouple wire probes require a path through the tissue. Whenever tissue is punctured to accomodate a foreign object, the patient is subject to painful discomfort and several risks. The most obvious risk is infection or contamination. Sterilization procedures can minimize this risk, but at increased cost. A more subtle risk associated with cancer treatment thermometry is metastatic induction. Mechanical injury of tumor cells can lead to metastases, or tumors at other sites in the body. Finally, the procedure of inserting several probes, to map out temperature distribution, can be traumatic, and unintentional movement of the patient can result in injury along the probe path. Consequently, truly noninvasive measurement techniques are preferred. Throughout this work, noninvasive measurement shall refer to procedures that do not compromise the integrity of the inherently closed surfaces formed by the tissues of the body. Thus, needle punctures (whether for inserting thermocouples or for drawing fluid samples) or surgical procedures of almost every kind would be considered invasive. In this context, x-rays and ultrasound transmitted through the body without rupturing the skin would be considered noninvasive. Note that defining a procedure as noninvasive does not imply that the procedure is free from biological effect. Excessive exposure to x-rays or any form of ionizing radiation is generally considered as dangerous and/or destructive to tissue. Therapeutic and hyperthermic levels of ultrasound are intended to affect tissue. The question of whether diagnostic exposure to ultrasound poses any danger is as yet unanswered.

Only a limited number of noninvasive thermometry alternatives are available at this time for mapping the spatial distribution of temperature. The most common is infrared surface thermography, which produces an image of the temperature distribution at the skin surface of the patient. This technique can be effective for locating and diagnosing highly vascularized tumors close to the surface. It has been a common procedure for breast cancer screening (Siedband and Holden, 1978). A more general approach, studied here, is the use of ultrasound to estimate temperature below the surface, in a two- or three-dimensional reconstruction.

Ultrasound computed tomography can be used to form cross sectional views of the speed and attenuation of ultrasound in a subject. The ultrasound is propagated into the body using transducers outside of the body. Thus the modality is noninvasive. By measuring the time-of-flight and frequency dependent loss of pulses of ultrasound passing through the body at a large number of angles, from a large number of views, it is possible to reconstruct images of the ultrasound speed and frequency dependent attenuation of the intervening tissue. Since both speed and attenuation are temperature sensitive (the speed generally increases and the attenuation generally decreases with increasing temperature, for smooth, nonfatty tissue), it is possible to estimate changes in temperature from changes in speed and attenuation. However, the key to the problem is an *a priori* knowledge of the thermal coefficients of speed and attenuation of ultrasound in biological media. This thesis draws together these coefficients into a common database, in order to determine what

data are available, and what areas are in need of study. Further, the accuracy of temperature estimation depends critically on the accuracy of the reconstruction (which depends on time, amplitude, and position measurement accuracies, as well as computational accuracy), and on the accuracy and applicability of the thermal coefficients. This thesis examines the errors present in a divergent beam ultrasound computed tomography system, and the variance in the available thermal coefficient data, in order to determine the requirements necessary to estimate temperature changes with an acceptable level of accuracy. Problems associated with refraction and diffraction are considered, and the applicability of diffraction tomography to differential thermography is described.

Some important clarifications in terminology are in order at this point. Contrary to popular usage, "velocity of propagation" and "speed of sound" are not interchangeable phrases. Velocity is a vector quantity, whereas speed is the scalar magnitude of the velocity. Thus, the term "velocity" will be reserved for discussions of abstract physics, or for measurements where the direction of the vector quantity is either explicitly or implicitly unambiguous. In all other applications throughout this work, the term "speed" will be used, since it is the formally correct word. Moreover, all uses of the word "speed" shall refer to the magnitude of the velocity of propagation of ultrasound, unless explicitly stated otherwise.

Attenuation and absorption are also subject to confusion. Attenuation describes the loss experienced by a wave as it passes through a medium. Amplitude attenuation describes a loss of amplitude. Intensity attenuation describes a loss of intensity, or equivalently, energy. Throughout this work, attenuation will always refer to intensity loss for discussions of physical phenomena. Absorption is a specific mechanism of attenuation, whereby energy is converted into another form - typically heat. Another mechanism for attenuation is scattering, where energy is redirected away from the direction of propagation of the original wave. For very homogeneous media, such as water or blood, scattering is small, so the distinction between absorption and attenuation is often not critical. For heterogeneous media, where the scattering is not a small effect, it is important to distinguish between reported values of absorption (loss due to heat conversion) and reported values of attenuation (total loss).

Another important distinction is between the attenuation and the attenuation coefficient, or equivalently, between the absorption and the absorption coefficient. Since attenuation is generally thought to depend exponentially upon the distance travelled by the wave, the attenuation coefficient is defined as the logarithm of the attenuation divided by the path length. While attenuation is dimensionless, the units of the attenuation coefficient depend on the type of logarithm used (natural, common, or other) and the units of distance used. All numerical values reported or described in this work are either amplitude attenuation coefficients or amplitude absorption coefficients.

Intensity attenuation will be reserved for discussions of physical phenomena. Since the intensity of a plane wave is proportional to the square of the pressure amplitude, the intensity attenuation coefficient is simply twice the amplitude attenuation coefficient.

Finally, the term "thermal coefficient" is used throughout this work to refer to the first order partial derivative, with respect to temperature, of a given function or ultrasound property. The speed thermal coefficient is thus the rate of change of the speed of propagation with respect to temperature. The thermal coefficient of the attenuation coefficient, also referred to as the attenuation coefficient thermal coefficient, or ACTC, is the rate of change of the attenuation coefficient with respect to temperature.

CHAPTER 2

LITERATURE REVIEW

Several authors have considered the possibility of exploiting the thermal dependency of the velocity of propagation and attenuation of ultrasound in biological media. Fry and Fry (1963) observed that the absorption part of the attenuation yielded elevated temperatures when tissue was heated with ultrasound. These temperature changes altered the ultrasound speed, and thus the acoustic impedance, giving rise to changes in the reflectivity of the tissue. Thus by heating the tissue with ultrasound, different B-scan images could be produced for a subject, with the differences highlighting the absorption (and the speed thermal coefficient) properties of the tissue. Later, Fry (1975) proposed heating as a general contrasting process to alter the visualizability of tissue, and bring out more detail.

Sachs et al. (1972) proposed a thermoacoustic sensing technique, known as TAST, which examined transmission time-of-flight measurements through ultrasound locally heated and unheated tissue. However, in order to make sense of the results, a large amount of tissue specific data was required, including absorption, specific heat, density, and the speed thermal

coefficient. These were combined into one term, the "P-factor," which Sachs *et al.* (1973) reported for several materials, including water, blood, fat, muscle, and several forms of tumors. Later, Sachs (1977) proposed this approach as a general tissue analysis system, reporting speed changes resulting from temperature changes of as little as 0.283°C, with a 400:1 signal-to-noise ratio, for normal brain.

Johnson *et al.* (1975), in examining the tomographic reconstruction of flow-velocity fields, concluded that, given a reconstruction of the speed of ultrasound for a subject and an *a priori* knowledge of speed as a function of temperature, one could estimate temperature. They predicted that a 0.1% accuracy in speed would give a 0.5°C accuracy in temperature. More to the point, Johnson *et al.* (1977a) suggested that changes in temperature could be estimated from changes in speed resulting from heating, given the speed thermal coefficient. Johnson *et al.* (1977b) proposed modelling the thermal dependence of the ultrasound speed for tissue, using the thermal dependence of water, estimated as a quadratic equation. Rajagopalan *et al.* (1979) provided more tissue specific data by using ultrasound computed tomography to examine the temperature dependencies of the ultrasound speed in several excised human tissues, including liver, kidney, spleen, muscle, breast fat and parenchyma, and spinal cord.

Nasoni *et al.* (1979) examined the thermal dependencies of the speed of ultrasound for several tissues, including both *in vitro* and *in vivo* data for canine kidney. They concluded that although the speed values varied between *in vitro* and *in vivo* measurements, the thermal dependence (dc/dT) remained within 3% (for kidney). This invariance suggests that *in vitro* speed thermal coefficient measurements could be used to estimate *in vivo* parameters.

Haney and O'Brien (1982) extended the concept of noninvasive thermography using ultrasound computed tomography to include frequency dependent attenuation as well as speed, and to suggest an algebraic reconstruction approach that would provide improved resolution accuracy (i.e., reduced resolution degradation) at a computationally reasonable price.

Peyrin *et al.* (1983) attempted to reconstruct temperature gradients in a polyvinyl chloride cylinder, using time-of-flight ultrasound tomography, but attributed their lack of quantitative success to problems with ultrasound refraction.

In all of the above, success in quantitative analysis relied heavily on *a priori* knowledge of tissue specific properties. It is this need for an *a priori* knowledge database that prompted the collection of thermal coefficients for speed and attenuation of ultrasound, for biological media. This database (Haney and O'Brien, 1985, in press) is contained in Appendices A and B. A summary of the available information (and an indication of where little or no information has been collected to date), is given in Chapter 3.

CHAPTER 3

THEORY

3.1 INTRODUCTION

The key to noninvasive temperature estimation using ultrasound is the recognition that both the velocity of propagation and the attenuation of ultrasound are sensitive to temperature. By using ultrasound computed tomography to obtain two-dimensional distributions of ultrasound speed and attenuation, before and after heating the tissue, a temperature change distribution can be estimated.

In general, the thermodynamics of liquids are sufficiently complex to resist description by a mathematically tractable equation of state. Instead, liquids are best described by partial derivatives evaluated in the vicinity of the equilibrium state of the liquid at the time of measurement.

In choosing to approximate a function by partial derivatives, an additional consideration, maximum error over a specified range, is introduced. The conventional approach to approximating a continuous differentiable function f(x), in the vicinity of a known point x_0, begins with the Taylor expansion:

$$f(x) = f(x_0) + (x-x_0)f'(x_0) + \frac{(x-x_0)^2}{2!} f''(x_0) + \ldots \quad (3.1)$$

As long as the function is continuous and infinitely differentiable, the complete series will yield the proper values for f(x) for any x, given only $f(x_0)$, and the derivatives of f(x) at x_0. However, in general, it may be prohibitive to calculate the infinite series, or the higher order derivatives may not be known. Thus an approximation, involving only a finite number of lower derivatives, may be chosen. Let g(x) be an approximation to f(x), using only the first N+1 terms. Then

$$g(x) = f(x_0) + \sum_{i=1}^{N} \frac{(x-x_0)^i}{i!} \frac{d^i f}{dx^i}\Big|_{x=x_0} \quad (3.2)$$

Clearly, $g(x_0)=f(x_0)$. Further, since both f(x) and g(x) are continuous (by definition for f, and by observation for g), the epsilon-delta definition of continuity provides an approach for determining the maximum error in estimating f as g, in the vicinity of x_0. In particular, for any desired degree of accuracy (error) e, one can find d such that

$$|f(x)-g(x)|<e \text{ as long as } |x-x_0|<d \quad (3.3)$$

This calculation can be carried one step further, into a dimensionless estimate, by scaling by 1/f(x). Thus, define

$$e' = |1-g(x)/f(x)|*100\% \quad (3.4)$$

Then, for any level of error, for example 5%, a value of d can be

determined such that as long as $|x-x_0|$ remains less than d, then e remains less than 5%. This range of values, $[x_0-d, x_0+d]$, describes the range of 95% accuracy of the approximation g(x), used to estimate f(x). Similarly, for a chosen range of values $[x_1, x_2]$, the maximum error can be computed.

Throughout much of the following, explicit mathematical representations are either not available or are not tractable. Thus, whenever an approximation is introduced, the maximum error associated with a specified range will accompany the approximation. For the majority of the cases in this work, when the independent variable x represents temperature, the value of the reference point x_0 will be chosen as 30°C, since this is a temperature for which published data are commonly reported. This touches on a major weakness of the available data base; for practical medical applications, data must be available within the 37-42°C temperature range. In examiniing the maximum error, the range of temperatures will often be 25 to 45°C. The choice of the lower temperature is motivated by experimental measurements made for this work, while the higher temperature has been chosen to include 42.5°C, a temperature of significance to hyperthermia applications.

3.2 MOLECULAR LEVEL THERMAL DEPENDENCY

The ultrasonic propagation properties of tissue are considered to be determined largely at the macromolecular level (Pohlhammer and O'Brien, 1980). This idea is supported by studies conducted at least thirty years ago. For instance, Carstensen et

al. (1953) found that the ultrasonic attenuation and speed in blood are determined mostly by protein content, and that the ultrasonic attenuation coefficient is directly proportional to the protein concentration. Several years later, it was shown (Carstensen and Schwan, 1959) that a small fraction of the attenuation in blood arose due to its cellular organization. An early study on liver tissue showed that approximately two thirds of its attenuation occurred at the macromolecular level, with the remaining one third being attributed to microscopic structure (Pauly and Schwan, 1971).

Later (Bamber et al., 1977), the ultrasonic attenuation coefficient and mean backscatter amplitude were measured in various tissues as a function of time after excision up to 120 hours post mortem. During this time period, the ultrasonic attenuation coefficient did not significantly change while the mean backscatter amplitude decreased substantially. It was suggested that the backscatter signal is associated with the relatively large parenchymal structures which are the first to disintegrate while the attenuation is associated with the macromolecular structure which degrades more slowly, thus lending support to the hypothesis that ultrasonic absorption occurs at the macromolecular level in biological materials.

The three tissue constituent materials of water, protein, and fat account for most of the tissue. Table 3.1 shows their ranges for some biological materials. Each of these will be briefly discussed because certain aspects of their temperature dependent behavior are known and thus may contribute to our understanding of

the temperature dependency of the ultrasonic propagation properties for biological tissues.

3.2.1 Water

Water is the most abundant tissue constituent, making up as much as 70 to 80 percent of many tissues. Its concentration is nonuniformly distributed throughout the body. Adipose tissue contains about 10% water, whereas blood contains about 83% water. The total body water is about 60% of body weight for young males, about 50% for young females, and about 76% for babies. Total body water tends to decrease with age. Lean body tissue contains about 72% water (Wolf, 1976; Ganong, 1967). Thus, due to its abundance and variability in tissues, the role of water is explored.

As an approach to understanding the thermal dependence of the speed of ultrasound in water, consider first the adiabatic propagation of a sound wave through an ideal gas. Here,

$$c^2 = \frac{RT\gamma}{M} = \frac{RTC_p}{MC_v} = \frac{RT}{M}\left(1 + \frac{R}{C_v}\right) \qquad (3.5)$$

where c is the speed of sound, R is the gas constant, T is the absolute temperature, M is the molecular weight of the gas, and γ is the ratio of the constant pressure and constant volume specific heats C_p and C_v, respectively (Lambert, 1977). If a relaxation process is involved in the propagation, removing energy from the otherwise reversible adiabatic process, then C_v varies with frequency, and

$$c^2 = \frac{RT}{M}\left(1 + \frac{R(C_{vl}+C_{vh}\omega^2\tau^2)}{(C_{vl}^2+C_{vh}^2\omega^2\tau^2)}\right) \qquad (3.6)$$

where $\omega=2\pi f$ is the radian frequency of the wave, τ is the relaxation time constant, and C_{vl} and C_{vh} are the two extreme values of the specific heat, reached at low and high frequencies, respectively. This is velocity dispersion. Two important factors arise in comparing this result to ultrasound propagation in water and biological tissue. First, over the frequency range of interest (0.5 MHz to 10 MHz), dispersion is generally considered to be a negligible effect. Carstensen and Schwan (1959) reported a "large" dispersion effect of 0.0916% change in velocity over this range of frequencies for human blood. Dunn et al. (1969) noted that the velocity dispersion is typically less than 1% for biological media. Second, the value of γ for water varies from 1.0005 to 1.015 from 0°C to 30°C, and is typically less than 1.006 for many tissues (Sehgal and Greenleaf, 1982). Thus the frequency dependent term of equation 3.6 can be considered to be very small. Therefore, one would expect an overall square root dependence between absolute temperature and speed of sound, at least for gasses. Thus

$$c = \sqrt{\frac{RT}{M}} \cong \sqrt{\frac{RT_0}{M}}\left(1 + \frac{T}{2T_0}\right) \qquad (3.7)$$

where, in the vicinity of 30°C (T_0=303.15 K), the higher order terms contribute less than 0.6% over the temperature range of 0 to 100°C, and contribute less than 0.03% from 25 to 45°C.

Another view is offered by considering a steady-state ultrasound plane wave propagating through a homogeneous medium, where the speed of sound is given by

$$c^2 = \frac{1}{\rho\beta} \tag{3.8}$$

where ρ is the mass density of the medium, and β is the compressibility (Edmonds and Dunn, 1981). If θ is the isobaric thermal expansion coefficient, such that

$$\theta = \frac{1}{V}\frac{dV}{dT}\bigg|_P \tag{3.9}$$

then

$$\rho(T) \tilde{=} \rho_0 + \frac{d\rho}{dT}\Delta T = \rho_0(1-\theta\Delta T) \tag{3.10}$$

Typical values of θ for water and saline in the range of 10 to 40°C, as well as a linear least squares fit to the data, are given in Table 3.2. The correlation coefficient (r) indicates a high confidence in correlation (better than 99.5% for water, better than 98% for saline). An even better fit could be obtained by using a higher order (quadratic) polynomial, but with so few points the statistical value of the improvement is suspect. For the saline fit, the probability is only 50% that the quadratic fit is justified over the linear fit. Using the linear fit for θ, a more complete estimate of ρ would be

$$\rho \tilde{=} \rho_0(1-\theta_1 T-\theta_2 T^2) \qquad (3.11)$$

However, due to the extremely small values of θ, one can estimate $\rho=\rho_0$ with less than 2.2% error over 25 to 45°C, for both water and saline.

If the ultrasonic propagation can be considered as an adiabatic process (ignoring losses due to attenuation), then the compressibility β can be estimated by the adiabatic compressibility β_s. Typical values of β_s for water in the range of 10 to 40°C, as well as linear and quadratic least squares fits to the data, are given in Table 3.3. The linear least squares fit to these data produces a rather unsatisfying result; the correlation coefficient for the linear fit shows a fair confidence of correlation (90%). The quadratic least squares fit is appreciably better. A statistical F-test applied to the relative change in χ^2 for the two fits indicates a better than 90% confidence that the quadratic fit is more appropriate than the linear fit. Note that since only four monotonically varying data points are available, a quadratic fit would be expected to produce a reasonable fit (and a cubic fit would produce a perfect fit), without regard to the underlying physics of the situation.

The decreasing trends of ρ and β_s imply an increasing trend in speed with temperature. If indeed β_s is quadratic, and is approaching a minimum (predicted at T=35.4°C by the quadratic fit in Table 3.3), then the speed should demonstrate a local maximum, assuming $\rho=\rho_0$ is essentially constant. Including the temperature dependence of ρ, the maximum would be expected near 40.0°C. As

will be seen below, the thermal dependence of the speed of ultrasound has been seen to exhibit a maximum in water, but at a significantly higher temperature (74°C), suggesting that the quadratic fit for β_s is not a good model.

Experimentally, the temperature dependence of the speed of ultrasound in water has been studied many times, with various empirical results. For example, Willard (1947) proposed:

$$c = 1557-0.0245(T-74)^2 \qquad (3.12)$$

where c is in meters per second, and T is in °C over the range of 25°C to 85°C. Other single component liquids (alcohols, hydrocarbons, ethers, etc.) show a linear temperature dependence over the temperature range of 20°C to 60°C. Only water appears to have a parabolic temperature dependence. This representation suggests a peak speed of 1557 m/s at 74°C. Willard further suggested that for low concentrations of other materials (principly salts) mixed with water, the peak speed and peak temperature vary linearly with concentration. For example, adding Na_2SO_4 increases the peak speed and decreases the temperature of the peak, to 1680 m/s and 63°C, respectively, at 1 M concentration (Stuehr and Yeager, 1965). The elevation of the speed associated with increasing saline concentration is seen clearly in Table 3.4.

Several other models for the speed of sound in water have been presented. At laboratory temperatures, for degassed water in the neighborhood of 19°C,

$$c = 1461+3.44(T-19)-0.0185(T-19)^2 \qquad (3.13)$$

where speeds and temperatures are measured in meters per second and degrees Celsius, respectively (Johnson et al., 1977a). Warning: the published reference reports the second order term of equation 3.13 as positive, i.e., +0.0185. However, careful analysis indicates that the sign of the second order term should be negative, as shown above. A 20°C change in water temperature will produce a speed change comparable to the difference between the speed of ultrasound in water and the speed of ultrasound in striated muscle. Higher order models (involving polynomials in T up the 5th order) have been reported in Millero and Kubinski (1975):

$$c = 1402.385 + (5.03522)*T - (58.3087*10^{-3})*T^2 + (345.300*10^{-6})*T^3 - (1645.13*10^{-9})*T^4 + (3.9625*10^{-9})*T^5 \quad (3.14)$$

and

$$c = 1402.38754 + (5.03711129)*T - (5.80852166*10^{-2})*T^2 + (3.34198834*10^{-4})*T^3 - (1.47800417*10^{-6})*T^4 + (3.14643091*10^{-9})*T^5 \quad (3.15)$$

and in Slutsky (1981):

$$c = 1402.73 + (5.03358)*T - (5.79506*10^{-2})*T^2 + (3.31636*10^{-4})*T^3 - (1.45262*10^{-6})*T^4 + (3.0449*10^{-9})*T^5 \quad (3.16)$$

where c is in m/s and T is in °C. Warning: the published references report the fourth order term of equation 3.15 as $1.47800417*10^{-5}$, and the fourth order term of equation 3.16 as

positive. However, careful analysis indicates that the equations should be corrected as shown above.

In each of the above cases a first order approximation can be found to linearize the model in the region of a specific temperature. In particular,

$$c(T) \cong c(T_0) + (T-T_0)\frac{dc}{dT} \tag{3.17}$$

where $c(T_0)$ is a reference speed known for temperature T_0, and dc/dT is the first order speed thermal coefficient. This approximation is valid only as long as the higher order terms are insignificant compared to the linear term. In all of the above models, the higher order terms contribute less than 0.48% over the temperature range of 25 to 45°C, for T_0=30°C.

Ultrasonic attenuation is often considered as two effects: scattering and absorption. When an ultrasound wave encounters a region of impedance differing from the preceding medium, a fraction of the wave energy is reflected. The energy in the reflected wave is a function of the impedance mismatch, and the size of the region. If the region is large (with respect to the wavelength of the ultrasound), the reflection is specular, and the reflected wave travels off at an angle equal to the angle of incidence of the incoming wave. However, if the size of the region is small with respect to a wavelength, some of the ultrasound energy is scattered in all directions (nonuniformly). The energy in this scattered ultrasound field which is lost from the incident wave is proportional to λ^{-4} for small spherical

scatterers; the energy scattered per unit length is proportional to λ^{-3} for small cylindrical scatterers (e.g., blood vessels), provided λ is larger than the scatterer (Morse and Ingard, 1968). Since λ=c/f, one would expect:

$$\lambda^{-4} = \frac{\lambda_0^{-4}}{(1+\Delta T/T_0)^2} \cong \lambda_0^{-4}\left(1 - \frac{2\Delta T}{T_0}\right) \qquad (3.18)$$

for a spherical scatterer, and

$$\lambda^{-3} = \frac{\lambda_0^{-3}}{(1+\Delta T/T_0)^{3/2}} \cong \lambda_0^{-3}\left(1 - \frac{3\Delta T}{2T_0}\right) \qquad (3.19)$$

for a cylindrical scatterer. In the vicinity of 30°C (T_0=303.15 K), the higher order terms contribute less than 0.76% over the temperature range from 25 to 45°C. Thus the temperature dependence of the loss due to scattering should be reasonably linear with temperature change over this range.

In examining absorption loss, one of the more studied models for absorption is relaxation (Wells, 1977; Carstensen, 1979). In a relaxation process, energy is converted from one mode (e.g., the ultrasound pressure wave) into another (adiabatic temperature increase, or particle velocity, or molecular rotation, etc.) in an oscillatory fashion. As long as the phases of the two modes are properly aligned, the process is reversible, and the ultrasound wave propagates without loss. When the phases of the modes are not aligned, energy is lost. Sehgal and Greenleaf (1982) considered pressure and temperature as modes that could model a number of different relaxation mechanisms. Carstensen (1979)

modeled the loss due to a single relaxation process, in terms of the absorption coefficient per unit wavelength:

$$\alpha\lambda = 2\alpha\lambda_{max} \frac{\omega\tau}{1+\omega^2\tau^2} \tag{3.20}$$

where $\omega=2\pi f$ is the radian frequency of the ultrasound wave, and τ is the relaxation time which characterizes the relaxation process. The absorption per wavelength exhibits a maximum at $\omega\tau=1$, where it has a value of $\alpha\lambda_{max}$. The relaxation time τ can be approximated by

$$\tau = A \exp\left(\frac{E}{RT}\right) \tag{3.21}$$

where A and R are constants, E is the activation energy of the process, and T is the absolute temperature (Carstensen, 1979). Combining equations 3.20 and 3.21, and differentiating,

$$\frac{d\alpha\lambda}{dT} = 2\alpha\lambda_{max}\left(-\frac{\omega\tau(1-\omega^2\tau^2)}{(1+\omega^2\tau^2)^2}\right)\frac{E}{RT^2} \tag{3.22}$$

Thus at low frequencies ($\omega\tau<<1$), $\alpha\lambda$ should be proportional to $\omega\tau$ (and thus α should be proportional to f^2), and the thermal dependence of the absorption coefficient per unit wavelength should be less than zero. At high frequencies ($\omega\tau>>1$), $\alpha\lambda$ should be proportional to $1/\omega\tau$, and the thermal dependence should be greater than zero. Finally, in the neighborhood of the relaxation frequency ($\omega\tau\tilde{=}1$), the thermal dependence should be zero. This behavior is well demonstrated in the neonatal mouse spinal cord absorption data of Johnston et al. (1979). For frequencies less

than 0.6 MHz, $\alpha\lambda$ decreases with increasing temperature over the temperature range of 2 to 40°C. For frequencies greater than 0.75 MHz, $\alpha\lambda$ increases with increasing temperature over the same range. In the neighborhood of 0.7 MHz, $\alpha\lambda$ varies by less than 25% over 2 to 40°C, compared to the change in $\alpha\lambda$ at 2°C as f varies from 0.26 to 1.0 MHz.

In either of the extreme cases ($\omega\tau<<1$ or $\omega\tau>>1$), one would expect the logarithm of $\alpha\lambda$ to be linear with $\log(\tau)$, which in turn should be proportional to 1/T (according to 3.21). Specifically:

$$\log(\alpha\lambda)\begin{cases} = \log(2\alpha\lambda_{max})+\log(\omega)+\log(A) + \dfrac{E}{RT}\log(e) & (\omega\tau<<1) \\ = \log(2\alpha\lambda_{max})-\log(\omega)-\log(A) - \dfrac{E}{RT}\log(e) & (\omega\tau>>1) \end{cases} \qquad (3.23)$$

Combining the terms into abstact constants leaves a relation of the form:

$$\log(\alpha\lambda) = a + \frac{b}{T} = a + \frac{b}{T_0(1+\Delta T/T_0)} \tilde{=} a' - b'\Delta T \qquad (3.24)$$

where the higher order terms contribute less than 0.25% over the 25 to 45°C temperature range, in the vicinity of 30°C (T_0=303.15 K). Thus, $\log(\alpha\lambda)$ (or $\ln(\alpha\lambda)$, the natural log) should be linear in ΔT, if a single relaxation process is responsible for the absorption.

In the real physical world, there is often a superposition of continuously distributed relaxation processes. Sehgal and Greenleaf (1982) considered the effect of a continuum of uniformly distributed relaxation times from 0 to τ', and arrived at

$$\alpha = \frac{2\omega}{c} \sin\left(\frac{\omega\tau' \ln(\gamma)}{2(1+\omega^2\tau'^2)}\right) \tag{3.25}$$

where γ is the ratio of specific heats. Since γ is typically close to 1 (see the discussion following equation 3.6), this equation can be reduced to two cases:

$$\alpha = \frac{\omega^2\tau'}{c} \ln(\gamma) \tag{3.26}$$

and

$$\alpha = \frac{\omega}{c} \ln(\gamma) \tag{3.27}$$

for low ($\omega\tau' << 1$) and high ($\omega\tau' >> 1$) frequencies, respectively. In the low frequency approximation, α is proportional to ω^2, as is found in various aqueous solutions of salts, acids and bases, which exhibit only a few relaxation processes. In the high frequency case, α is proportional to ω. As $\omega\tau'$ approaches unity, the frequency dependence becomes stronger than linear in ω, but weaker than quadratic (ω^2). This frequency dependence is observed experimentally in many biological tissues. The thermal dependence of this model shows the same properties as those in equation 3.22. For water, $\ln(\gamma)$ increases 25 times, while τ' decreases by two orders of magnitude as temperature increases from 0 to 30°C. At

low frequencies, the τ' decrease more than offsets the $\ln(\gamma)$ increase, so $d\alpha/dT$ is negative. However, at high frequencies, only $\ln(\gamma)$ is present, so $d\alpha/dT$ is positive. Note that the speed of sound c changes only by a factor of 1.07 over this range, and thus does not contribute very much to the change (Sehgal and Greenleaf, 1982).

From the standpoint of experimental measurements, the ultrasonic absorption of water is considered to be equal to the attenuation since water is an isotropic, homogeneous liquid. The ultrasonic loss in water is much less than that in soft tissues, although the ultrasonic speed is comparable. Thus tissues containing exceptionally large amounts of water exhibit a relatively low ultrasonic attenuation, as compared to tissues with less water. The frequency dependency of the attenuation and absorption coefficients of tissue differ from water in that, for tissue, the loss coefficients are roughly linearly proportional to frequency, whereas for water, the absorption coefficient is proportional to the square of the frequency. As with speed, the addition of salts, in low concentrations, alters the attenuation, producing increases for some salts and decreases for others, depending on the salt involved and the frequency of the ultrasound (Stuehr and Yeager, 1965). At 37°C, the frequency-free absorption coefficient is

$$\alpha/f^2 \text{ @ } 37^{\circ}C = 15.7*10^{-17} \text{ s}^2/\text{cm} \qquad (3.28)$$

where α is the ultrasonic absorption coefficient in Np/cm and f is the ultrasonic frequency in hertz (Pinkerton, 1949). Table 3.5

shows how the frequency-free absorption coefficient for water varies with temperature. The thermal coefficient for the absorption coefficient varies from -0.62 to -0.26 $*10^{-17}$ $s^2/cm/^oC$ over the temperature range of 25°C to 45°C. Due to this variation, it is apparent that a linear temperature dependency model, comparable to equation 3.17, is inadequate. This view is supported by the poor value of the correlation coefficient for the linear fit presented in Table 3.5. Consequently, a quadratic fit is considered. Also, prompted by equations 3.23 and 3.24, linear and quadratic fits to $\ln(\alpha/f^2)$ are included in Table 3.5. In spite of the relatively small value of the linear correlation coefficient (0.879), the data show a better than 99.9% level of confidence in correlation. A statistical F-test applied to the change in χ^2 between the linear and quadratric fits shows a 99.9% confidence that the quadratic fit is justified over the linear fit. These observations are not surprising in light of the large temperature range involved.

Note that the linear correlation coefficient of the log fit (0.970) is distinctly larger than for the nonlog fit. Nonetheless, the log-linear correlation coefficient also indicates a better than 99.9% confidence in correlation, as does the nonlog fit. A statistical F-test of the log-linear and log-quadratic fits produces exactly the same conclusions (i.e., 99.9% confidence) as the preceeding nonlog fits, presumably for the same reasons. Statistically, these two models are comparable at the 0.1% level of confidence. However, an examination of the standard deviations in the estimated parameters shows that the standard

deviation in the log parameters ranges from 0.5 to 7.6%, whereas the standard deviation in the nonlog parameters ranges from 4.6 to 16.3%. Thus one would expect a subtle improvement in using the log fit.

3.2.2 Protein

There are two distinct types of proteins. One provides structural features to the body, while the other provides necessary metabolic functions. The major structural protein, collagen, is believed to play an important role in the acoustical properties of tissues. There are several reasons for this. One reason is that collagen, a high tensile strength insoluble fiber, is the most abundant protein in the human body, constituting from 25 to 33 percent of the total protein, and, therefore, about 6 percent of the body weight (White et al., 1968). A second reason is that there is evidence which shows that collagen exhibits different acoustic properties from those of the other common tissue constituents (Fields and Dunn, 1973; Goss and O'Brien, 1979; Pohlhammer and O'Brien, 1980). It is known, for example, that collagenous fibers exhibit a static elastic modulus (Young's modulus) approximately 1000 times greater than that of other tissues (Fields and Dunn, 1973). Since ultrasonic speed is proportional to the square root of the elastic modulus, this suggests that the ultrasonic speed would be greater for collagen than for other constituents. Direct measurements of ultrasonic speed in tendon threads show this to be the case (Goss and O'Brien, 1979; Edwards and O'Brien, 1979). The higher speed in

3.2.3 Fat

Fat is an almost water free tissue. Thus, total body water is largely inversely dependent upon the total amount of body fat. Babies generally have less fat than young males, and young males generally have less fat than young females. This is reflected in the average total body water percentages of 76, 60, and 50, respectively (Bradley, 1972).

At least 10% of the body weight is lipids (fat). The most abundant type of lipid is triglycerides (neutral fat) which is found throughout the body, and especially in adipose tissue (White et al., 1968).

There are no known reports of the temperature dependent ultrasonic propagation properties for lipids. However, the ultrasound speed and attenuation of two oils, castor oil and phenylated silicone Dow-Corning 710, are known at 1 MHz (Dunn et al., 1969). Both oils exhibit a negative thermal dependency for both speed (Table 3.7) and attenuation coefficient (Table 3.8). The speed thermal coefficient, dc/dT, for castor oil remains fairly constant around -4.2 m/s/^{o}C over the range of 5^{o}C to 35^{o}C, while for Dow-Corning 710, the coefficient varies from -3.7 to -2.8 m/s/^{o}C. The thermal coefficient for the attenuation coefficient, dA/dT, varies from -10.0 to -2.0 $cm^{-1}/^{o}C$ for castor oil over the range 5^{o}C to 35^{o}C, while for Dow-Corning 710, the coefficient varies from -6.5 to 1.6 $cm^{-1}/^{o}C$ over the range 15^{o}C to 35^{o}C. Fyke et al. (1979) also found a negative thermal dependency for ultrasonic attenuation for castor oil, mineral oil, and an

of the speed and attenuation coefficient for aqueous collagen suspension are positive and negative, respectively. At 8.87 MHz and a collagen concentration of 0.5 g per 100 cm^3, around 15°C, the thermal coefficient for speed, dc/dT, is 3.28 m/s/°C. When the concentration is 14.2 g per 100 cm^3, the speed thermal coefficient is 0 (around 15°C), indicating a peak in speed as a function of temperature.

Frequency-free attenuation coefficients for collagen suspensions are reported in Table 3.6. The thermal coefficient of the attenuation coefficient, $d(A/f^2)/dT$, varies from -2.02 to $-0.06 * 10^{-17}$ $s^2/cm/°C$, depending on frequency and concentration.

The above data are too limited in temperature range to perform a significant least squares fit. However, two interesting conclusions can be drawn. First, the data decrease with increasing frequency, indicating that A is not proportional to f^2. A linear fit of log(A) to log(f) suggests that for these data, $A = af^b$ for $1.69<b<1.77$ ($r=0.747$, 0.670) at 10°C, and $1.01<b<1.10$ ($r=0.955$, 0.986) at 20°C. Note that the fit to the 20°C data is markedly better than the fit at 10°C. Second, dA/dT is less than zero for this data. These two observations suggest that from the standpoint of the relaxation models presented earlier, $\omega\tau<1$ but it is not the case that $\omega\tau<<1$.

collagen implies that collagen also has a higher characteristic acoustic impedance. This in turn implies that there will be an impedance mismatch between collagen and surrounding tissue, and that collagen is therefore responsible for much of the reflection and scattering that occur in tissues. This idea is supported by Fields and Dunn (1973), for instance, who have suggested that collagen is largely responsible for the echographic visualizability of soft tissue.

Although collagen is the most prevalent protein, the nonstructural proteins must also be considered, since qualitative relationships have been shown to exist between ultrasonic propagation properties and the total protein concentration. For example, in an attempt to characterize tissues according to their ultrasonic attenuation, a number of tissues including brain, liver kidney, blood, and articular tissues were examined and grouped according to their function, such as: 1) metabolic material transport, 2) fat and water storage, 3) protoplasmic activity, physiological function, 4) structural supporting, stress conveying, high in stuctural proteins, 5) framework protection, 6) gasseous exchange (Dunn, 1976; Johnston et al., 1979). Upon examination of this classification, it was found that there is a relatively narrow range of attenuation values within each group, and that the speed of sound increases and the attenuation approximately doubles from group to group in order of increasing attenuation. Furthermore, as one proceeds in this manner, tissues of ever increasing structural protein content are encountered. This suggests that ultrasonic attenuation can be used to

characterize tissues according to functional criteria, and/or their protein concentration.

The propagation properties of aqueous solutions of hemoglobin have been measured more comprehensively than those of any other solution of biological significance. One of the earliest works in this area is that of Carstensen et al. (1953), who investigated the ultrasonic absorption and speed in blood, plasma, and solutions of serum albumin and hemoglobin, and concluded that the acoustical properties of blood are largely determined by the protein concentration. A number of other investigators have measured the propagation properties of hemoglobin solutions (Gramberg, 1956; Carstensen and Schwan, 1959; Edmonds, 1962; Schneider et al., 1969; Edmonds et al., 1970, O'Brien and Dunn, 1972a, 1972b) at frequencies ranging from 35 kHz to 1.0 GHz, thoroughly covering a major portion of the frequency range of relaxation absorption.

Experimentally, Lang et al. (1978) found $\log_e(\alpha/f^2)$ for human breast cyst fluid to vary roughly linearly with temperature, with a value of $-0.01\ ^{o}C^{-1}$ over the range of 25 to 40°C. They also concluded that at 25°C, from 1.7 to 115 MHz, the absorption coefficient is $0.0088*f^{1.42}$ cm^{-1} for cyst liquid, and $0.0066*f^{1.41}$ cm^{-1} for plasma.

Ultrasound speed and attenuation coefficient have been determined in aqueous suspensions of collagen over an extended frequency range at 10°C and 20°C (Goss and Dunn, 1980). As with aqueous solutions of other biopolymers, the temperature dependence

oil-polymer mixture under study as a potential tissue phantom. Least squares fits (linear for speed; linear, quadratic, and log(A) linear for attenuation coefficient) are included in Tables 3.7 and 3.8.

Both of the linear correlation coefficients in Table 3.7 show a 99.9% level of confidence in correlation. Although a statistical F-test applied to the change in χ^2 for linear vs quadratic fits shows a 95% level of confidence that the quadratic fit is justified, the parameters show a very small relative standard deviation (less than 1% for castor oil; less than 3.3% for Dow-Corning 710) for the linear fit, which is significantly degraded by the quadratic fit (up to 21.5% standard deviation for both oils).

The linear correlation coefficients (0.961 and 0.956) in Table 3.8 show a 99 and 95% level of confidence in correlation for castor oil and Dow-Corning 710, respectively. Although the quadratic fits are an improvement (and justified at the 99% confidence level for castor oil, but only at the 75% level for Dow-Corning 710), the log-linear fit is distinctly better (99.9 and 99.8% level of confidence in correlation for castor oil and Dow-Corning 710, respectively). A log-quadratic fit is somewhat justified for Dow-Corning 710 (at the 90% level of confidence), but completely unjustified for castor oil (at the 50% level of confidence).

3.2.4 Summary Of Molecular Level Thermal Dependencies

The thermal properties of the three principle tissue constituents, water, protein, and fat, can be summarized as follows.

For water, the ultrasound speed tends to show a locally quadratic behavior with temperature. In the vicinity of 37°C, the first derivative is positive, indicating that the speed increases with increasing temperature, while the second derivative is negative, indicating the presence of a local maximum at a higher temperature. Several water based solutions show this same behavior, and changing the concentration of the solute shifts the temperature of the peak speed. The absorption coefficient in water tends to increase with the square of the frequency, and decrease with temperature. Although the absorption coefficient shows a locally quadratic behavior, as does speed, no local minimum is found in the range of 0 to 100°C, suggesting that a more sophisticated function may be applicable. An exponential decay model is attractive, and fits the available data at least as well as does the quadratic model. In the vicinity of 37°C, the first derivative is negative, indicating a decreasing absorption coefficient with increasing temperature, while the second derivative is positive, indicating that the absorption coefficient decreases less rapidly at higher temperature.

Aqueous collagen suspensions show increasing speed with increasing temperature, as does water. Also, changing the concentration of the collagen changes the speed thermal

coefficient and shifts the temperature of the peak speed. From 10 to 20°C, the attenuation coefficient decreases with increasing temperature. Insufficient data are available for further qualification of this observation. However, human breast cyst fluid shows an exponential decrease (decay) in attenuation coefficient with increasing temperature, not unlike the behavior of the attenuation coefficient in water.

The speeds of ultrasound in both castor oil and Dow-Corning 710 show a locally linear thermal dependence, giving decreasing speeds with increasing temperatures, at a rate comparable to the increase in speed in water (approximately 3 to 5 m/s/°C). The attenuation coefficient also shows the same type of thermal behavior as water, in so far as exhibiting a decreasing attenuation coefficient with increasing temperature, but the decrease becomes less rapid at higher temperatures.

3.3 TISSUE LEVEL THERMAL DEPENDENCY

Appendices A and B are a compilation of temperature dependent measurements of ultrasound speed and attenuation in biological tissues and fluids. Although many authors have published data on speed and attenuation measurements at various temperatures, only those articles that showed a temperature dependence, or provided sufficient data to approximate a temperature dependence, were included.

Some of the information is second hand: references marked m*1 or m*2 were measurements reported by m, although the data were taken from the extensive compilations of Goss et al. (1978) or Goss et al. (1980), respectively. All pertinent temperature information in Parry and Chivers (1979) is included in the data from Goss et al. (1978) and Goss et al. (1980).

3.3.1 Ultrasound Speed Table

Appendix A reports values of ultrasound speed (m/s) as a function of temperature (^{o}C) at various frequencies (MHz). For each biological material, any available physiological state or age information is included. The ultrasonic frequency of the measurement is indicated where reported. In many cases, speed information was available only in the form of graphs. Thus, speed values marked with an (*) were interpolated from graphs. Where a speed value was not reported but a speed thermal coefficient was available, the missing speed value was linearly estimated, and marked with a (#). The precision of the speed measurement, where available, is provided in parentheses following the speed, either in percent, or as one standard deviation. The speed thermal coefficient, where reported, follows the error (m/s/^{o}C). For a large number of cases, the speed thermal coefficient was not reported, and hence was estimated by the author as the difference in speed divided by the difference in temperature. These estimated coefficients are marked with a (#).

3.3.2 Ultrasound Attenuation Coefficient Table

Appendix B reports values of ultrasound attenuation coefficients (dB/cm) as a function of temperature (^{o}C) at various frequencies (MHz). For each biological material, any available physiological state or age information is included. The ultrasonic frequency of the measurement is indicated where reported. In many cases, attenuation coefficient information was available only in the form of graphs. Thus, attenuation coefficient values marked with an (*) were interpolated from graphs. The precision of the attenuation coefficient measurement, where available, is provided in parentheses following the coefficient, either in percent, or as one standard deviation. The thermal coefficient of the attenuation coefficient, where reported, follows the error (dB/cm/^{o}C $*10^{-3}$). For a large number of cases, the thermal coefficient of the attenuation coefficient was not reported, and hence was estimated by the author as the difference in attenuation coefficient divided by the difference in temperature. These estimated coefficients are marked with a (#).

The results of Dunn (1962), Dunn and Brady (1974a and 1974b), and Johnston et al. (1979) were all based on the same experimental apparatus, and thus represent the same experiment at different frequencies.

As an overview of the available data, and as an index, Tables 3.9 and 3.10 are provided. Table 3.9 is a summary of the ultrasound speed data in Appendix A, indicating the tissues that have been studied and the range of values that have been reported.

Table 3.10 is a summary of the ultrasound attenuation coefficient data in Appendix B. Casual examination reveals that by comparison to speed, little data have been reported on the thermal dependency of the attenuation coefficient for many tissues. Less casual examination reveals that many tissues have not been reported at all (e.g., lung, pancreas, tendon).

3.4 ULTRASOUND COMPUTED TOMOGRAPHY

A wealth of excellent references exist for describing computed tomography (Gordon, 1974; Mersereau and Oppenheim, 1974; Kak, 1979; Horn, 1979; Herman, 1980; and countless others). At the abstract level, measurements are made in some two-dimensional geometry of a process that can be represented as line integral projections of a two-dimensional function. Appropriate computations can then be applied to these integral projections to reconstruct the underlying two-dimensional function. All of this can be extended to higher dimensional systems.

3.4.1 Measurements

For divergent beam ultrasound computed tomography, acoustic propagation measurements are made in a sector shaped region of tissue; see Figure 3.1. The sector is then rotated about a central axis, and the measurements are repeated for many angles of view. The divergent beam geometry is preferred over the more familiar parallel beam beam geometry (where measurements are made along parallel lines, forming a rectangular shaped, rather than sector shaped, region) for large scale, high speed systems, since

the transducers can be mounted on a nonmoving ring. In Figure 3.1, the distance from the transmitter to the receiver is fixed, and the center of curvature for the sector is located at the transmitting transducer. Thus the receiver traces out a circular arc, while the transmitter rotates about its position. With only minor changes in the mathematics, this geometry can be changed to produce a high speed system by placing several transmitters and receivers in a ring; see Figure 3.2. In this configuration, the signal from each transmitter is sampled by a sector-shaped collection of fixed position receivers, rather than one moving receiver. The center of curvature for this sector is located at the center of rotation of the system, rather than at the transmitter. This difference causes all of the sector angles of the fixed ring system to be 1/2 as large as the angles in the single pair transmitter-receiver case. The differences in transmitter-receiver distance are also easy to accomodate. Since no mechanical motion is required in the ring configuration, data can be collected as fast as the electronics permits.

Two physical quantities can be readily measured with ultrasound tomography: time-of-flight and amplitude attenuation. The time required for an ultrasound pulse to propagate through a medium is equal to the distance traveled divided by the speed of propagation. For a heterogeneous medium, the total time-of-flight is the integral of the inverse speeds:

$$t = \int \frac{dx}{c(x)} \qquad (3.29)$$

The simplest approach to measuring the time-of-flight for a pulse of ultrasound traveling between two transducers is to measure the amount of time between the generation of the pulse, and the time when the received signal exceeds some predetermined threshold. This approach is susceptible to many sources of error, such as time walk and time hop, both due to attenuation (Crawford and Kak, 1981). A more robust approach is to correlate the received signal with a copy of the transmitted signal, and measure the time difference from the shift in the correlation peak. Let q(t) be the transmitted signal, and s(t) be the received signal. If the propagation of ultrasound does not change the character of the signal significantly, other than to attenuate the signal and to produce a delay due to the propagation time, then s(t)=Aq(t-t'), where A describes the amplitude attenuation and t' is the time-of-flight. By correlating q and s,

$$R(t") = \int q(t)s(t-t")dt = \int q(t)Aq(t-t'-t")dt \qquad (3.30)$$

the time-of-flight can be determined from the location of the peak of the correlation curve:

$$t' = t" \iff \max(R(t")) \text{ over } t" \qquad (3.31)$$

In general, the transmitted signal q(t) is not available, since it would require ideal measurements made with ideal transducers. However, a reasonable alternative is to use the received signal through a reference medium of known properties as the kernal of the correlation. Let $s_w(t)$ be the signal received if the ultrasound were to propagate through a water path (with speed c_w) of distance equal to that in the tomography system. The

time-of-flight difference, $\Delta t'$, defined by

$$\Delta t' = \int \frac{dl}{c_w} - \int \frac{dl}{c(x,y)} \qquad (3.32)$$

can be extracted from

$$\Delta t' = t'' \iff \max(R(t'')) = \max(\int s_w(t)s(t-t'')dt) \qquad (3.33)$$

As will be seen later, the reconstruction of tomographic data is greatly simplified if the object being imaged can be assumed to have finite size and magnitude, and to be surrounded by a region of zero magnitude. For water-based tomographic systems, the rays at the edges of each sector pass through open water (see Figure 3.1). This provides a convenient source for the reference signal $s_w(t)$, and satisfies the above property (i.e., $\Delta t'=0$ at the edges of each sector).

If the correlation is performed digitally,

$$R(nt'') = t''\sum s_w(mt'')s((m-n)t'') \qquad (3.34)$$

then the values of s, s_w, and R are known only at discrete points in time (...-2t", -1t", 0, t", 2t",...). Superficially, this implies that the temporal resolution for estimating $\Delta t'$ is equal to the sampling period t". McGill and Dorfman (1984) have presented a straightforward approach to improve this resolution (without involving increased sampling rates) using the Fourier transforms of the signals to determine the location of the peak of the correlation. A computationally simpler approach, used by Foster (1985) is to estimate $\Delta t'$ from a parabolic fit to the

correlation at its peak. Let nt" be the time that maximizes R(nt"). Then, by fitting a parabola to R((n-1)t"), R(nt"), and R((n+1)t") (using the notation R(-1), R(0), and R(1), without loss of generality),

$$\Delta t' = \left(n + \frac{R(-1)-R(1)}{2(R(-1)+R(1))-4R(0)} \right) t" \qquad (3.35)$$

This provides a simple and effective estimate of $\Delta t'$.

The second physical quantity, attenuation, is also an integral process. The intensity of an ultrasound wave is assumed to decrease exponentially with distance, as it travels through an attenuating medium. The underlying physical mechanisms of this process were examined in section 3.2. Let I_r be the received intensity, and I_i be the transmitted intensity of the ultrasound wave. Then,

$$I_r = I_i \exp(-2Ad) \qquad (3.36)$$

where A is the amplitude attenuation coefficient, and d is the distance traveled. For a heterogeneous medium, if specular reflection can be ignored, the attenuation is also an integral process:

$$I_r = I_i \exp\left(-\int 2A(x,y)\,dl\right) \qquad (3.37)$$

As with the time-of-flight, the transmitted intensity is not readily available. However, the attenuation with respect to the attenuation through a comparable water path can be determined using data from the edges of each sector as a reference:

$$I_r = I_w \exp(-\int 2(A(x,y)-A_w)\,dl) \tag{3.38}$$

where A_w is the attenuation coefficient of water. Again, as with time-of-flight, preprocessing is required to obtain the integral process of interest. Specifically,

$$\Delta A = \int (A(x,y)-A_w)\,dl = -\ln(I_r/I_w)/2 \tag{3.39}$$

Two problems exist in this approach. The first is that the "measured intensity" of a pulse is an ambiguously defined concept. An American Institute of Ultrasound in Medicine document distinguishes between temporal average and temporal peak intensity (AIUM, 1984). The second problem is specular reflection. The energy lost from a wave, as a portion of it reflects off of a tissue interface, is not an exponential process. Fortunately, attenuation due to scattering and absorption is frequency dependent (see section 3.2), whereas specular reflection is largely frequency independent. The Fourier transform provides a convenient mechanism for avoiding both problems by finding the frequency sensitive portion of the loss. Since the intensity of a plane wave is proportional to the square of the amplitude of the wave, it is convenient to use the amplitude of the received signal to determine the amplitude attenuation coefficient. Let $S_w(\omega)$ and $S(\omega)$ be the Fourier transforms of the water path and sample signals, respectively. Then

$$|S(\omega)| = K\ |S_w(\omega)|\ \exp(-\Delta A(\omega)) \tag{3.40}$$

or

$$\Delta A(\omega) = -\ln \frac{|S(\omega)|}{|S_W(\omega)|} - \ln(K) \qquad (3.41)$$

where K descibes the frequency independent loss due to reflections (Crawford and Kak, 1981). Since $\Delta A(\omega)$ approaches 0 as ω approaches 0, one approach is to use $S_W(0)$ and $S(0)$ to normalize K out of the equation. Unfortunately, the expected values of $S_W(0)$ and $S(0)$ are zero. Thus $S_W(0^+)$ and $S(0^+)$, the values of S_W and S in the neighborhood of $\omega=0$, must be used to estimate $S_W(0)/S(0)$:

$$\Delta A(\omega) = -\ln \frac{|S(\omega)|/|S(0^+)|}{|S_W(\omega)|/|S_W(0^+)|} \qquad (3.42)$$

Note that this asssumes $A(0^+)<<K$. If a specific frequency dependency model is assumed (e.g., $\Delta A=A_0 f^b$), then a least squares fit can be used to provide some noise immunity (by using many data points to estimate a few parameters).

In both cases, time-of-flight and frequency dependent attenuation measurements are made along discrete lines of a sector; see Figure 3.3. Let χ be the angle of the line with respect to the center line of the sector. The sectors are measured at discrete view angles. Let θ be the angle between some frame of reference and the center line of the sector. Thus the data are collected as a function of two angles: θ and χ. If the sectors are uniformly sampled in angle χ, the geometry is called equiangular divergent beam tomography. The values of the measured and extracted property are denoted $g(\theta,\chi)$.

3.4.2 Reconstruction

The reconstruction of the underlying function from the integral projections is a mathematically straightforward but computationally demanding task. The two most common approaches, convolution backprojection and algebraic reconstruction, are described below.

Since the following reconstruction mathematics is indifferent to whether time-of-flight or frequency dependent attenuation is being reconstructed, the notation $g(\theta,\chi)$ does not need to reflect which property is being processed.

3.4.2.1 Convolution Backprojection

The most commonly used approach to tomographic reconstruction is convolution backprojection. The details can be found in many sources (e.g., Horn, 1979; Kak, 1979; Kak, 1980). For equiangular divergent beam geometry,

$$g(\theta,\chi) = \int f(x,y)\,dl \tag{3.43}$$

and

$$f'(x,y) = \int_0^{2\pi} \frac{1}{L^2} \left(g(\theta,\chi) D\cos(\chi)\right) \circledast (h(\chi))\,d\theta \tag{3.44}$$

where

$$h(\chi) = \frac{1}{2}\left(\frac{\chi}{\sin(\chi)}\right)^2 \frac{1}{2\pi} \int |\omega| \exp(j\omega\chi)\,d\omega \tag{3.45}$$

and where D is the distance from the transmitting transducer to the center of rotation, and L is the distance from the transmitting transducer at view angle θ, to the point (x,y).

Philosophically, this approach arises from the projection slice theorem, where the one-dimensional Fourier transform of the integral projection data provides a line (or slice) of the two-dimensional Fourier transform of the underlying function. Rather than collect all of the data, fill in all of the two-dimensional Fourier space, and then invert, convolution backprojection takes advantage of the fact that all of the mathematical processes involved are linear. Thus the contribution of each individual integral projection is separately filtered (convolved), and added (backprojected) into the final solution. The function $h(\chi)$ is the kernal of the convolution, and the integral over θ is the summation of the individual views.

The filter function $h(\chi)$ is to a large extent a spatial high pass filter. The Fourier transform $H(\omega)$ is proportional to $|\omega|$, along with some geometry dependent factors. Thus $H(0)=0$, and $H(\omega)$ increases with increasing ω. If digital signal processing is used, so that $\chi=n\chi'$ and $\omega=m\omega'$, then it is tempting to sample $H(m\omega')$ such that $H(0)=0$ for $m=0$. However, a significant error is introduced by this choice, since $m=0$ describes not only $\omega=0$, but also $-\omega'/2\leq\omega\leq\omega'/2$. Over this range, $H(\omega)$ varies by a nonnegligible amount. A better estimate of the discrete frequency space function is available from the discrete Fourier transform of the discrete spatial domain function (Kak, 1980). Thus

$$h(n\chi')\begin{cases} = \dfrac{1}{8\chi'^2} & n=0 \\ = 0 & n \text{ even} \\ = \dfrac{-1}{2\pi^2\sin^2(n\chi')} & n \text{ odd} \end{cases} \qquad (3.46)$$

and $H(m\omega')$ can be obtained from the FFT of $h(n\chi')$. Digital convolution is then possible by multiplying $H(m\omega')$ by $G(\theta,m\omega')$ and taking the inverse FFT. Note that both spatial domain functions, $h(n\chi')$ and $g(\theta,n\chi')$ must be zero padded to prevent the cyclic convolution by Fourier space multiplication from producing spatial aliasing (Kak, 1979).

3.4.2.2 Algebraic Reconstruction Techniques

An alternative approach to tomographic reconstruction is offered by modelling the integral projections as linear summations. Consider

$$g(\theta,\chi) = \int f(x,y)\,dl = \iint A(\theta,\chi,x,y)\,f(x,y)\,dxdy \qquad (3.47)$$

where $A(\theta,\chi,x,y)$ is the contribution that $f(x,y)$ makes to the measurement $g(\theta,\chi)$. Rearranging the two-dimensional arrays of image points and data points into vectors (using lexigraphical ordering):

$$g = Af \quad \text{or} \quad g_i = \sum_j A_{ij} f_j \qquad (3.48)$$

Thus the reconstruction problem has been converted to a conventional problem of linear equations: given g and A, find f.

To clarify the notation, f(x,y) will always describe a real continuous function in two independent variables x and y. When this function is sampled into a two-dimensional M*N matrix, the elements of the matrix will be denoted f_{mn}, and the value of the element will be f(mx',ny'), where x' and y' are the spatial sampling rates in the x and y dimensions, respectively. Finally, when the two-dimensional matrix is rearranged by stacking one column upon another to form a one-dimensional vector, the elements of the vector will be denoted f_j, where the value of the element is f_{mn} such that $j = m + (n-1)M$.

Before approaching the solution of g=Af, consider the form of the geometric description matrix A. Each row i of the A matrix describes the interaction between the object function f and the ultrasound beam at angles θ and χ, to form measurement i. The most simple model for this process is $A_{ij}=1$ if beam i passes through pixel j, and zero otherwise. This is an attractive model since Af becomes a multiplication-free computation. Note that this assumes that f and g are scaled according to unit distance, so that the "size" of a pixel is unity.

A more realistic model is to let $A_{ij}=L_{ij}$, where L_{ij} is the length of the portion of beam i that passes through pixel j; see Figure 3.4.

In both of the above models, the majority of the elements of A are equal to zero. Specifically, if the underlying function f(x,y) is sampled into an M*N matrix, so that the vector f is 1*MN, and integral projections are measured at K angles and L

views, so that the measurement vector g is 1*KL, then the matrix A is KL*MN. Although this value may be very large (if K, L, M, and N, are all 64, then KL*MN is greater than $16*10^6$), it is necessary to store and maniuplate only the nonzero elements of A. Each row i describes the interaction of a beam of ultrasound with a line of pixels through the object. Clearly, however, not every pixel in the object is in line with each beam. To be specific, if beam i enters the object at (m,n) and exits at $(m+\Delta m, n+\Delta n)$, then the number of pixels involved in the beam, N_{pix}, is constrained by

$$\max(|\Delta m|, |\Delta n|) \leq N_{pix} \leq |\Delta m| + |\Delta n| \qquad (3.49)$$

Thus for each row of A (each beam), only N_{pix} out of MN values in the A matrix are nonzero. A very conservative upperbound on N_{pix} is M+N, corresponding to a beam crossing diagonally through the rectangular region described by the sampled f matrix. If the beam is modeled as having a finite width, then the number of pixels involved is roughly $w*N_{pix}$, where w is the width of the beam, measured in pixel scale.

The occupancy of the matrix A, measured as the percent of nonzero elements in the matrix, is thus

$$S = 100\% \frac{N_{pix}}{MN} \leq 100\% \frac{(M+N)}{MN} \qquad (3.50)$$

For a 64*64 array for f, $S \leq 3.125\%$. This is an important consideration, since the occupancy of a matrix determines the amount of computation required to manipulate the matrix.

The model $A_{ij}=L_{ij}$ is based on the assumption that in the neighborhood of point j, f_j can be treated as a constant. This is a strong assumption of spatial bandlimitedness. A less strict assumption is that f(x,y) varies sufficiently slowly in the neighborhood of the point j that the line integral for the ray passing near j can be evaluated from a bilinear interpolation of f_j and the values of f for the nearest neighbors to j. Specifically,

$$g_i = \int \sum_m \sum_n f_{mn} \mathrm{tri}(m-x)\,\mathrm{tri}(n-y)\,dl \qquad (3.51)$$
$$= \sum_m \sum_n f_{mn} \int \mathrm{tri}(m-x)\,\mathrm{tri}(n-y)\,dl = \sum_m \sum_n A_{ij} f_{mn}$$
$$j=m+(n-1)M$$

where

$$\mathrm{tri}(z) = \begin{cases} 1+z & -1 \le z \le 0 \\ 1-z & 0 \le z \le 1 \\ 0 & \text{otherwise} \end{cases} \qquad (3.52)$$

The bilinear interpolation approximates f(x,y) in terms of f_{mn} and the eight nearest neighbors to point (m,n)<=>j. Since the line integral can be evaluated independent of the value of f_{mn}, but instead depending only on the geometry of the data collection, the contribution of f_{mn} to measurement i (i.e., A_{ij}) can be predetermined before data collection, and reused for many measurements. Although an explicit representation for A_{ij} can be determined (since the interpolation function is relatively simple and can be integrated by conventional mathematics), the general solution is sufficiently awkward to make numerical solution attractive.

This model causes the number of nonzero entries in A to increase by roughly a factor of four. Thus the occupancy of A becomes roughly 12.5% for a 64*64 object array. However, the interpolation in this model is effectively equivalent to increasing the underlying sampling rate, and using larger matrices. The reduction in error and equivalent sampling rate comparison for this model is addressed in section 3.6.3, and the results of a computer simulation analysis are presented in Chapter 5.

The solution of g=Af lends itself to many approaches. The most direct is to invert A to find f from g. In general, however, A is a rectangular matrix (KL*MN), and even when the number of measurements has been chosen to equal the number of pixels (KL=MN), there is no guarantee of nonsingularity. Thus pseudoinverse matrices can be used. As will be seen below, computationally more attractive methods of algebraic reconstruction are often used. However, an appreciation of direct methods is required for later noise related variance analyses. Of the three types of pseudoinverse matrices, the common underlying definition is that $A^{\%}$ is the pseudoinverse of A if and only if $A^{\%}$ satisfies:

$$A = AA^{\%}A \tag{3.53}$$

(Pratt, 1978). Conditional and least squares inverses, the two most general of the pseudoinverses, always exist, but may not be unique. The generalized inverse is the most constrained of the pseudoinverses, and is unique if it exists at all. In general, if

$A^{\#}$ is a least squares pseudoinverse (i.e., $A^{\#}$ satisfies 3.53 above, as well as $AA^{\#}=(AA^{\#})^T$), then

$$f' = A^{\#}g \tag{3.54}$$

provides the best (least squares) estimate of f given g and A. Note that if a generalized inverse A^- exists, then f' is not only a least squares solution, but moreover, it has minimum norm.

The least squares pseudoinverse is readily available (Luenberger, 1969):

$$\begin{aligned} A^{\#} &= (A^TA)^{-1}A^T \text{ iff } (A^TA)^{-1} \text{ exists} \\ &= A^T(AA^T)^{-1} \text{ iff } (AA^T)^{-1} \text{ exists} \end{aligned} \tag{3.55}$$

The first case describes an overconstrained system, where the number of measurements exceeds the number of pixels. This is often the configuration of choice. If no noise is present, a unique solution will exist if the measurements are consistent. The second case describes an underconstrained system, where at best a continuum of nonunique solutions can be found. In this case, f' will have minimum norm over the set of nonunique solutions.

Although the matrix A^TA (or AA^T) is very large (MN*MN, or KL*KL for AA^T), and solving matrix inversions is very time- and space-consuming, this computation can be performed once for a given geometry, and used countless times to reconstruct any number of objects studied with the same geometry. Thus the cost of computing $(A^TA)^{-1}$ can be amortized over a large number of later reconstructions. As noted earlier, only the nonzero elements of

the matrix need to be stored and manipulated. A further economy can be achieved by recognizing that each value of the matrix is used once in the reconstruction. Thus the entire matrix need never reside in the central memory of the computer performing the reconstruction, but instead could reside on a magnetic disk or tape. Current computer technology readily supports the concept of performing the calculations associated with one row of the matrix, while the next row is being concurrently loaded from disk (using direct memory access). Specialized computer systems, or "reconstruction engines," can be readily designed to take advantage of the intensely parallel nature of the computation involved.

For individual reconstructions (i.e., other than the mass produced reconstructions suggested above), a computationally attractive alternative to direct inversion is iterative approximation. The name "algebraic reconstruction technique," or ART, is conventionally used to describe only iterative approaches, not direct solutions. The essence of additive iteration, (additive ART) is

$$f^{n+1} = f^n + D(g, Af^n) \tag{3.56}$$

where f^0 is some initial guess for f, Af^n is the projection of guess f^n, and D(a,b) is a directed measure of how close vector a is to vector b. An excellent example is the projection iterative method described by Huang (1977):

$$f^{n+1} = f^n + \frac{g_i - A_i f^n}{A_i^T A_i} A_i \qquad (3.57)$$

where A_i is the i'th row of the A matrix. One full iteration is defined by evaluating 3.57 for each of the I rows of A. Repeated iterations of this method will produce one of the following results: i) convergence to the solution, if a unique solution exists, ii) convergence to the (least squares) nearest solution (from the starting guess) if the solution is not unique, or iii) cyclic convergence (i.e., $f^n=f^{n+I}$ but $f^n \neq f^{n+1}$) if no solution exists. This last case arises if the system is overconstrained, and noise in the system causes the equations to become inconsistent.

Perhaps the most common variation on the above is the use of relaxation parameters (Herman et al., 1975):

$$f^{n+1} = f^n + rD(g, Af^n) \qquad (3.58)$$

where r is chosen to alter the rate of convergence. For r>1, the iteration will rapidly approach the solution, but may overshoot and produce artifacts in the final image. For r<1 (underrelaxation), convergence is slowed, but artifacts due to overshoot are reduced. The choice of r=0.75 is popular (Herman, 1975; Johnson et al., 1977b).

3.4.2.3 Limited Viewing Angles

A significant problem arises in applying divergent beam ultrasound computed tomography to human body studies. Specifically, for uniform estimation of the underlying function, 360 degrees worth of viewing angles must be available. (The outer integral over θ in the convolution backprojection runs from 0 to 2π.) Since ultrasound will not propagate readily from soft tissue to bone, or from tissue to air (as in the lungs or in the occasionally gas-filled gastro-intestinal tract) due to reflection, very few areas of the body are readily available for 360 degrees of data acquisition. The principle exception to this is mammography, where ultrasound computed tomography has been used.

For the rest of the body, only limited viewing angles are available. Algebraic methods, such as ART, are formulated independent of the underlying geometry. Thus missing angles can be accomodated by simply deleting rows from the A matrix. For iterative solutions, this runs the risk of making the solution less stable. For direct solutions, the pseudoinverse matrix must be recomputed, which may not be economical for a single reconstruction. Convolution backprojection, on the other hand, is not designed to work with less than complete data. One approach to this problem is to iterate between convolution backprojection and ART, using the algebraic representation of the problem to estimate the projections that would have been measured at the missing angles (Heffernan and Robb, 1983).

3.4.3 Interpretation Of Reconstruction

Independent of the reconstruction method used, the measured projection data are manipulated to recover the underlying object function. In the case of the time-of-flight data, inverse speeds are reconstructed:

$$\Delta t = \int \frac{dl}{c_w} - \int \frac{dl}{c(x,y)} = \int f(x,y)\,dl$$
$$\Rightarrow f(x,y) = \frac{1}{c_w} - \frac{1}{c(x,y)} \tag{3.59}$$

If the time-of-flight is measured in microseconds, and the physical dimensions of the tomography system are measured in millimeters, then f(x,y) will have units of μs/mm. To recover the ultrasound speed,

$$c(x,y) = \frac{1}{(1/c_w - f(x,y))} \tag{3.60}$$

where c(x,y) will have the units of mm/μs.

For frequency dependent attenuation, the log of the loss is used:

$$\Delta A(\omega) = -20\log \frac{|S(\omega)|}{|S_w(\omega)|} = \int (A(x,y) - A_w)\,dl$$
$$\Rightarrow f(x,y) = A(x,y) - A_w \tag{3.61}$$

The reconstructed attenuation coefficient function f(x,y) will have units of dB/mm, assuming as before that the system dimensions are measured in millimeters. The object attenuation coefficent,

as a function of frequency, is readily available from:

$$A(\omega,x,y) = f(x,y) + A_w \qquad (3.62)$$

See section 3.2 for values of A_w.

3.5 DIFFERENTIAL TOMOGRAPHY AND DIFFERENTIAL THERMOGRAPHY

If the relationship between speed and temperature, or attenuation and temperature, is known precisely, and all of the relevant tissue properties are known for the tissue under investigation, then a single measurement of ultrasonic properties should be sufficient to determine the temperature. The large range of variation in ultrasound properties and thermal coefficients in Tables 3.9 and 3.10 suggests that a single measurement would be insufficient to properly characterize the tissue temperature. Note however that the tables are not very comprehensive: Table 3.10 is missing data in many entries, and both tables omit several tissues, including blood vessel, intestinal wall, and pancreas, as well as the many forms of abnormal tissues and tumors. In light of the relatively small amount of available data, one may question whether the available data are truly representative of the temperature dependent interaction of ultrasound with biological media. Regardless, given the data currently available, absolute noninvasive thermography does not seem promising at this time.

However, estimating a temperature change resulting from the application of some external energy source is still tractable. If a Taylor expansion of the ultrasound speed (or attenuation coefficient) as a function of temperature can be validly modeled as a first order polynomial, as in equation 3.17, then

$$c_1 - c_0 = \frac{dc}{dT} \Delta T \text{ or } \Delta T = \frac{c_1 - c_0}{dc/dT} \tag{3.63}$$

where c_0 is the speed measured before heating, and c_1 is the speed measured after heating. The same applies for the attenuation coefficient. If a first order polynomial is not sufficient to model the temperature dependency over the temperature range of interest, then a second order polynomial may be tried. However, to estimate temperature, equation 3.63 is still applicable, with

$$\left.\frac{dc}{dT}\right|_{T_0'} = \frac{dc}{dT} + \frac{d^2c}{dT^2} T_0' \tag{3.64}$$

where T_0' is an estimate of the starting temperature. This is a linearization of the quadratic polynomial in the neighborhood of T_0', and as such, T_0' need not be equal to T_0, the true starting temperature, as long as the second order term of the quadratic contributes little due to the difference between T_0' and T_0 or T_1 (i.e., the temperature change must be small). As will be seen in Chapter 5, the second order polynomial approach is more appropriate for attenuation coefficients than for speed. Note that applying two doses of heating, and measuring three speeds (or attenuations) does not in general improve the solvability of the problem. With two doses of heat, there will be two temperature

changes to compute, and thus no net information has been gained. Even if the energy in the two heat doses is the same, the temperature change may not be constant unless the specific absorption rate of the tissue is independent of temperature in this temperature range. In this case, if the temperature dependence is linear, the three measurements will represent three points along the same line, and no real information will have been obtained by the third measurement (although the variance of the estimation may improve due to better signal to noise statistics). If the temperature dependence is quadratic then the three points could be fit to a parabola, and thus all be useful. However, in the case of quadratic (i.e., nonlinear) temperature dependence, one would not expect a constant specific absorption rate (i.e., a linear response). Thus two equal exposures would probably not yield two equal temperature changes. Thus little should be gained by making more than two measurements.

An interesting alternative to linear estimation exists in the case of ultrasound speed. If equation 3.5 is valid for tissue,

$$\frac{c_1^2}{c_0^2} = \frac{RT_1\gamma_1/M}{RT_0\gamma_0/M} = \frac{T_1\gamma_1}{T_0\gamma_0} = \frac{T_0+\Delta T}{T_0}\,\frac{\gamma+\Delta\gamma}{\gamma} \tag{3.65}$$

If $\Delta\gamma$ is small with respect to γ, then

$$\frac{\Delta T}{T_0} = \frac{c_1^2}{c_0^2} - 1 \tag{3.66}$$

should estimate temperature changes, assuming T_0 is known or can be guessed. Sehgal and Greenleaf (1982) reported $\ln(\gamma)$ changing

by a factor of 25 over the temperature range of 0 to 30°C for water. This corresponds to $\Delta\gamma = 0.015$ for $\gamma = 1.015$ (or 1.47%). In the case of *in vivo* measurements, if T_0 can be estimated as body temperature (e.g., 37°C, or 310.15 K), then ΔT becomes readily available from two speed measurements.

For attenuation modeled as a relaxation process, the temperature dependence of the relaxation time has the effect of shifting the $\alpha\lambda$ relaxation curve in frequency space such that $\omega_0\tau_0 = \omega_1\tau_1$. This conclusion arises from the fact that all occurrences of τ in the relaxation model (both the single relaxtion model in equation 3.20, and the multiple process model, equation 3.25, represented as $\alpha\lambda$) are in products with ω. Thus any percentage decrease in τ is indistinguishable from the equivalent percentage increase in ω. If $A\lambda_0(\omega)$ is the frequency dependent attenuation coefficent of the first measurement (before heating), and $A\lambda_1(\omega)$ is the attenuation coefficient of the second measurement, then the peak of their cross correlation in log frequency space will identify the effective shift of the curve:

$$\Delta\omega \Leftrightarrow \max\int A\lambda_0(\ln(\omega))A\lambda_1(\ln(\omega)-\ln(\omega'))d\ln(\omega) \qquad (3.67)$$

where $\omega_1 = \omega_0\Delta\omega$. The above integral can be simplified by recognizing that $d\ln(\omega) = d\omega/\omega$. Given the effective shift in frequency space,

$$\ln(\Delta\omega) = \frac{E}{RT_1} - \frac{E}{RT_0} = \frac{E\Delta T}{RT_0^2(1+\Delta T/T_0)} \cong \frac{E\Delta T}{RT_0^2} \qquad (3.68)$$

where E is the activation energy, and R is a constant. E and R

can be collapsed into one tissue specific parameter for the sake of modeling. Thus the log of the frequency shift should be proportional to the temperature change, which can be estimated if T_0 is known or can be guessed.

With the exception of the ratio of squared speed method, all of the above requires an *a priori* knowledge of tissue specific parameters, which may not be directly measurable in a noninvasive manner. For this reason, Appendices A and B, containing literature values for speed and attenuation coefficient for various biological tissues, have been compiled. An analysis of these data with the above models is presented in Chapter 5.

3.6 ERROR ESTIMATION

A noninvasive estimate of internal temperature would be of little value without an estimate of the variance associated with that temperature. Several sources of error are inherent in ultrasound property measurements. These errors are then propagated through the tomographic reconstruction process, and finally influence the outcome of the temperature estimation. The following material examines the errors in measurement and estimation that are independent of the experimental facility that might be used to make the measurements. Experiment-specific error sources associated with the apparatus used in this study will be examined in Chapter 5.

3.6.1 Physical Sources Of Experiment Independent Error

Conventional ultrasound computed tomography measurements are based on the assumption that the ultrasound wave propagates along a straight path through the tissue under investigation. Although this assumption is valid for x-ray tomography, there are several physical mechanisms that introduce errors in ultrasound propagation measurements. When a wave passes from a region of one speed of propagation to a region of another speed at an angle other than normal incidence, the wave path bends according to Snell's Law: the ratio of the speeds is equal to the ratio of the sine of the angle of incidence to the sine of the angle of transmission. If the second region can be modeled as a layer with parallel sides, then compared to straight path propagation, the ultrasound will follow a slightly longer path through a layer of relatively higher speed, and a slightly shorter path through a layer of relatively lower speed; see Figure 3.5. If time-of-flight is measured with respect to time-of-flight through a homogeneous reference medium, the effect of refraction is to decrease the variation in time-of-flight due to the inhomogeneities, and thus result in underestimation of the speed differences. Peyrin *et al.* (1983) attributed their difficulties in tomographic reconstruction of PVC cylinders to refraction error. Refraction will also change the amplitude of the received pulse by directing the pulse slightly away from the receiving transducer. This will not change the spectral content of the received signal, however, if the bending is frequency independent. Thus refraction (by itself) should not have a major effect on

attenuation as measured by equation 3.42.

Velocity dispersion causes different frequencies of ultrasound to propagate at different speeds. If refraction is present to bend the beam, then dispersion will broaden the beam due to variation of transmission angles resulting from frequency dependent variations in speeds. If dispersion is present, the spectral characteristics of the ultrasound wave will be altered, producing errors in estimating the attenuation. Time-of-flight estimation can also be affected if the spectral characteristics of the received pulse are changed sufficiently to affect the correlation (with a water path reference signal) used to estimate time delay. Note that dispersion has been assumed to be negligible in section 3.2, and is included in the discussion here only for completeness.

The interaction of an ultrasound wave with edges, or regions comparable in size to a wavelength of the ultrasound, results in frequency dependent scattering, or diffraction. Since the effect is frequency dependent, diffraction changes the spectral characteristics of the received pulse, and thus alters both the attenuation and the time-of-flight estimation. One approach that addresses diffraction and refraction problems is diffraction tomography, where the ultrasound far field is sampled for each viewing (illumination) angle, in order to obtain a sufficient amount of information to reconstruct the wave field in the tissue under investigation. Pan and Kak (1983) present a comparison of various diffraction tomographic reconstruction algorithms. The sophistication of the model used to describe the interaction of

ultrasound with the tissue determines the completeness with which diffraction and refraction are accounted for. Unfortunately, the sophistication of the model also determines the complexity of the solution. Thus ultrasound diffraction tomography appears to be the most comprehensive (and the most difficult) approach to fully analyze the interaction of ultrasound with tissue. Since the temperature estimation procedures of section 3.5 are independent of the reconstruction algorithm used, they should be equally applicable to diffraction tomography.

3.6.2 Errors In Property Estimation

If the time-of-flight is estimated from the location of the peak of a correlation between a known, noise-free reference signal, and a time-delayed, scaled, noisy copy of that signal, and the noise has a zero mean and is independent, then the expected value of the measured time delay $\Delta t'$ is equal to the true time delay. The variance of the time delay is given by

$$\mathrm{var}(\Delta t') = \frac{N}{EB^2} \tag{3.69}$$

where N is the power of the noise, E is the power of the received signal, and B is the normalized rms bandwidth

$$B^2 = (2\pi)^2 \frac{\int f^2 |S_w(f)|^2 df}{\int |S_w(f)|^2 df} - (2\pi)^2 \left(\frac{\int f |S_w(f)|^2 df}{\int |S_w(f)|^2 df} \right)^2 \tag{3.70}$$

where $S_w(f)$ is the Fourier transform of $s_w(t)$, the reference signal (Burdic, 1984). For ultrasound tomography, the individual

reference signals at the edges of each fan are not noise-free. However, a relatively clean estimate can be formed by averaging these signals over several fans. Also, the received signal through the tissue is not simply a scaled noisy copy of the reference signal. The frequency dependency of the attenuation (which is the basis for the determination of the attenuation) changes the spectral characteristics of the received signal. Fortunately, the experimental variance of the water path measurements can be readily determined from the tomographic data by correlating the signals at the edges of the fans with each other. Note that the expected value of $\Delta t'$ for these fans is zero. The experimental variance of the tissue measurements can be determined from the data only if a large number of pulses of ultrasound are recorded for each sector and viewing angle. However, in light of the effect of attenuation on the spectral characteristics of the tissue path signals, one would expect equation 3.69, and the experimental variance of the water path measurements, to be a lower bound on the variance of the tissue path time delay estimation. The results of nontomographic (i.e., fixed position) measurements of water and a tissue mimicking phantom material are presented in Chapter 5.

The attenuation estimation can also be examined. If the received signals can be modeled as a clean signal plus zero-mean, independent noise, then the expected value of the Fourier transform of the received signal is equal to the Fourier transform of the expected signal (i.e., the clean signal). The variance of the Fourier transform is more difficult to analyze without a

specific noise distribution, since the bandlimited discrete Fourier processing that is performed produces aliasing of high frequency noise. The attenuation is determined as the log of the ratio of the Fourier transforms of water and tissue path signals, so that the expected value of the attenuation will be the true attenuation if the noise distribution has a sharp peak at zero (i.e., zero mean and a small variance). The experimental variance of the attenuation of the water path signals can be readily determined from the tomographic data, since all of the signals at the edges of each fan can be used. Note that as with the time delay estimation, the expected value of $\Delta A(\omega)$ for the water path measurements is zero. The variance of the tissue path attenuation should be the same as the variance of the water path attenuation, since the logarithm converts an exponential decrease into a biasing shift, as long as the noise decreases with the signal amplitude. If the noise does not follow the decrease in signal due to the tissue, then the variance of the tissue attenuation will be greater than the water path attenuation variance. Note that as with the time delay estimation, determining the experimental variance of the tissue measurements requires a large number of recorded pulses of ultrasound. Thus the water path attenuation can be used as a lower bound for the tissue attenuation. The results of nontomographic (i.e., fixed position) measurements of water and a tissue mimicking phantom material are presented in Chapter 5.

3.6.3 Impact On Reconstruction

The effect of noise on convolution backprojection can be readily analyzed if the noise can be assumed to be independent (from measurement to measurement). If f' is the reconstructed estimation of f, then the expected value of f' is f if the expected value of the noise is zero (i.e., the noise has zero mean). The variance of f'(x,y) can be determined from

$$\mathrm{var}(f'(x,y)) = \int_{o}^{2\pi} \frac{1}{L^4} (\mathrm{var}(n) D^2 \cos^2(\chi)) \circledast (h^2(\chi)) d\theta \qquad (3.71)$$

where the above variables have the same interpretaion as in equation 3.44 (Kak, 1979). As noted in the previous section, the experimental variance of the noise can be estimated from the variance of data at the edges of each fan (i.e., the water-path only signals). Thus $\mathrm{var}(n) = \mathrm{var}(g_w)$.

The effect of noise on algebraic reconstruction can be readily analyzed. Let n_i be a random variable representing the noise associated with measurement g_i, such that $g = Af + n$. Let f' be the least squares estimate of f given g and A, as produced by the least squares pseudoinverse matrix $A^{\#}$ (i.e., $f' = A^{\#}g$). If the noise is independent and has zero mean, then the expected value of f' is f, and the variance of the noise can be estimated from

$$\mathrm{var}(n) = \frac{1}{KL} ((g-Af')^T (g-Af')) \qquad (3.72)$$

and the image variance can be estimated from

$$\mathrm{var}(f'_j) = \mathrm{var}(n)A^{\#}_{jj} \qquad (3.73)$$

(Katz, 1978). If the statistical properties of the noise can be determined a priori, this information can be used to weight the pseudoinverse matrix to provide a better fit. Aside from the water path variance at the edges of each fan, this a priori information is not available in general for ultrasound computed tomography.

If an iterative method is used, such as the projection iterative method shown in equation 3.57, then the presence of noise may prevent the solution from being unique. The cyclic convergence of the projection iterative technique does not insure a minimum variance solution. Moreover, the variance estimate of f'_j still requires $(A^TA)^{-1}_{jj}$ as shown in equation 3.73. Thus iterative algebraic reconstruction may be easier to compute, but the method forfeits a direct estimate of the variance of the reconstructed image.

The choice of binary, linear, or interpolated modeling for the A matrix results in decreasing modeling error at the expense of increasing computation. If the underlying continuous, bandlimited function f(x,y) is discretely sampled at a sufficiently high rate (specifically, greater than twice the highest frequency present in the function), then f(x,y) can be recovered from f_{mn} by convolving the samples with an appropriate low pass filter. (The details of the Nyquist sampling theorem are not critical to this discussion. A thorough presentation of this topic can be found in any text on digital signal processing.) This

is a computationally expensive task, however, since recovering each point (x,y) involves information from all of the M*N sample points. Both the binary and the linear models assume that f(x,y) changes sufficiently slowly that it can be modeled as a constant for each pixel. Computationally this is attractive, since the value of f(x,y) can be estimated from the sampled point f_{mn} nearest to (x,y). The mean squared error between the true value of the function f(x,y) and the estimated value f'(x,y) is a measure of the error associated with using f' for calculations rather than f. For a given function f(x,y), this error will in general decrease as the sampling rate increases, since the pixels will be smaller and will better fit the continuous function. Note however that increasing the sampling rate in both the x and y directions results in a squared increase in the computation time required to manipulate all of the points. The interpolated model estimates f(x,y) in terms of the nearest neighbor f_{mn}, as well as the eight neighbors of (m,n). As noted earlier in the analysis of the interpolated model, the contribution of f_{mn} and its neighbors to any given measurement should involve roughly four times more computation than for the linear model (since some of the neighbors of (m,n) would already be involved in the beam computation for the linear model). However, the mean squared error between the true value f(x,y) and the interpolated estimated value f"(x,y) will tend to be less than the mean squared error for the simple nearest neighbor estimate used by the binary and linear models, since the interpolated model will tend to follow the function from pixel to pixel, while the nearest neighbor model remains constant until the pixel-pixel boundary, where it changes abruptly to the value of

the next pixel. One measure of the benefit vs cost of the interpolated model over the linear model is the degree to which the linear model sampling rate needs to be increased to obtain the same level of mean squared error obtained by the interpolated model. Since the interpolated model requires four times more computation, if the linear model requires more than a factor of two increase in the sampling rates for both x and y to obtain a comparable mean square error, then it would be cost effective to choose the interpolated model over the linear model. Unfortunately, mean squared error is not a linear function, so it is not possible to study the set of continuous bandlimited functions as a superpostion of basis functions. It is also not tractable to evaluate a priori the mean squared error for all possible functions. For these reasons, a computer simulation was performed to examine the mean squared errors resulting from linear and interpolated modeling of two-dimensional sine wave fields of various frequencies. Since superposition can not be used, the calculated mean squared errors can not be used directly for studying arbitrary functions. However, the trends in mean squared error for the various frequencies are indicative of the expected behavior for regions of arbitrary functions. The results of this analysis are presented in Chapter 5.

It should be noted that previous studies have shown that the variance exhibited by convolution backprojection (parallel beam geometry) is close to the theoretical algorithm independent lower bound on variance (Kak, 1979). Thus the only apparent advantage of algebraic reconstruction over convolution reconstruction is the

ability to estimate the variance of the noise (and thus the variance of the reconstruction) from all of the data present, whereas convolution backprojection estimates the noise variance only from the water path signals at the edges of each fan.

3.6.4 Impact On Interpretation

The interpretation of the reconstruction further modifies the variance of the estimation. For ultrasound speed as deterimined by equation 3.60, the variance of the interpreted speed is

$$\mathrm{var}(c) = c^4 \left(\frac{1}{c_w^4} \mathrm{var}(c_w) + \mathrm{var}(f) \right) \tag{3.74}$$

where $\mathrm{var}(c_w)$, the variance of the speed of water measurement used for a reference, is independent of the variance of f. If this value is sufficiently small, or otherwise not available, as may be the case for values taken from the literature, then $c^4\mathrm{var}(f)$ is a useful lower bound.

For attenuation, as determined by equation 3.62, the variance of the interpreted attenuation is the sum of the reconstructed variance and the variance of the reference water attenuation:

$$\mathrm{var}(A) = \mathrm{var}(f) + \mathrm{var}(A_w) \tag{3.75}$$

assuming the variance of A_w is independent of the variance of f. If $\mathrm{var}(A_w)$ is not available (as may be the case for values taken from the literature), then var(f) is a useful lower bound on the actual variance.

3.6.5 Impact On Temperature Estimation

All of the previously examined variances combine to influence the variance of the estimated temperature change. For linear (or linearized quadratic) models, such as equation 3.63, the variance of the temperature change is

$$\mathrm{var}(\Delta T) = \frac{\mathrm{var}(c_1)}{(dc/dT)^2} + \frac{\mathrm{var}(c_0)}{(dc/dT)^2} + \mathrm{var}(dc/dT)\frac{\Delta T^2}{(dc/dT)^2} \qquad (3.76)$$

assuming that the variations in c_1, c_0 and dc/dT are all independent. This equation applies equally for linear models of attenuation. The variances of the thermal coefficients, as available from the literature, are presented in Chapter 5.

If equation 3.66 is applicable for estimating temperature change from the ratio of speeds, then

$$\mathrm{var}(\Delta T) = T_0^2\left(4\,\frac{c_1^2}{c_0^4}\,\mathrm{var}(c_1) + 4\,\frac{c_1^4}{c_0^6}\,\mathrm{var}(c_0)\right) \qquad (3.77)$$

if T_0 is known, and the variations in c_1 and c_0 are independent. If T_0 is estimated, then a third term, $(\Delta T/T_0)^2\mathrm{var}(T_0)$, must be added.

If equation 3.68 is applicable for estimating temperature change from the shift of the attenuation spectrum, then

$$\mathrm{var}(\Delta T) = T_0^2\,\frac{R^2}{E^2}\,\frac{\mathrm{var}(\Delta\omega)}{\Delta\omega^2} \qquad (3.78)$$

where the variance in the frequency shift can be determined by the

same variance analysis as was applicable for the time delay estimation, as shown in equations 3.69 and 3.70. For the frequency shift case, however, the "time domain" signal $s_w(t)$ is $A(\omega)$, while the "frequency domain" spectrum $S_w(\omega)$ is $a(t)$, the Fourier transform of the attenuation spectrum (i.e., the Fourier tranform of the log of the Fourier transform of the received signal). Again, if T_0 is not known and must be estimated, an additional term of $(\Delta T/T_0)^2 \mathrm{var}(T_0)$ must be added.

CHAPTER 4

EXPERIMENTAL FACILITY

4.1 PHYSICAL DESCRIPTION

The ultrasound computed tomography apparatus involves a 62.1 * 62.1 * 41.0 (depth) cm (inside dimensions) Plexiglas tank, holding approximately 148 liters of water. In the bottom center of the tank, a triaxial shaft transmits mechanical power from the three drive motors below to a 25.5 * 19.0 * 18.5 cm water-proof gearbox inside the tank. A coaxial shaft exits the top of the gearbox to provide a shaft for mounting the transmitting transducer, and a boom arm for mounting the receiving transducer. The water temperature is controlled by a Haake E-2 heater-circulator in the tank. See Figure 4.1.

The distance from the central axis to the transmitting transducer is typically 10.4 cm. The distance from the trasmitter to the receiver is typically 20.4 cm. Thus each sector is 20.4 cm "deep," and roughly centered at the center of rotation. See Figure 4.2.

4.2 MECHANICAL DESCRIPTION

Details of the mechanics and control electronics for this system can be found in Lerner (1979) and Berkwits (1980). However, the salient features are repeated here. The tank provides three degrees of rotational freedom: i) the gearbox and transducers rotate as a unit about the central axis of the system; ii) the transmitter and receiver boom arm rotate in alignment above the gearbox to sweep out sector shaped regions; iii) the receiver boom can swing independent of the transmitter, in order to measure the ultrasound beam profile. All three motions are produced by d.c. motors, driven by integrated pulse proportional control from an interface driven by a SYM-1 microcomputer. Angle encoders with 0.1^{o} resolution are attached to each drive shaft entering the grearbox, to provide the SYM-1 with angle position information. The SYM-1 communicates with a Perkin-Elmer 7/32 minicomputer via a 16 bit parallel I/O cable. The SYM-1 acts as a slave to the 7/32, accepting motion commands and providing angle information on request. The SYM-1 also asynchronously signals the 7/32 during each data acquisition sector, to indicate that the transmitter and receiver are in proper orientation for data collection. For this thesis, only the first two degrees of freedom (base and fan) are used. Moreover, the transmitter is mechanically coupled to the receiver boom arm, to insure constant alignment. The base angle encoder is in direct mechanical connection with the grearbox, so that θ measurements have a resolution of 0.1^{o}. However, the fan position encoder is coupled to the transmitter and receiver through the 2:3 ratio gears in the

gearbox. Thus the measurements of sector angle χ have a resolution of 0.15^{o}. The base is capable of rotating 180^{o}. For this work the fan only swings out 40.8^{o} sectors (collecting data from the central 33.6^{o} section for reasons explained in the following chapter), although larger sectors are possible.

4.3 ELECTRICAL DESCRIPTION

Pulses of ultrasound (at a 4 kHz repetition rate) are produced by a Panametrics 5050 PR pulser-receiver, connected to a Panametrics 1 inch diameter, 5 MHz center frequency, focussed (f=5 inches) transducer. The ultrasound propagates through the water in the tank to a 1 mm diameter PZT disk hydrophone probe (mounted on the end of a 4.9 cm section of coaxial hardline). The center frequency of the probe is 20 MHz.

The received signal from the probe is returned to the amplifier circuits of the Panametrics 5050 PR, before being passed through a variable attenuator (0, 1, 2, 3, and 6 dB) to a 50 MHz, eight bit analog to digitial data acquisition system. This system consists of two TRW 1007J 25 MHz A/D converters, operating interleaved, connected to 8 Kbytes of high speed memory. Thus, 160 microseconds of raw rf signal can be digitized. In practice, however, 2.40 microseconds (120 data points) are sufficient to capture the 5 MHz pulse. The data from the acquisition system are then read into a Perkin-Elmer 7/32 minicomputer for storage and analysis.

4.4 SETUP AND PROCEDURES

Due to the size of the tank (148 liters), the use of highly degassed saline is prohibitive. Instead, the tank is filled with tap water, and heated to 45°C the night before an experiment. Outgassed bubbles are brushed off of the underwater surfaces. The water is then allowed to cool overnight, to reach a typical initial temperature of 23°C. The water is then warmed to 25°C, and the first set of data are collected.

The processes of warming and data collection is repeated for 30, 35, and 40°C. At 40°C, few or no bubbles are present, indicating that the heating/degassing process removes most of the air to prevent gross ultrasound diffraction due to bubbles comparable in size to a wavelength of ultrasound.

To minimize physiological changes to the tissue due to exposure to tap water, an acoustically transparent normal saline cell is used. The cell consists of a saline filled latex condom. A 5.08 cm diameter lucite disk at the bottom (sealed end) and a 5.08 cm diameter lucite tube near the top (open end) produce a 12 cm long (average length) cylindrical region for the tissue. The disk and tube have a notched edge to allow rubber bands outside of the cell to hold the lucite pieces in place.

The tissue under examination is cut approximately into a 2.54 cm disk, and held in place against a 2.54 cm diameter lucite disk by means of a thin latex band. A rod attached to the 2.54 cm disk holds the tissue sample at the proper depth in the saline cell. See Figure 4.3.

A tissue mimicking phantom material, supplied by Dr. E. L. Madsen of the University of Wisconsin at Madison, was also studied, but in a nontomographic modality. A 2.54 cm thick sample of material, with Saran wrap front and back layers, was inserted into the beam, with the transducers at a stationary position. Ultrasound pulses were recorded after passing through the sample. and compared to pulses passing through a direct water path when the sample was removed. Each pulse was digitized into 120 samples by the 50.05 MHz analog to digital converter. The amplitude of the water path pulse was adjusted (by varying the pulser controls and the gain of the receiver) to nearly fill (90%) the dynamic range of the eight bit converter at the temporal peak of the pulse. Four received water path signals, and four sample path signals, were temporally averaged to form one water-sample pulse pair for later analysis. This temporal averaging was also done for 64 water path signals and 64 sample path signals. The entire process (both 4 and 64 averages) was repeated on separate occasions, at 20.5^{o}C and 22.5^{o}C, respectively. Time-of-flight and frequency dependent attenuation were determined for each pulse pair. This experiment provided an estimate of system performance and noise levels. independent of the tomographic reconstruction processing. Measurements were repeated for a 5.08 cm sample of the same material, as well as a 2.54 cm sample of castor oil. The results (which were compared to measurements made by several other laboratories by Madsen and Frank, 1984) are presented in Chapter 5.

4.5 DATA ACQUISITION AND ANALYSIS

Each 33.6^{o} fan is divided into 57 data collection positions. Data collection consists of sampling 120 points of the raw received signal, to capture the 5 MHz center frequency pulse. An adaptive timing program on the 7/32 attempts to keep the leading edge of the pulse positioned approximately 1/3 of the way into the 120 byte buffer, by changing the time when data recording begins. The value of the starting time is stored with the data, so that no information is lost. This insures that all of the pulse is captured. After each fan, the base rotates to the next viewing angle. Fifty views are collected over 180^{o}. Fans are collected alternately clockwise and counterclockwise, for every other view, to minimize excess fan motion. One complete scan requires approximately 11 minutes. The data are stored on magnetic tape for later analysis.

The first step in the data analysis is to extract the differences in time-of-flight between the measurements at the edges of the fans (assumed to pass through water only, and thus used as reference waveforms), and those in the middle of the fan. The time-of-flight difference is determined by correlating the reference waveform with the subject waveform. The correlation maximum, and its two neighboring points, are fit to a parabola to estimate the true location of the peak. This location, along with the starting time of the waveforms, determines the time-of-flight difference for the subject waveform.

Eight frequency dependent attenuation coefficient estimates, from 3.52 to 6.26 MHz, are also made. The log of the magnitude of the Fourier transform of the reference waveform is subtracted from the log spectrum of the subject waveform, and scaled by -20 to give dB of attenuation. The above range of frequencies is dictated by the energy content of the reference pulse.

Following data extraction, intermediate filtering and backlash correction (to account for the fact that alternate scans are collected clockwise then counterclockwise) are applied. The data are also balanced, so that the edges are always zero or positive. This handles the case of the edge of the saline cell coinciding with the edge of the sector.

The nine files (one time-of-flight, eight attenuation) are then reconstructed by convolution-backprojection, as described by Kak (1979). The resulting time image is then converted to a speed image, as described by equation 3.60. The eight attenuation images are dimensionally correct as is. The constant attenuation difference for the water (equation 3.62) can be subtracted at leisure.

CHAPTER 5

RESULTS

5.1 ANALYSIS OF LITERATURE DATA

Appendices A and B contain a compilation of temperature dependent ultrasound property measurements of biological media available from scientific literature. Appendix A reports values of ultrasound speed as a function of temperature; Appendix B reports values of ultrasound attenuation coefficient as a function of temperature. Following each set of related measurements, the results of least squares fits to the data are presented. If two or more measurements were reported, a linear least squares fit is presented. If three or more measurements were reported, a quadratic least squares fit is presented as well. Let yi represent the i'th measurement, and let x_i represent the corresponding temperature. Define

$$Y_k = \sum_i y_i x_i^k \quad \text{and} \quad X_{jk} = \sum_i x_i^{j+k} \tag{5.1}$$

for $0 \leq j,k \leq J=K$. If the data are to be fit to a J'th order polynomial:

$$y(x) = B_0 + B_1 x + B_2 x^2 + \ldots + B_J x^J \tag{5.2}$$

then the least squares fit is given by

$$B = X^{-1}Y \quad \text{or} \quad B_j = \sum_k X^{-1}{}_{kj} Y_k \tag{5.3}$$

Unless specified otherwise, all statistical computations are drawn from Bevington (1969).

For each fit, several auxilliary parameters are included. The standard deviations of the fit coefficients are included in parentheses beneath the coefficient. These are found from

$$\sigma^2{}_j = s^2 X^{-1}{}_{jj} \quad \text{and} \quad \text{s.d.} = \sigma_j \tag{5.4}$$

where the variance of the data with respect to the fit, s^2, is defined by

$$s^2 = \frac{1}{N-J-1} \sum_i (y(x_i) - y_i)^2 \tag{5.5}$$

This variance (also known as the unexplained variance) is presented in the form var=... in the appendices, on the same line as the standard deviations.

The correlation coefficient (the square root of the ratio of the explained variance to the total variance) is presented in the form r=..., and is computed from

$$r = \sqrt{\frac{\sum (y(x_i) - \bar{y})^2}{\sum (y_i - \bar{y})^2}} \tag{5.6}$$

The probability that random data could have produced a value of r as large as the value computed from the available data is presented in the form P_r=..., where the value has been computed by

a program given by Bevington (1969). This probability, which is strictly valid only for linear least squares fits, is a measure of confidence that the data are correlated to a staight line (specifically, that the data are not random, or correlated to some function very much different from a straight line). Thus small values of P_r indicate high confidence. For subsequent processing, 0.05 (95% confidence) is used as a threshold for accepting linear fits as applicable approximations for modeling the data.

Where four or more measurements have been reported, both linear and quadratic fits can be compared to determine if the quadratic fit is a statistically significant improvement over the linear fit. Although both fits are present for data sets of only three measurements, at least four measurements are required to evaluate the relative merit of the fits. Let F be defined as

$$F = \frac{(N-J)(s_1)^2 - (N-J-1)(s_2)^2}{(s_2)^2} \qquad (5.7)$$

where $(s_1)^2$ is the unexplained variance of the linear fit, and $(s_2)^2$ is the unexplained variance of the quadratic fit. Then F has a two-dimensional chi-squared distribution, with 1 and N-J-1 degrees of freedom, respectively. Large values of F indicate that the unexplained variance of the quadratic fit is much smaller than the unexplained variance of the linear fit, and thus that the quadratic fit better models the data than does the linear fit. The probability that random data could have accounted for a value of F as large as the value computed from the available data is presented in the form P_F=..., where the value has been taken from

a table in Bevington (1969). Since this is a tabular estimate, the actual value of the probability is less than or equal to the reported value. Thus small values of P_F indicate a high confidence that the quadratic fit is justified over the linear fit. As with the probability of correlation, the value of 0.05 (95% confidence) is used as a threshold for accepting quadratic fits as applicable approximations for modeling the data.

5.1.1 Analysis Of Ultrasound Speed Data

The statistical tools of section 5.1 were applied to the speed data in Appendix A to find linear and quadratic least squares fits to the ultrasound speed as a function of temperature. The results are included in that appendix. As a summary of the significance of these calculations, Table 5.1 is provided, indicating the total number of sets of data available for study (grouped according to tissue), the number of sets for which linear least squares fits could be examined (i.e., sets with three or more measurements), the number of sets for which the probability of correlation was statistically significant at the 0.05 (95% confidence) level, the number of sets for which quadratic least squares fits could be compared to linear fits (i.e., sets with four or more measurements), and the number of sets for which the quadratic fit was a statistically significant improvement over the linear fit at the 0.05 (95% confidence) level.

Of those sets of measurements that provided a sufficient amount of data to examine the linear least squares fit, the majority (65 out of 72) showed a high probability of correlation (95% or better) with a straight line, suggesting that a linear least squares fit is a good model for ultrasound speed as a function of temperature. Of those sets of measurements that provided a sufficient amount of data to examine a quadratic least squares fit as well, less than half (24 out of 57) showed a high probability (95% or better) that the quadratic fit was justified over the linear fit. Notable cases include: blood, where only 1 out of 5 quadratic fits were justifed; liver, where 4 out of 5 quadratic fits were justified; and brain, where 10 out of 25 quadratic fits were justified. The weight of these numbers suggest, in general, that blood would be best fit by a linear temperature model, that liver would be best fit by a quadratic temperature model, and that brain is somewhere in between. For the other tissues, only small numbers of sets of data are available, and conclusions drawn from them would be suspect.

Graphs of dc/dT *vs* c at $37^{o}C$, based on the linear and quadratic fits for which the confidence exceeded 95%, are presented in Figures 5.1, 5.2, and 5.3. Figure 5.1 describes the speed thermal coefficients of various fluids (aqueous and vitreous humor, blood, milk, and water); 5.2 describes the speed thermal coefficients of various nonfatty tissues (breast muscle and parenchyma, cornea, lens, liver, kidney, central nervous system tissue, psoas muscle, sclera, skeletal muscle, and spleen); 5.3 describes the speed thermal coefficients of various fatty tissues

(breast fat and parenchyma, peritoneal fat, and stomach (omentum) fat).

Two observations are immediately apparent from the graphs. First, the central nervous tissue values are distinct in speed values from the other nonfatty tissues, and share the same range of values (both in speed and in thermal coefficients) as the fluids. Second, the fatty tissues are distinct from the nonfatty tissues and fluids, both in terms of lower speeds, and lower (negative) speed thermal coefficients.

5.1.2 Analysis Of Squared Speed Ratio Thermal Model

To test the hypothesis that the speed of ultrasound in biological media is proportional to the square root of the absolute temperature, and thus that temperature change could be estimated with equation 3.66, the following statistical model was used:

$$\left(\frac{c_1}{c_0}\right)^2 - 1 = a + b\,\frac{T_1 - T_0}{T_0} \qquad (5.8)$$

If speed is indeed proportional to the square root of the absolute temperature, then the expected value of a is 0, and the expected value of b is 1. Speed <u>vs</u> temperature data from Appendix A were used to test this hypothesis by two approaches. For each set of N measurements (only if $N \geq 4$), N-1 relative speed changes and relative temperature changes were computed. Approach 1 computed the changes relative to the first speed and temperature reported for that set. Approach 2 computed the i'th changes relative to

the i+1'th speed and temperature reported for that set. Thus Approach 1 considered changes with respect to a (relatively) fixed starting point, whereas Approach 2 focused only on incremental changes. For both approaches, the coefficients a and b were determined by least squares fit. The standard deviations of the coefficients, the unexplained variance, linear correlation coefficient, and the probability of correlation were also determined.

To test the hypothesis that a=0, a statistical t-test was used on the parameter

$$t = \frac{a\sqrt{N-2}}{s_{yx}\sqrt{N+1+\bar{x}^2/s_x^2}} \qquad (5.9)$$

where s_{yx} and s_x are defined by

$$s_{yx} = \sqrt{\frac{(N-2)s^2}{N}} \quad \text{and} \quad s_x = \sqrt{\frac{\Sigma x^2 - N\bar{x}^2}{N}} \qquad (5.10)$$

and $\bar{x}$ is the mean value of the temperatures. For each least squares fit, the hypothesis a=0 was rejected if t exceeded the 95% confidence value for the Student's t distribution given by a table in Spiegel (1961).

To test the hypothesis that b=1, a statistical t-test was used on the parameter

$$t = \frac{(b-1)\sqrt{N-2}}{s_{yx}/s_x} \qquad (5.11)$$

For each least squares fit, the hypothesis a=0 was rejected if t

exceeded the 95% confidence value for the Student's t distribution given by a table in Spiegel (1961).

Tables 5.2 and 5.3 show the results of Approaches 1 and 2, respectively. Each table indicates the number of data sets available for study (grouped according to tissue type) with four or more measurements, the number of sets for which the probability of correlation (using equation 5.8 as a model) was at least 95%, the number of sets for which the hypothesis a=0 was accepted at the 95% level of confidence, the number of sets for which a=0 might be marginally accepted (i.e., rejected at the 95% level but accepted at the 99.5% level), the number of sets for which the hypothesis b=1 was accepted at the 95% level of confidence, and the number of sets for which b=1 might be marginally accepted (i.e., rejected at the 95% level but accepted at the 99.5% level).

Several observations can be made concerning Table 5.2 and Approach 1. Of the 57 available data sets, most (47) provided a good (95% confidence) linear least squares fit to equation 5.8, and more than half (37) accepted the hypothesis a=0. However, much less than half (15) accepted the hypothesis b=1. In particular, for those tissue groups with several available data sets (blood, liver, and nervous tissue), the acceptance of b=1 was not strong (2 out of 5, 1 out of 5, and 11 out of 26, respectively). These numbers suggest that equation 5.8, and thus equation 3.66, and the general concept that ultrasound speed may be proportional to the square root of absolute temperature, is probably a poor model for estimating temperature in biological tissue. The strong acceptance of a=0 does not contradict this

conclusion, but merely supports the notion that zero temperature change corresponds to zero speed change. The rejection of b=1 by water is consistent with the earlier model of water as having a quadratic (rather than square root) temperature dependence, and that the change in specific heat with temperature (equation 3.65) is not negligible in water.

The most apparent conclusion to be drawn from Table 5.3 points to the weakness in Approach 2. Of the 57 data sets available, only 12 provided an adequate least squares fit to the model. This is not an indictment of the model (since Approach 1 gave a fairly strong correlation response: 47 out of 57). Rather, the problem lies in the fact that most of the relative temperature and speed changes were huddled together. Approach 2 computed the i'th change with respect to the i'th and i+1'th measurements. Since the temperature measurements tended to be uniformly spaced (e.g., 10, 20, 30, ...), the relative temperature change tended to be constant (e.g., $10^{o}C$), varying only in the division by the absolute temperature. As a result, the least squares fitting process was called upon to find a line through a series of y values, all with nearly the same x value. Such a process is highly sensitive to noise, and thus it is not surprising that the overall performance of Approach 2 was poor.

5.1.3 Analysis Of Ultrasound Attenuation Coefficient Data

The statistical tools of section 5.1 were applied to the attenuation coefficient data in Appendix B to find linear and quadratic least squares fits to the ultrasound attenuation

coefficient as a function of temperature, and to the natural log of the attenuation coefficient as a function of temperature. The results are included in that appendix. As a summary of the significance of these calculations, Table 5.4 is provided, indicating the total number of sets of data available for study (grouped according to tissue), the number of sets for which linear least squares fits could be examined (i.e., sets with three or more measurements), the number of sets for which the probability of correlation was statistically significant at the 0.05 (95% confidence) level, the number of sets for which quadratic least squares fits could be compared to linear fits (i.e., sets with four or more measurements), and the number of sets for which the quadratic fit was a statistically significant improvement over the linear fit at the 0.05 (95% confidence) level. The numbers for the natural log fits to the attenuation measurements are included in parentheses in the table.

Of those sets of measurements that provided a sufficient amount of data to examine the linear least squares fit, less than half (36 out of 90, and 42 out of 90 for the log fits) showed a high probability of correlation (95% or better) with a straight line, suggesting that a linear least squares fit is not necessarily a good model, either for the attenuation coefficient as a function of temperature, or for the log of the attenuation coefficient as a function of temperature. Notable cases include: blood, where 5 out of 6 linear fits were good; peritoneal fat and kidney, where 0 out of 7 and 0 out of 5 fits were good, respectively; and spleen, where 5 out of 10 fits were good, but 8

out of 10 log fits were good. These numbers suggest that a linear least squares fit to the attenuation coefficient, or the log of the attenuation coefficient, as a function of temperature, would be a good choice for blood and a poor choice for peritoneal fat and kidney. In choosing between fitting the attenuation coefficient or the log of the attenuation coefficient, only liver and spleen show a bias toward the log fit. Thus the log-linear fit, while perhaps applicable to some special cases, does not in general seem appropriate.

Of those sets of measurements that provided a sufficient amount of data to compare a quadratic least squares fit to the linear fit, less than a third (19 out of 66) showed a high probability (95% or better) that the quadratic fit was justified over the linear fit. In choosing between fitting the attenuation coefficient or the log of the attenuation coefficient, only blood showed a bias toward the log fits, and only brain and spinal cord showed a bias away from the log fit. The lack of strong evidence supporting the linear or the quadratic fits suggests that the data available either follow a function more sophisticated than a straight line or a parabola, or that the data available have a fairly high noise content, considering the amount of data available. The lack of strong evidence supporting log fits vs nonlog fits also suggests sophisticated functions or high noise. From a purely economical standpoint, the additional cost of computing the log fits seems unjustified in light of the lack of supporting evidence.

Graphs of dA/dT vs A at 37°C, based on the linear and quadratic fits for which the confidence exceeded 95%, are presented in Figures 5.4, 5.5, and 5.6. Figure 5.4 describes the attenuation coefficient thermal coefficients (ACTC's) of blood; 5.5 describes the ACTC's of various nonfatty tissues (heart, liver, central nervous system tissue, and spleen); 5.6 describes the ACTC's of various fatty tissues (peritoneal fat and unspecified fat).

Several observations can be made concerning these graphs. The majority of the ACTC's are negative, for all three groups (blood, nonfatty, and fatty tissues), suggesting that in general the attenuation coefficient decreases with increasing temperature for most biological media, for frequencies between 0.1 and 10 MHz. In comparison to the relaxation models in Chapter 3 (either equation 3.20 or equation 3.25), this would suggest $\omega\tau<1$. The attenuation coefficients of blood are distinctly smaller than those of the nonfatty and fatty tissues. This is an expected observation, arising in the difference in densities between the media. The ACTC's of blood, however, are comparable to those of the nonfatty and fatty tissues, at comparable attenuation coefficient levels. The distinction between fatty and nonfatty tissues is less well defined. At lower attenuation coefficient levels, the ACTC's of the two groups are comparable. At higher attenuation coefficient levels, the ACTC's of the nonfatty tissues appear greater (more negative) than those of the fatty tissues. However, due to the small number of data points available, this is not a strongly supported conclusion. Overall, the graphs show an

increasing (i.e., increasingly negative) trend in the ACTC's with increasing attenuation coefficient levels. Although not shown in the graphs, there is a general trend of increasing attenuation coefficient with increasing frequency. This trend is clearly visible in the numerical values in Appendix B.

5.1.4 Analysis Of Frequency Shift Thermal Model

Data from Appendix B were used to test the hypothesis that temperature change could be estimated from a change in relaxation time, as detected by a shift in frequency, for attenuation due to relaxation absorption. As argued in Chapter 3, an increase in temperature should result in a decrease in relaxation time. Due to the symmetric relationship between time and frequency in the relaxation mathematics, a decrease in relaxation time should be equivalent to a shift of the absorption spectrum, $\alpha\lambda(f)$, to higher frequencies. This shift should be linear in log-frequency, so that $\alpha\lambda(\log(f))$ at one temperature should match $\alpha\lambda(\log(f)+\log(\Delta f))$ at another. The log-frequency shift, $\log(\Delta f)$, should then be proportional to the temperature change, according to equation 3.68, for changes that are small compared to the absolute starting temperature. Thus the model

$$\log(\Delta f) = a + b\Delta T \qquad (5.12)$$

can be used to test if the log-frequency shift varies with the temperature. If the log-frequency shift is indeed proportional to the temperature change, then the expected value of a is 0, and the expected value of b is greater than 0, and should vary from tissue

to tissue, since it incorporates tissue specific parameters.

For each set of attenuation coefficient values from Appendix B where at least three temperature measurements were available for each of at least three frequencies, the data were preprocessed as follows. First, the attenuation coefficient was divided by the frequency. The objective of this computation was to obtain a value proportional to the absorption per unit wavelength, $\alpha\lambda$, since $\lambda = c/f$. Since speed values were not available for these measurements, it was not possible to incorporate the temperature dependence of the speed in this analysis. This represents a potential source of error. The second step was to convert the frequency of each measurement to log-frequency. Then, for each of the N(N-1)/2 pairs of temperatures (assuming N temperatures reported for each frequency), the log-frequency shift $\log(\Delta f)$ was determined iteratively, by performing linear and quadratic least squares fits to the data set formed by $A(\log(f))/f$ for the first temperature, combined with $A(\log(f)+\log(\Delta f))/f$ for the second temperature. The value of $\log(\Delta f)$ was iteratively adjusted to minimize the variance of the fit. Double precision (64 bit) computations were used to insure at least four digits of accuracy in the value of $\log(\Delta f)$. For each of the N(N-1) fits (linear and quadratic combined), the values of $\log(\Delta f)$ and the temperature difference divided by the square of the absolute temperature (see equation 3.68), along with the appropriate r or F statistic, were produced.

Of the 22 independent data sets, an average of 9 log(f) - temperature change pairs were generated per set. Of these 206 pairs, 50 were rejected from further analysis on the basis of inadequate probability of correlation (at the 95% level of confidence), leaving 156 pairs. For those data sets that retained at least three pairs, a linear least squares fit to equation 5.12 was computed. A quadratic fit was computed as well, principally because it was easier to perform both linear and quadratic fits using the computer program employed, than to suppress the quadratic fit. There is no special physical significance to a quadratic fit in the context of this analysis. The results of these fits are presented in Table 5.5.

Several observations can be made concerning Table 5.5 and this analysis. Although the amount of data available for this analysis was not large (22 sets), nearly 76% of the data (156 out of 206 log-frequency - temperature change pairs) showed an acceptable level of confidence that the absorption spectrum at one temperature matched the shifted absorption spectrum at another temperature. However, of the 16 sets of data that had enough data points to test equation 5.12, only four sets showed an acceptable level of confidence that the log-frequency shift varied linearly with temperature change. Three possibilities are suggested by these observations: either the linear and quadratic fits used in the iterative process of determining the log-frequency shift were poor estimators of absorption spectrum similarity, or the log-frequency shift does not in general vary linearly with the temperature change, or there was too much noise in the available

data to allow this analysis. The lack of temperature dependent speed information for this data (discussed earlier) may have contributed to the noise in this case.

Of the four sets that did show a significant linear relationship between log-frequency and temperature change, only the bone and one of the liver data showed a reasonable possibility that $a=0$. For the blood (and the quadratic fit to the spleen), a was greater than twice its standard deviation different from 0. For the odd liver data set, b was less than 0, which is contrary to the physics of the model.

The major weakness of this model lies in separating the absorption spectra from the attenuation spectra, and aligning them at different temperatures. The process of sliding one spectrum against another in log-frequency space does not take into consideration losses due to reflection or scattering. Two conditions would make this analysis ideal. First, a large number of frequencies should be used to measure the attenuation spectrum at different temperatures. More frequencies imply better statistics and better noise immunity. This can be achieved readily by the use of broadband pulse measurements, such as those used by the tomographic apparatus described in this work. The second condition is to collect attenuation measurements in the neighborhood of the relaxation maximum ($\omega\tau=1$). By obtaining a uniquely identifiable reference point, i.e., the peak of the absorption spectrum, it is possible to normalize the spectra at different temperatures, and thus minimize the errors due to reflection and scattering. This second condition can be difficult

to realize, since the frequency of the absorption peak tends to be large. Using a continuum of relaxation processes as a model, Sehgal and Greenleaf (1982) estimated the frequency of the peak for kidney to be greater than 1.1 MHz, for liver to be greater than 7.7 MHz, and for blood to be greater than 16.7 MHz. Although practical for kidney, these measurements would be challenging for liver, since 7 MHz implies a loss of 5 to 10 dB/cm. To employ a broadband pulse covering from 3.5 to 14 MHz (with 7 MHz in the middle of the log-frequency space) would imply high frequency attenuation on the order of 10 to 20 dB/cm. For a 2.54 cm section of tissue (as used in the tomographic apparatus described in Chapter 4), this would require a system with a dynamic range of at least 25.4 to 50.8 dB, assuming no noise. The eight bit A/D converter used by the apparatus provides at best 42 dB of dynamic range, since each bit contributes 6 dB, but one bit is lost since the signal is bipolar. Further, although the converter samples at 50 MHz, the input bandwidth is less than 10 MHz (designed to prevent aliasing in the 25 MHz components of the converter), which would additionally complicate the high frequency measurements.

5.2 ANALYSIS OF TANK PARAMETERS

The errors introduced by the physical apparatus used to collect the data necessary for reconstructing speed and attenuation coefficient are unique to each facility. Only the errors and limitations associated with the apparatus available for this research will be discussed. These errors fall into two general catagories: mechanical and electrical.

5.2.1 Mechanical Errors

As described in Chapter 4, the data were collected at 57 points of a 33.6° fan. The 3:2 gear ratio in the fan beam mechanics implies that the 0.6° angle between data points within each fan corresponds to 0.4° angle change as measured by the angle encoder. This encoder has a 0.1° resolution, with a ±0.05° uniform error. The mechanical linkage introduces wobble and backlash errors as the receiver is swept across the fan. To minimize these errors, data were collected while the receiver was in motion (to avoid start/stop vibration and positional error), and the mechanical limits of travel of the fan were set four data points (i.e., 3.6°) wider than the 33.6° data collection width, on each side (for a total of 40.8°), to allow the receiver time to speed up before and slow down after data collection. A backlash analysis was performed by correlating the time-of-flight projections from pairs of successive fans (i.e., successive views). The object under investigation (a 25.4 mm diameter disc of excised rat liver) was assumed to offer an essentially nonvarying profile over the 3.6° difference in viewing angles corresponding to two successive views (of the 51 views collected over 180° of total viewing angle). Since the receiver sweeps out fans in alternating directions (left-to-right for one fan, then right-to-left for the next), the location of the correlation peak is an indication of the degree of backlash between sweeps. The variation in the location of the peak is an indication of the degree of wobble. This analysis showed a zero mean position error for the points in each fan, but the error was distributed over ± 1

point width (i.e., 0.6^{o} actual position, or 0.4^{o} encoder position). Note that this is eight times larger than the encoder resolution error (0.05^{o}), which has thus been considered negligible for this case. The random position error blurs together the data in each projection, resulting in a random, spatially varying, anisotropic distortion in the reconstructed image. The spatial extent of the blurring can be considered by examining the distance traveled by the receiver between data points. Since the distance from the receiver to the center of rotation of the fan was 204 mm, the receiver traveled 2.136 mm between data points within each fan. Thus the spatial extent of the blurring in the reconstructions should be on the order of (less than) 2 mm.

A separate analysis of information content obtained from the 57 points for each of 51 views showed that reconstruction onto a 32 by 32 point matrix would give an information ratio (number of measured values to number of reconstructed pixels) of 2.84 to 1 (i.e., this would represent an overconstrained system) with a pixel scale of 2.03 mm. The use of a higher density matrix (with a smaller spatial scale and thus a higher spatial resolution) was not justified in light of the above distortion scale. Note also that collecting more points per fan (up to four times more would be possible, limited by the 0.1^{o} resolution of the angle encoder) would also be unjustified, due to wobble error and subsequent spatial distortion.

5.2.2 Electrical Errors

Electrical errors arose both from electrical noise and the use of an eight bit, 50.05 MHz analog to digital converter. Experimentally, the values reported by the A/D were biased, with a mean of 132 (rather than 127.5, the middle of the 0 to 255 range of this device), and random noise was typically on the order of 1 step when the gain of the receiver was set to give near full scale signal levels (10 to 245) at the peak of the pulse. In the absence of noise, the quantization error of the A/D would be 0.5 (one half of a step), comparable to half of the experimental noise. For water path signals, the standard deviation of the 120 points of the sampled waveform was typically between 25.8 and 29.3, varying according to the settings of the pulser-receiver (which produced differing waveforms for different settings). Overestimating the standard deviation of the noise as 1, the ratio of signal energy to noise energy (estimated by the ratio of signal variance to noise variance) was on the order of 666:1 to 859:1 for water path signals, and significantly less for sample path signals, corresponding to the attenuation of the signal by the sample. The noise had a direct impact on attenuation estimation, and an indirect impact on time-of-flight estimation, as will be seen in the following section.

5.3 ANALYSIS OF PROPERTY ESTIMATION

The study of castor oil and a tissue mimicking phantom material as supplied by Dr. E. L. Madsen (see Chapter 4) provided an experimental basis for examining the errors introduced by i)

time-of-flight estimation by windowed correlation, and ii) frequency dependent attenuation by spectral subtraction (see Chapter 3).

Theoretically, equation 3.69 provides an estimate of the error introduced in the time-of-flight calculations. Using the variance of the signal and the variance of the noise as estimates of the energy in the signal and the energy in the noise, respectively, and the rms bandwidth as calculated by equation 3.70, the variance in the time-of-flight estimation was calculated as 14 to 21 $*10^{-6}$ μs^2 for water, 14 to 17 $*10^{-4}$ for castor oil, and 0.8 to 3.0 $*10^{-4}$ for the phantom material. The mean values of the time-of-flight difference for these measurements were 0.0 μs (since the water path was the reference), 0.3 to 0.4, and 0.77 to 0.80, respectively, varying with temperature. Experimental variances, obtained by comparing time-of-flight determinations between the 4 pulse average and 64 pulse average data sets (see Chapter 4), were on the order of 6 $*10^{-6}$ for castor oil, and between 10^{-4} to 10^{-7} for the phantom material. Since only a small number of determinations (two to four) were used to estimate these experimental variances, it is not surprising that the experimental variances are less than the theoretical variances.

The ratio of noise variance to signal variance (1.1 to 1.5 $*10^{-3}$ for water, 2 to 3 $*10^{-2}$ for castor oil, and 0.5 to 1.8 $*10^{-2}$ for the phantom material) implies a comparable error in spectral estimation, prior to the attenuation estimation by subtraction of the logs of the spectra. The mean values of the attenuation coefficient difference (at 1 MHz) corresponding to the above

measurements were 0.0 dB/mm (since the water path was the reference), 0.61 to 0.70, and 0.47 to 0.56, respectively, varying with temperature. Experimental variances, obtained by comparing the attenuation coefficient determinations of the 4 pulse average and 64 pulse average data sets (see Chapter 4), were of the order of 10^{-3} for castor oil, and between 10^{-3} and 10^{-5} for the phantom material.

5.4 EXPERIMENTAL RESULTS - RAT DATA

A cooperative study between the Bioacoustics Research Laboratory and the Food Science Department of the University of Illinois was undertaken to determine the relationship between acoustic properties and tissue constituents in normal and alcohol induced fatty liver in white laboratory rats. The animals were pair fed, so that for each pair of rats, one received an alcohol rich diet, while the other received an isocaloric normal diet. Between January 16 and February 14, 1984, nine pairs of rats, ranging in time on diet from 7 to 36 days, were sacrificed, and their livers were examined. Four separate ultrasound measurements were performed on each liver: a Scanning Laser Acoustic Microscope (SLAM) was used to measure speed and attenuation at 100 MHz, a radiation force balance was used to measure the attenuation coefficient at 1.4, 4.2, 7.0, and 9.8 MHz, a transient thermoelectric effect apparatus was used to measure the absorption coefficient at 1 MHz, and the ultrasound computed tomography apparatus described in this work was used to measure speed and attenuation coefficient over the range of 3.3 to 6.3 MHz. The

tissue was also subjected to biochemical assay to determine lipid (fat) content. This study was described by Haney et al. (1984).

Due to limited resources, the tomographic reconstructions could not be performed at the time of the data acquisition. Consequently, for each of the nine pairs of livers, the full digitized signals (120 samples per pulse, 57 sector angles by 51 views) were stored on magnetic tape. For each liver, data were collected at 25, 30, 35, and 40°C. As the temperature increased, both the time-of-flight and the attenuation decreased. This behavior is consistent with a positive speed thermal coefficient and a negative attenuation coefficient thermal coefficient, as are common in Appendices A and B.

Subsequent reconstructions using convolution backprojection onto a 32 by 32 point array were disappointing. The reconstructed speed images showed a reasonable value for the speed in water (1.5 $\pm$0.01 mm/μs), elevated values for saline (1.52 to 1.55 mm/μs), and an unreasonable variation in liver speed (1.54 to well over 1.6 mm/μs), with the distinction between saline and tissue difficult at best. The expected values at 25°C are 1.496, 1.497, and roughly 1.58 mm/μs (using Table 3.4 for the first two estimates, and Appendix A for the last), respectively. Figure 5.7 shows a typical speed image (rat T-1033), and the "best" speed image (rat T-1026) produced.

The reconstructed attenuation coefficient images were equally dissapointing. Each attenuation data set consisted of eight images at frequencies from 3.3 to 6.3 MHz. Figure 5.8 shows

typical (rat T-1033) and "best" (rat T-1026) images for the attenuation coefficient at 4.1 MHz. A conventional model for attenuation coefficient is $A=A_0f^b$, where f is in MHz, and $1\leq b\leq 2$. A least squares fit to this model, using the eight attenuation images, refused to produce acceptable fits for any of the livers. A comparable least squares fit, performed with the attenuation coefficient data at 4.2, 7.0, and 9.8 MHz from the radiation force balance, produced excellent fits for all 18 livers. Including the 1.4 MHz data also measured by the radiation force balance somewhat degraded the fits, but not to the extent seen in the tomographic reconstructions.

Two sources of difficulty are immediately apparent to explain the lack of acceptable results for this experiment. First, any wobble or backlash would have had a severe impact on the high contrast edges between the saline and the liver tissue. Although the spatial extent of this noise should have been limited, it would make data near the edges of the tissue fairly useless for subsequent analysis. The second difficulty is related to the question of the beam path. Although the beam width was assumed to be small (approximately 5λ, or 1.5 mm), the tissue thickness being imaged was only 3 to 4 mm. Even a minor alignment error could result in the ultrasound beam being split, and simultaneously traveling inside and outside of the tissue, following two paths of different speed and attenuation. Reflections at the edges of the acoustic cell and at the edges of the tissue may have been responsible for the elevated saline speed values. In general, the fundamental assumption that the ultrasound beam followed a

straight path through the sample, may not have been justified. This is a major weakness in ultrasound tomography in general.

5.5 ANALYSIS OF RECONSTRUCTION

5.5.1 Convolution Backprojection

For tomographic reconstruction, the impact of noise can be studied from equation 3.71. A simple model was chosen to describe a 25.4 mm diameter disc of liver tissue located at the center of rotation of the water filled tomography system. The following parameters were used: 1.58 mm/μs speed for liver; 1.49 mm/μs speed for water; 20°C. Data were simulated for 57 points over 33.6° of fan angle, and 51 views over 180° of view angle. Time-of-flight differences varied from 0.0 (through water only) to 0.971 μs (through the diameter of the disc), as a function of fan angle. This corresponded to a local inverse speed of 0.0 μs/mm in the water, and 0.03823 μs/mm in the tissue. (Inverse speed is the amount of time per unit distance the pulse is delayed, relative to the water-only path, by passing through a given region; see Chapter 3.) Figure 5.9 shows the inverse speed image model used for this analysis.

Reconstruction was performed by convolution backprojection onto a 32 by 32 point array, where the width of the array was set equal to the width of the fan at the center of rotation. For a transmitter to center distance of 104 mm, the array width was 62.8 mm. The noise-free reconstruction produced numerically reasonable inverse speeds: 0.000357 μs/mm for water (0.0 expected), and

0.03863 $\mu s/mm$ for tissue (0.03823 expected), with variances of $3.58 *10^{-6}$ and $8.50 *10^{-6}$ $\mu s^2/mm^2$, respectively. Since this was a noise-free reconstruction, the variances describe the nonuniformity in the reconstruction, produced by limited viewing angle artifacts and computational roundoff errors. Figure 5.10 shows the reconstructed inverse speed image.

Equation 3.71 was used to examine how noise in the data affects the reconstruction. The variance in the time-of-flight was chosen as 10^{-6} $\mu s^2/mm^2$ for the water, and 10^{-4} $\mu s^2/mm^2$ for the tissue. The computation reported a mean variance of $4.16 *10^{-4}$ $\mu s^2/mm^2$ for the water inverse speeds, and $9.51 *10^{-4}$ $\mu s^2/mm^2$ for the tissue inverse speeds. The variances in these estimations were $2.57 *10^{-8}$ and $6.40 *10^{-8}$, respectively. This "variance of variances" can be interpreted again as arising from limited view angle artifacts and computational limitations, and indicates the degree of variability in the "reconstruction variances" given above. Note that the mean variances are two orders of magnitude larger than the variances in the noise-free mean reconstruction. Thus, in this simulation, the error introduced by the convolution backprojection computation is small, at least compared to the error propagated through the convolution backprojection computation (originating in the projection data). Figure 5.11 shows the reconstructed variance image.

5.5.2 Algebraic Reconstruction

For algebraic reconstruction, the relative merits of linear *vs* interpolated modeling were examined by computer simulation. A two-dimensional wave field was defined by $f(x,y)=g(x)*h(y)$, where $g(x)=\sin(2\pi nx+\phi)$ and $h(y)=\sin(2\pi ny)$, for $0\leq x,y\leq 1$. This field was sampled by a 16x16 point array, for values of n from 1 to 7 cycles across the array. The case n=0 is uninteresting, since f is constant, and both linear and interpolated modeling provide error free results. For values of n greater than 7, the Nyquist sampling rate criterion is not satisfied. For a given ϕ, these 7 wave fields defined a family. Eleven families, corresponding to values of ϕ from 0 to $\pi/2$, were simulated, for a total of 77 wave fields. Figure 5.12 shows an example of a wave field, with n=3 and $\phi=\pi/10$.

The mean squared error between f(x,y) and the linear (nearest neighbor) model was computed by numerical integration, with 19x19 steps for each of the 16x16 pixels. The mean squared error between f(x,y) and the interpolated model was computed at the same resolution. An earlier simulation using only a 9x9 step per pixel resolution differed from the 19x19 step resolution results by only 1.7%. Due to the computational costs, analysis at higher resolutions (beyond 19x19) was considered unjustified. Figures 5.13 and 5.14 show the effective wave fields used by the nearest neighbor and linear interpolated models, respectively for the field shown in Figure 5.12.

Two results were immediately apparent from the simulation. First, the value of the phase ϕ for the 11 families of wave fields was insignificant. For a given value of n, all 11 phases yielded the same mean squared error for the linear model, and the same mean squared error for the interpolated model. This is an expected result due to the underlying digital signal processing assumption that opposite edges of the wave field are continuations of each other (i.e., the top edge is continuous with the bottom edge, and the left edge is continuous with the right edge). The second result, which was anticipated but not strictly expected, was that the mean squared error of the linear model was larger than the mean squared error of the interpolated model, varying from 1.5 times larger at the highest frequency, to 36 times larger at the lowest frequency. The mean squared error itself decreased with decreasing frequency, by over two orders of magnitude for the linear model, and by nearly three orders of magnitude for the interpolated model, over the range of frequencies studied.

Comparing the mean squared errors to determine equivalent sampling rates, the mean squared error of the interpolated model at the highest frequency (7 cycles) fell between the mean squared errors of the linear model at 5 and 6 cycles. The most favorable estimate, 7/5, suggests that if the linear model sampling rate were increased by a factor of 1.4, it would be comparable to the interpolated model at high frequencies. At the lowest frequency (1 cycle), the mean squared error of the linear model fell midway between the mean squared errors of the interpolated model at 2 and 3 cycles. Using the estimate 2.5, this suggests that if the

linear model sampling rate were increased by a factor of 2.5, it would be comparable to the interpolated model at low frequencies. Chapter 3 argued that since the interpolated model is four times more computationally expensive to compute than the linear model, the interpolated model would be economical only if the effective sampling rate difference were a factor of two (in each of two dimensions) or better. At high frequencies, this criterion is not satisfied, and thus the interpolated model is not cost effective over the linear model at high frequencies. At low frequencies, the criterion is satisfied, suggesting that interpolated modeling would be cost effective over linear modeling at low frequencies. The break even point, where the effective sampling rate factor is two, is reached in the neighborhood of less than 2 cycles for the linear fit, and less than 3.5 for the interpolated fit.

These results are consistent with an analysis by Parker et al. (1983), who examined the one-dimensional interpolation problem, and observed that the linear (nearest neighbor) approach acted as a low pass filter that effectively passed low frequency signals, but poorly attenuated high frequencies beyond the upper limit set by the Nyquist rate. The interpolated approach was superior in attenuating these high frequency out-of-band signals, but at the price of attenuating some of the high frequency in-band signals (i.e., signals within the Nyquist limit). Thus a signal rich in high frequency (in-band) energy would be poorly handled by the interpolated model.

Therefore, if the function (image) under analysis is smoothly varying, in the sense that it has been oversampled by at least a factor of 2 in each dimension (i.e., more than twice as many data points than are required by the Nyquist sampling criterion, in each direction, have already been sampled), then the interpolated model is cost effective over the linear model. This conclusion can be broadened to include functions sampled at the Nyquist rate, but with only relatively small regions of high frequency variations. In general, however, functions sampled at or near the Nyquist rate in order to minimize data acquisition and storage costs will not be cost effectively handled by the interpolated model. Therefore, in general, the linear model will be more cost effective than the interpolated model. Considering the observation (Kak, 1979) that reconstruction by convolution backprojection exhibits a variance close to the theoretical lower bound, further study of algebraic reconstruction for purposes of establishing a lower bound on the variances associated with differential thermography is unjustified. However, the use of algebraic reconstruction in an application that requires the variance of the reconstruction to be determined from all of the available data may still be appropriate.

5.6 ANALYSIS OF TEMPERATURE ESTIMATION

The effects of the various error sources can be combined to examine the net error in estimating temperature. In the convolution backprojection analysis, a variance of $9.5*10^{-4}$ $\mu s^2/mm^2$ was reported for the time-of-flight reconstruction of data

with an inherent variance of 10^{-4}. Assuming the variance in the speed in water to be negligible, equation 3.74 predicts that the variance in the estimated speed of sound in the tissue should be $5.9*10^{-3}$. The first half of equation 3.76 predicts that the variance in the speed will contribute $5.3*10^{-3}{}^{o}C^{2}$ to the variance in the temperature, if the speed thermal coefficient dc/dT is modeled as 1.5 mm/μs/°C. The last portion of the equation deals with the error introduced by the variance in the speed thermal coefficient. If the standard deviation of the speed thermal coefficient is modeled as 0.1 (which is consistent with the least squares models in Appendix A), and the temperature change is estimated as 5.5°C (corresponding to a shift from 37°C to 42.5°C, which would be an expected shift for hyperthermia applications), then the variance contributed to the temperature estimation by the speed thermal coefficient will be $0.1344^{o}C^{2}$. This variance is 25 times greater than the variance introduced by the data collection and reconstruction process. The standard deviation of the total variance would then be 0.3738°C. It is readily apparent that the determining factor in this analysis is the variance in the speed thermal coefficient. To achieve a minimally acceptable standard deviation of 0.25°C (corresponding to an accuracy of 0.5°C modeled as a 2 standard deviation limit), the standard deviation in the speed thermal coefficient would have to be reduced to 0.068 μs. This implies that the speed thermal coefficient must be at least 22 times larger than its standard deviation. Of the eight sets of liver data in Appendix A, only two sets have such small standard devations. Of the 42 sets of liver attenuation coefficient data in Appendix B, only one set has the thermal coefficient greater

than 20 times its standard deviation. Since equation 3.76 is equally valid for attenuation coefficient based temperature estimates as for speed based temperature estimates, this implies that the majority of the available attenuation coefficient data is incapable of estimating a 5.5°C change in temperature with a 0.5°C accuracy. Note that to reach the level where the variance due to the uncertainty in the speed thermal coefficient is comparable to the variance due to the data collection and reconstruction, the standard deviation of the speed thermal coefficient would have to be reduced to 0.0198 μs. This corresponds to a factor of more than 75 between the speed thermal coefficient and its standard deviation. It is clear that much work needs to be done to improve the statistics of both the speed and attenuation coefficient thermal coefficients.

CHAPTER 6

CONCLUSIONS

This dissertation has attempted to study the nature of the problem of noninvasive differential thermography using divergent beam ultrasound computed tomography. Several conclusions have been presented throughout the analysis. In summary,

i) Both ultrasound speed and frequency dependent attenuation coefficient are temperature sensitive, and in principle, measuring changes in these properties could be used to estimate temperature change. Ultrasound speed tends generally to increase with temperature for nonfatty tissue, and decrease with temperature for fatty tissue. The ultrasound attenuation coefficient tends to decrease with temperature for both fatty and nonfatty tissues, but the rate of decrease tends to be greater for fatty tissues. However, a critical factor in temperature estimation, based on speed or attenuation coefficient, is a thermal property database for biological tissue.

ii) Attempts to apply a Taylor expansion approximation to the thermal properties of tissue by fitting simple polynomial models to the thermal dependence of speed have shown that over the temperature range from 10 to 40^{o}C, speed tends to be linear in temperature for most tissues, although liver may be better modeled by a quadratic thermal dependence. A linear model for the attenuation coefficient in blood also seems appropriate, but the attenuation coefficients of most other biological media tend to follow a quadratic, or more complicated dependence on temperature. Working with the log of the attenuation coefficient does not provide substantially better results. However, a serious question must be asked concerning the amount of error in the available information. Careful, reproducible measurements of the thermal properties of tissue are called for.

iii) Two more sophisticated models, derived from the physics of simple systems, did not provide substantially better results than the simple polynomial models. The ratio of squared speeds model suggested that speed does not depend strictly on the square root of the absolute temperature. The frequency shift model also failed to show a strong dependence of the shift of the absorption spectrum on the temperature. Although difficult to perform, this model calls for further study at higher frequencies, to identify whether the problem lies in the data or the model.

iv) There is a high degree of variability in the measured properties reported in the scientific literature, suggesting both that absolute thermometry is not possible without further data, and that relative thermometry is also in doubt without more refined data. A "role call" of tissues described by scientific literature shows that a significant amount of basic sonometry needs to be performed to build up the available knowledge base.

v) To measure speed and attenuation coefficient noninvasively, ultrasound computed tomography can be used. With the apparatus available, time-of-flight can be measured with a variance of 1 part in 10^4, and attenuation can be measured with a variance of 1 part in 10^2 to 10^3. Images of speed and attenuation coefficient can then be reconstructed with a variance of 1 part in 10^3. To perform the reconstruction, convolution backprojection is computationally efficient, and provides a variance close to the theoretical limit. The noise introduced by the computation is small compared to the noise propagated through the computation, originating in the measured data. Algebraic reconstruction provides the advantage that the variance of the reconstruction can be determined from all of the available data, while convolution backprojection is limited in its ability to extract variance information from the data, and relies on external determinations of data variance. Interpolated modeling for algebraic reconstruction can be cost effective for smoothly varying oversampled data, but in

general may not be justified.

vi) Several difficulties need to be resolved with the facilities available in the Bioacoustics Research Laboratory at the University of Illinois at Urbana-Champaign. Backlash and wobble in the mechanics of the scanner introduce anisotropic spatial distortions that can not be readily removed, either by averaging or by digital signal processing techniques. Resolution of this problem either calls for the use of tensioned belts (to remove backlash), or significant redesign to minimize mechanical errors in general. Although the dynamic range of the analog to digital conversion for digitizing the ultrasound pulses is good, the bandwidth is too limited to study absorption spectral shifts. This limitation is in the process of solution (Embree, 1986) in the development of a data acquisition system for other ultrasound devices in the lab. Finally, proper support of tissue samples suggests the design of a system with the mechanics either above, or to the side of the sample under study.

vii) Using the available literature data for thermal coefficients, and the divergent beam ultrasound computed tomography apparatus in the Bioacoustics Research Laboratory, differential temperature estimation could be performed with a standard deviation on the order of $0.5^{o}C$, for temperature shifts of $5.5^{o}C$ (i.e., from $37^{o}C$ to $42.5^{o}C$). The critical factor in this estimation is the variance in the speed thermal coefficient, based on data from the tissue database.

A major theme in the above discussion is the need for more thermal property measurements, covering more tissues, with greater repeatability. Since thermal property measurements are no better than the underlying parameter measurements, this calls for better ultrasound speed and attenuation coefficient measurements to be made from imaging systems. Diffraction, refraction, multipath, and limited view problems limit the applicability of conventional ultrasound computed tomography. The general problem of inverse scattering, and diffraction tomography in specific, holds the key to forming quantitative ultrasound property images. Advanced imaging techniques, as well as basic sonometry to increase the size and reliability of the tissue database, are the necessary steps toward furthering noninvasive temperature estimation through ultrasound imaging.

TABLES

Table 3.1. Tissue Constituents

Percentage concentration ranges for the three constituent materials of water, total protein, and fat for various biological materials. Those in parentheses were calculated (Pohlhammer and O'Brien, 1980).

Biological Material	Water	Total Protein	Fat	References
Brain	72-85	(6-11)	8.6	a,b,c,d
Cartilage	70-73	20-25		e,b,f
Cerebro-Spinal Fluid	99	0.015-0.040	0.00	a,g
Eye-Aq/Vit humor	99-99.9	0.01-1.0	0.004-0.007	a,b,f,h,i
Fat	10^{-3}5	3.2-17.0	50-86	c,j,d,k
Heart	63-79.2	15-19	3.6-21	b,c,d
Kidney	75.9-82.7	15.4-16.8	3.3-6.7	b,c,d
Liver	66.9-80.3	16.5-21.2	3.7-10	b,c,d,l
Milk-whole	87-88	3-4	3.5-5	d,g
Striated Muscle	63-75.7	17.3-21.8	4.0-13.3	b,c,d
Plasma	90-95	5.4-8.0	0.9-2.0	m,a,j,g,n,o
Spleen	74.4-77.4	17.1-18.8	3.0-3.9	b,c,d
Testis	84.0-85.0	(9-11)	0.045	p,q
Tongue	61-74.3	13.7-18.5	5.3-23	d

a Altman and Dittmer, 1961
b Chvapil, 1967
c Ruch and Patton, 1966
d Watt and Merrill, 1963
e Robb-Smith, 1954
f Mathews, 1975
g White et al., 1968
h Van Heyningen, 1962
i Dawson, 1972
j Wolf, 1976
k Galton, 1971
l Freese and Lyons, 1979
m Nyborg, 1975
n Carstensen et al., 1953
o Ganong, 1967
p Neufeld, 1937
q Wolf and Leathem, 1955

Table 3.2. Thermal Expansion Coefficients

Thermal expansion coefficients for distilled degassed water, and normal (0.9%) saline (Edmonds and Dunn, 1981).

T (^{o}C)	θ - water (C^{-1}) $*10^{-5}$	θ - saline (C^{-1}) $*10^{-5}$
10	9.45	8.46
20	21.19	23.89
30	30.75	29.94
40	38.93	40.07

$\theta_w = 0.580 + 0.980*T$ $(*10^{-5})$ r=0.997
$\theta_s = 0.370 + 1.009*T$ $(*10^{-5})$ r=0.985

Table 3.3. Adiabatic Compressibility

Adiabatic compressibility for distilled degassed water (Edmonds and Dunn, 1981).

T (^{o}C)	β_s water (m^2/N) $*10^{-11}$
10	47.842
20	46.161
30	45.443
40	45.338

$\beta_s = 48.254 - 0.0823*T$ $(*10^{-11})$ r=0.919
$\beta_s = 50.224 - 0.279*T + 0.00394*T^2$ $(*10^{-11})$ r=0.999

Table 3.4. Speed of Sound in Seawater

Speed of sound in seawater at 1 atm as a function of salinity and temperature. Speeds are in m/s (Millero and Kubinski, 1975).

T	Saline Concentration				
(°C)	0%	10%	20%	30%	40%
0	1402.39	1415.85	1429.17	1442.48	1455.84
5	1426.15	1438.99	1451.63	1464.31	1477.12
10	1447.24	1459.52	1471.57	1483.68	1495.94
15	1465.88	1477.64	1489.20	1500.79	1512.51
20	1482.28	1493.58	1504.70	1515.83	1527.05
25	1496.62	1507.51	1518.25	1528.97	1539.73
30	1509.06	1519.59	1529.98	1540.34	1550.69
35	1519.74	1529.96	1540.04	1550.07	1560.09
40	1528.80	1538.76	1548.54	1558.29	1568.05

Table 3.5. Absorption Coefficient in Water

Frequency-free ultrasonic absorption coefficient as a function of temperature in water (Pinkerton, 1949).

T (°C)	α/f^2 (s^2/cm) $*10^{-17}$
0	56.9
5	44.1
10	35.8
15	29.8
20	25.3
30	19.1
40	14.61
50	11.99
60	10.15
70	8.71
80	7.89
90	7.24
100	6.87

$\alpha = 39.69 - 0.4167*T$ r=0.879

$\alpha = 49.45 - 1.167*T + 0.00777*T^2$ r=0.978

$\ln(\alpha) = 3.733 - 0.02093*T$ r=0.970

$\ln(\alpha) = 3.982 - 0.0401*T + 0.0002*T^2$ r=0.999

Table 3.6. Attenuation Coefficient in Collagen

Summary of collagen suspension frequency-free attenuation coefficient data as a function of collagen concentration and frequency (Goss and Dunn, 1980).

	A/f^2 (s^2/cm) $*10^{-17}$				
	10°C	20°C	10°C	20°C	
freq	c=0.49%	c=0.52%	c=0.23%	c=0.34%	c=0.17%
8.87	35.5	33.1	14.0	19.3	10.1
14.8	25.9	18.7	9.9	12.5	5.8
20.7	28.2	14.7	11.2	9.3	4.6
26.7	28.7	13.8	14.0	10.0	3.2
32.6	30.2	10.0	11.0	9.2	2.5
38.6	26.6	7.6	10.6	6.6	1.0
44.4	25.2	7.0	9.9	6.9	0.6
50.5	18.5	5.3	9.5	5.4	0.4
56.4	15.4	-	7.1	3.2	3.5

Table 3.7. Speed of Sound in Oil

Speed of ultrasound as a function of temperature for castor oil and phenylated silicone Dow-Corning 710 oil (Dunn et al., 1969).

T (°C)	castor oil (m/s)	Dow-Corning 710 (m/s)
0	1580	1446
10	1536	1409
20	1494	1378
30	1452	1349
40	1411	1321

$c_{co} = 1579.0 - 4.22*T \quad r=1.000$
$c_{dc} = 1442.6 - 3.10*T \quad r=0.998$

Table 3.8. Attenuation Coefficient in Oil

Ultrasound attenuation coefficient at 1 MHz as a function of temperature for castor oil and phenylated silicone Dow-Corning 710 oil (Dunn et al., 1969).

T (^{o}C)	castor oil (cm^{-1})	Dow-Corning 710 (cm^{-1})
0	0.26	-
10	0.16	0.135
20	0.096	0.070
30	0.057	0.040
40	0.037	0.024

$A_{co} = 0.2318 - 0.00549*T$ r=0.961

$A_{co} = 0.2582 - 0.0108*T + 0.00013*T^2$ r=1.000

$\ln(A_{co}) = -1.3506 - 0.0493*T$ r=1.000

$A_{dc} = 0.1580 - 0.00363*T$ r=0.956

$A_{dc} = 0.2193 - 0.0098*T + 0.00012*T^2$ r=0.998

$\ln(A_{dc}) = -1.4673 - 0.0574*T$ r=0.998

Table 3.9. Summary of Appendix A

Summary of Appendix A, indicating tissues, temperature ranges, speed ranges, speed thermal coefficient ranges (at 37°C) and species reported.

Tissue	Temps °C	Speed Values m/s	Thermal Coefs @37°C m/s/°C	Species hbcefmp
Blood	10-44	1475-1590	1.30: 2.00	h c
Bone	-	-	-	
Breast, parenchyma and fat	22-43	1471-1572	-0.07: 2.52	h
Cerebrospinal Fluid	24-25	1509-1515	-	h
Eye	29-37	1560-1572	1.50	h
aqueous h.	4-37	1462-1530	1.86: 2.03	p
cornea	4-37	1537-1588	1.37: 1.62	h p
lens	4-37	1617-1673	0.69: 1.10	h p
sclera	4-37	1609-1656	0.97: 1.20	h p
vitreous h.	4-37	1458-1542	1.81: 2.95	hb p
Fat	20-37	1430-1581	-7.4	b
breast	22-43	1435-1481	-0.24: 1.48	h
orbit	20-37	1462-1582	-7.06	h
peritoneal	10-60	1345-1680	-7.14:-2.81	b
stomach	35-44	1394-1455	-3.43:-2.56	c
Heart	35-43	1592-1602	1.25	c
Kidney	17-44	1508-1589	1.05: 1.35	h c
Liver	5-65	1490-1690	0.20: 1.40	hbc p
Milk	10-50	1483-1560	0.60: 1.50	b
Muscle breast	22-43	1543-1580	1.31: 1.86	h
ext. to eye	20-37	1612-1631	1.21	h
psoas	17-41	1459-1581	1.05: 1.11	h
skeletal	35-43	1588-1630	0.56: 1.23	c
Nervous Tissue brain	0-67	1424-1580	0.67: 2.86	h c f
optic nerve	20-37	1615-1644	-1.71	h
spinal cord	17-41	1456-1544	0.78: 2.20	h
Spleen	17-43	1528-1609	1.22: 10.6	h c
Water	23-45	1492-1536	1.51: 2.80	

h human
b bovine
c canine
e equine
f feline
m murine
p porcine
- no data reported

Table 3.10. Summary of Appendix B

Summary of Appendix B, indicating tissues, temperature ranges, attenuation coefficient ranges, thermal coefficient of attenuation coefficient ranges (at 37°C), and species reported.

Tissue	Temps °C	Atten Coefs dB/cm	Thermal Coefs @37°C dB/cm/°C *10^{-3}	Species hbcefmp
Blood	10-40	0.009-1.15	-5.00:-0.10	h c
Bone	5-60	28.5-81.0	120.0:200.0	e
Breast	-	-	-	
Cerebrospinal Fluid	-	-	-	
Eye	-	-	-	
aqueous h.	-	-	-	
cornea	-	-	-	
lens	-	-	-	
sclera	-	-	-	
vitreous h.	-	-	-	
Fat	4-49	2.00-20.8	-577.:-83.3	p
breast	-	-	-	
orbit	-	-	-	
peritoneal	10-60	2.00-16.0	-1143.:147.	b
stomach	-	-	-	
Heart	10-37	0.09-0.70	-5.81: 2.86	c
Kidney	4-37	0.50-12.6	52.9: 88.2	p
Liver	4-65	0.89-24.0	-294.: 225.	hb p
Milk	-	-	-	
Muscle				
breast	-	-	-	
ext. to eye	-	-	-	
psoas	-	-	-	
skeletal	-	-	-	
Nervous Tissue				
brain	10-58	0.30-9.00	-84.2:-14.3	b f
optic nerve	-	-	-	
spinal cord	2-45	0.10-1.13	-10.0:-2.50	m
Spleen	10-58	1.00-31.8	-465.: 26.3	b

h human
b bovine
c canine
e equine
f feline
m murine
p porcine
- no data reported

Table 5.1. Results of Least Squares Fits to Appendix A

Summary of least squares fits to the speed data in Appendix A, indicating tissues, number of data sets available, number of data sets with three or more measurements, number of data sets with significant probability of correlation (95% level of confidence), number of data sets with four or more measurements, and number of data sets with significant probability that a quadratic fit is justified over a linear least squares fit (95% level of confidence).

Tissue	Number of Data Sets Available				
	total	$N \geq 3$	$P_r \leq 0.05$	$N \geq 4$	$P_F \leq 0.05$
Blood	8	6	4	5	1
Bone	-	-	-	-	-
Breast, parenchyma and fat	2	2	2	2	1
Cerebrospinal Fluid	1	-	-	-	-
Eye					
aqueous h.	1	1	1	1	1
cornea	2	2	2	2	0
lens	4	2	2	2	1
sclera	2	2	2	2	1
vitreous h.	4	3	3	3	0
whole	1	-	-	-	-
Fat					
breast	1	1	1	1	0
orbit	1	-	-	-	-
peritoneal	1	1	1	1	1
stomach	3	2	2	-	-
unspecified	1	-	-	-	-
Heart	1	-	-	-	-
Kidney	7	4	4	1	1
Liver	13	8	6	5	4
Milk	2	2	2	2	2
Muscle					
breast	1	1	1	1	0
ext. to eye	1	-	-	-	-
psoas	1	1	1	1	0
skeletal	6	4	4	-	-
Nervous Tissue					
brain	27	26	24	25	10
optic nerve	1	-	-	-	-
spinal cord	1	1	0	1	0
Spleen	2	2	2	1	0
Water	1	1	1	1	1
Totals	96	72	65	57	24

Table 5.2. Results of Square Speed Ratio Model (fixed)

Results of least squares fit of speed *vs* temperature data to equation 5.8, using Approach 1 (fixed reference), indicating number of data sets available, number of data sets with a significant probability of correlation (at the 95% level of confidence), number of data sets for which the hypothesis a=0 was accepted at the 95% level of confidence, number of data sets for which the hypothesis a=0 could be marginally accepted, number of data sets for which the hypothesis b=1 was accepted at the 95% level, and number of data sets for which the hypothesis b=1 could be marginally accepted.

Tissue	Number of Data Sets					
	total	$P_r \leq 0.05$	a=0	a=0 marginal	b=1	b=1 marginal
Blood	5	3	3	0	2	1
Breast						
parenchyma	1	1	1	0	0	0
and fat	1	0	0	0	0	0
Eye						
aqueous h.	1	1	1	0	0	1
cornea	2	2	2	0	0	2
lens	2	2	2	0	0	1
sclera	2	1	1	0	0	1
vitreous h.	3	1	1	0	0	1
Fat						
breast	1	1	1	0	0	0
peritoneal	1	1	1	0	0	1
Kidney	1	1	0	1	0	0
Liver	5	4	3	1	1	1
Milk	2	2	2	0	0	2
Muscle						
breast	1	1	1	0	0	0
psoas	1	1	1	0	1	0
Nervous Tissue	26	23	15	6	11	8
Spleen	1	1	1	0	0	1
Water	1	1	1	0	0	0
Totals	57	47	37	8	15	20

Table 5.3. Results of Square Speed Ratio Model (incremental)

Results of least squares fit of speed vs temperature data to equation 5.8, using Approach 2 (incremental change), indicating number of data sets available, number of data sets with a significant probability of correlation (at the 95% level of confidence), number of data sets for which the hypothesis a=0 was accepted at the 95% level of confidence, number of data sets for which the hypothesis a=0 could be marginally accepted, number of data sets for which the hypothesis b=1 was accepted at the 95% level, and number of data sets for which the hypothesis b=1 could be marginally accepted.

Tissue	Number of Data Sets					
	total	$P_r \leq 0.05$	a=0	a=0 marginal	b=1	b=1 marginal
Blood	5	1	0	0	0	0
Breast						
parenchyma	1	0	0	0	0	0
and fat	1	0	0	0	0	0
Eye						
aqueoue h.	1	0	0	0	0	0
cornea	2	1	0	1	1	0
lens	2	0	0	0	0	0
sclera	2	0	0	0	0	0
vitreous h.	3	1	1	0	1	0
Fat						
breast	1	0	0	0	0	0
peritoneal	1	0	0	0	0	0
Kidney	1	0	0	0	0	0
Liver	5	1	1	0	1	0
Milk	2	2	0	1	0	1
Muscle						
breast	1	0	0	0	0	0
psoas	1	1	1	0	0	1
Nervous Tissue	26	4	0	3	1	2
Spleen	1	0	0	0	0	0
Water	1	1	1	0	0	0
Totals	57	12	4	5	4	4

Table 5.4. Results of Least Squares Fits to Appendix B

Summary of least squares fits to the attenuation coefficient data in Appendix B, indicating tissues, number of data sets available, number of data sets with three or more measurements, number of data sets with significant probability of correlation (95% level of confidence), number of data sets with four or more measurements, and number of data sets with significant probability that a quadratic fit is justified over a linear least squares fit (95% level of confidence). Numbers in parentheses describe the results of linear and quadratic fits to the natural log of the measurements.

Tissue	Number of Data Sets Available				
	total	$N \geq 3$	$P_r \leq 0.05$	$N \geq 4$	$P_F \leq 0.05$
Blood	13	6(6)	5(5)	6(6)	0(3)
Bone	3	3(3)	3(3)	3(3)	0(0)
Breast	-	-	-	-	-
Cerebrospinal Fluid	-	-	-	-	-
Eye					
aqueous h.	-	-	-	-	-
cornea	-	-	-	-	-
lens	-	-	-	-	-
sclera	-	-	-	-	-
vitreous h.	-	-	-	-	-
whole	-	-	-	-	-
Fat					
breast	-	-	-	-	-
orbit	-	-	-	-	-
peritoneal	7	7(7)	0(0)	3(3)	2(2)
stomach	-	-	-	-	-
unspecified	5	2(2)	2(2)	2(2)	0(0)
Heart	24	6(6)	2(2)	6(6)	0(0)
Kidney	5	5(5)	0(0)	-	-
Liver	42	42(42)	14(17)	32(32)	12(12)
Milk	-	-	-	-	-
Muscle					
breast	-	-	-	-	-
ext. to eye	-	-	-	-	-
psoas	-	-	-	-	-
skeletal	-	-	-	-	-
Nervous Tissue					
brain	7	5(5)	3(3)	5(5)	2(0)
optic nerve	-	-	-	-	-
spinal cord	5	4(4)	2(2)	4(4)	2(1)
Spleen	10	10(10)	5(8)	5(5)	1(1)
Totals	121	90(90)	36(42)	66(66)	19(19)

Table 5.5. Results of Frequency Shift Analysis

Results of fitting linear and quadratic curves to the data set formed by combining the absorption spectrum at one temperature with the log-frequency shifted absorption spectrum at another temperature. Included in the table are the number of data sets available (grouped by tissue), the number of data sets with at least three log-frequency - temperature change pairs, the number of data sets with a significant probability of correlation (at the 95% level of confidence), and the number of data sets with a significant probability that a quadratic fit is justified over a linear least squares fit (95% level of confidence).

Tissue	Number of Data Sets			
	total	$M \geq 3$	$P_r \leq 0.05$	$P_F \leq 0.05$
Blood	4	2	1	0
Bone	1	1	1	0
Fat	2	1	0	0
Heart	4	1	0	0
Kidney	1	1	0	0
Liver	7	7	2	0
Nervous Tissue, brain	1	1	0	0
Spleen	2	2	0	1
Totals	22	16	4	1

FIGURES

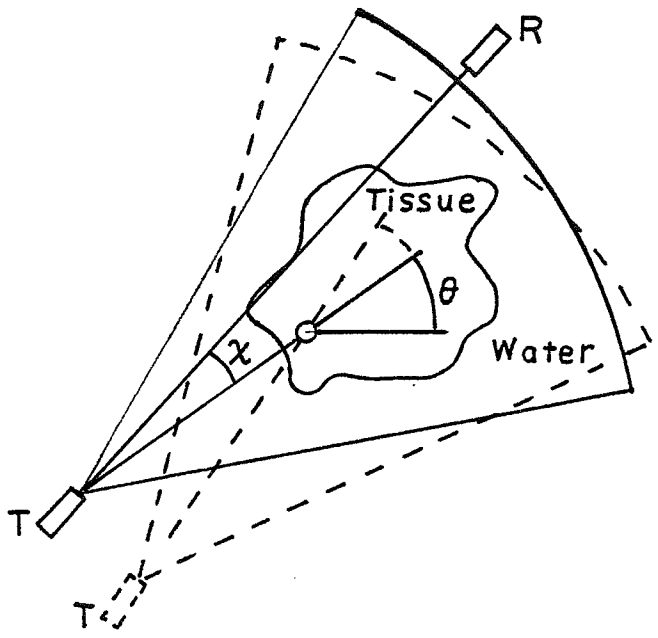

Figure 3.1. Divergent beam geometry with a single transmitter-receiver pair. For each sector, the tranmitter turns and the receiver sweeps so as to maintain a constant alignment. Sectors are repeated at multiple view angles (θ).

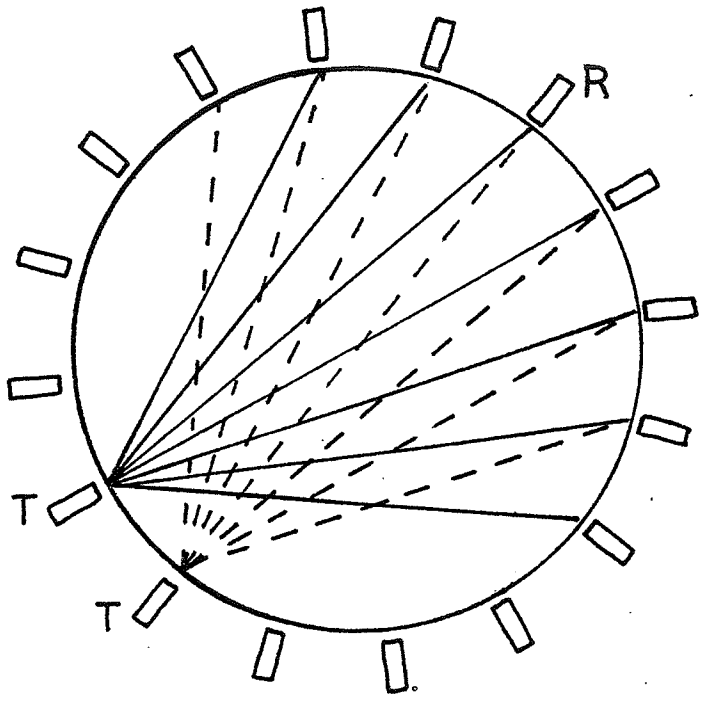

Figure 3.2. Divergent beam geometry with multiple fixed position transducers. Each transducer serves both as a transmitter (for one view) and as a receiver (for all of the other views).

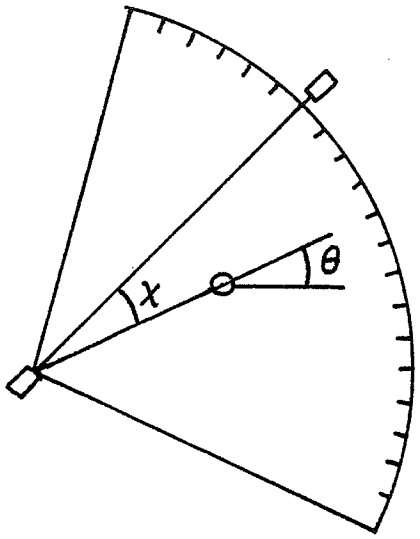

Figure 3.3. Divergent beam data collection geometry with a single transmitter-receiver pair. Data are collected at multiple discrete sector angles (χ), then the apparatus is rotated about its central axis for multiple view angles (θ).

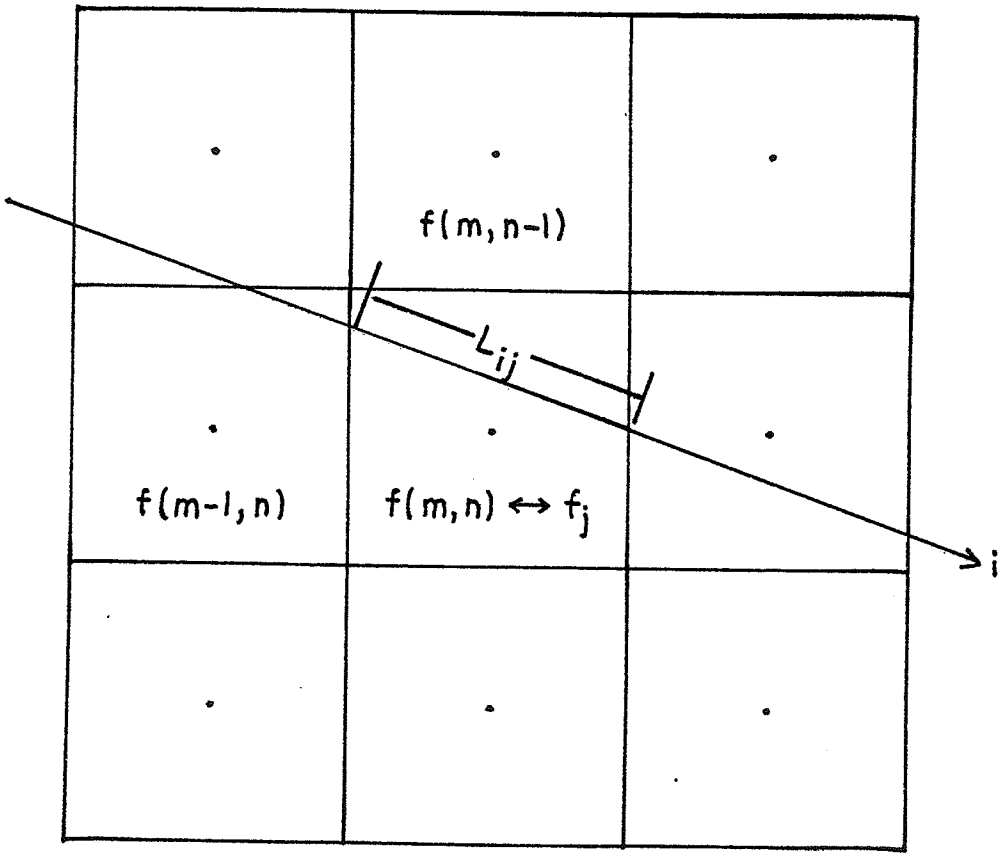

Figure 3.4. Algebraic reconstruction geometry. The object function f(x,y) is sampled into f_{mn}, and the points are uniquely labeled so $f_{mn} <=> f_j$ ($1 \leq m \leq M$, $1 \leq n \leq N$, $1 \leq j \leq MN$). The influence of pixel j on beam i is approximated by $L_{ij} f_j$, where L_{ij} is the length of beam i that passes through pixel j.

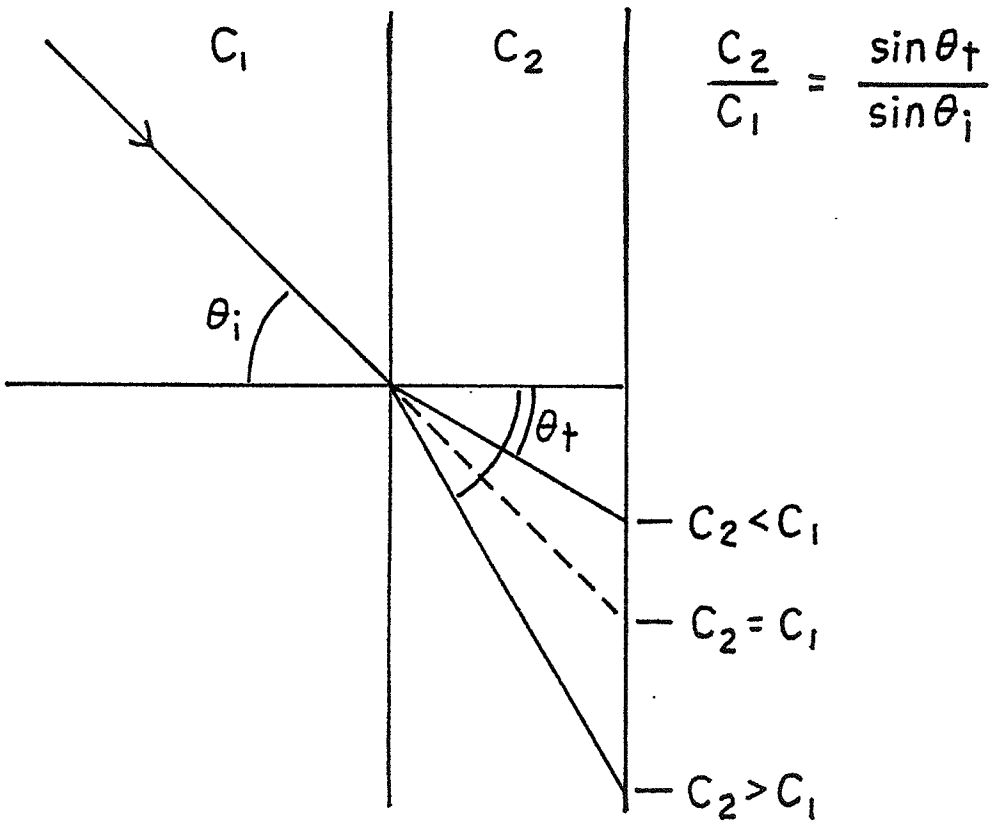

Figure 3.5. Refractive bending. By Snell's Law, the ratio of the speeds is equal to the ratio of the sines of the transmitted and incident angles. Thus if $c_2>c_1$, the beam will follow a "longer" path through the medium of higher speed (longer with respect to the straight line path), and arrive at a later time, leading to an underestimation of c_2. Equivalently, if $c_2<c_1$, then c_2 will tend to be overestimated.

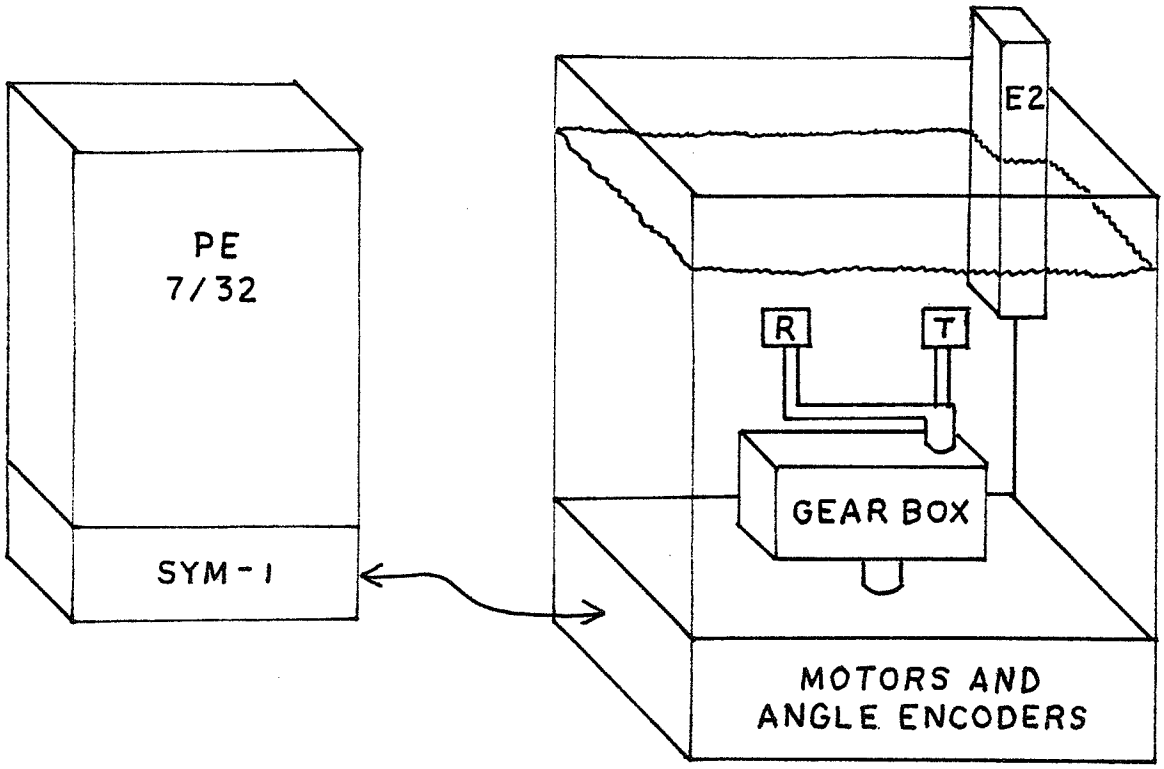

Figure 4.1. The ultrasound computed tomography tank, showing the water bath tank, transducers, drive mechanics, and heater circulator (E-2) for temperature control. The PE 7/32 computer directs all operations and data acquisition. The SYM-1 microcomputer acts as a slave processor to control the motors and monitor the transducer angles.

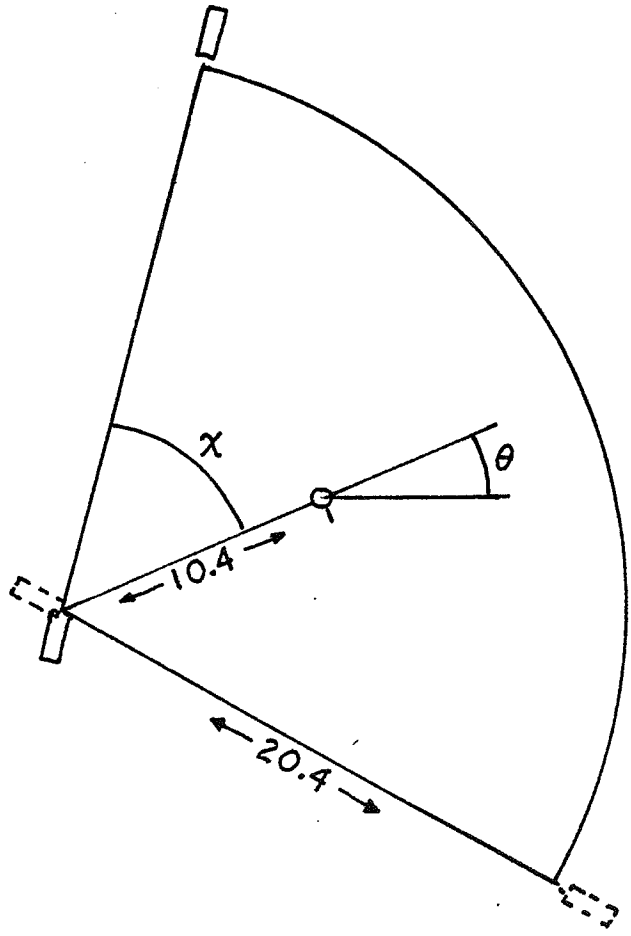

Figure 4.2. Divergent beam sector dimensions. The sector angle spans $-16.8^{\circ} \leq \chi \leq 16.8^{\circ}$ in 57 steps; the view angle spans $0^{\circ} \leq \theta \leq 180^{\circ}$ in 51 steps (typical values).

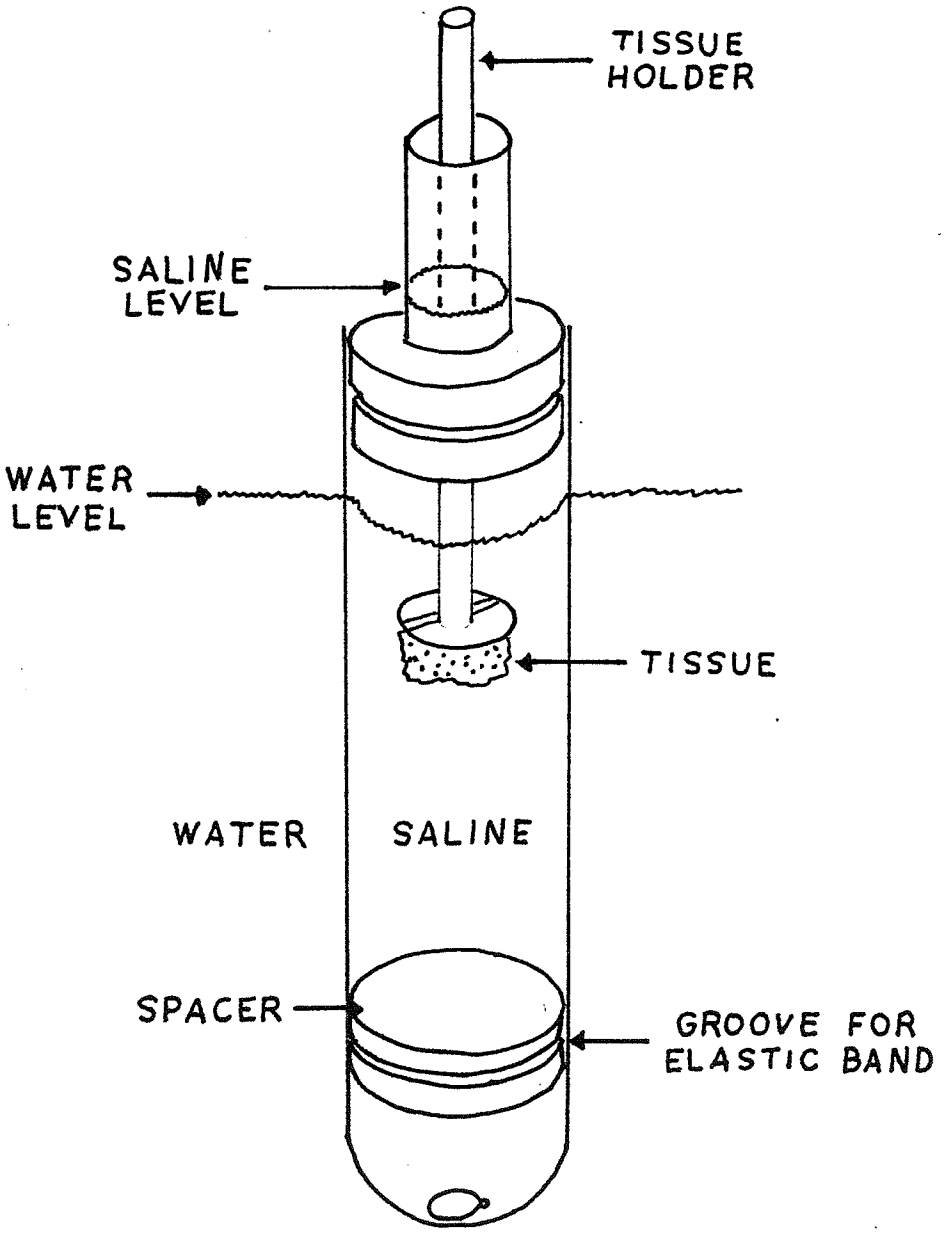

Figure 4.3. Saline cell and tissue holder. The lucite spacer disk is held in place by an elastic band around the outside of the cell. The saline level is kept higher than the surrounding water level to maintain a positive pressure on the cell walls and keep the cell from collapsing. A 13 g lead fishing weight assists in providing stability. The tissue sample is held in place against the tissue holder disk by means of a 5 mm (typical) wide latex band (the same material as the cell wall).

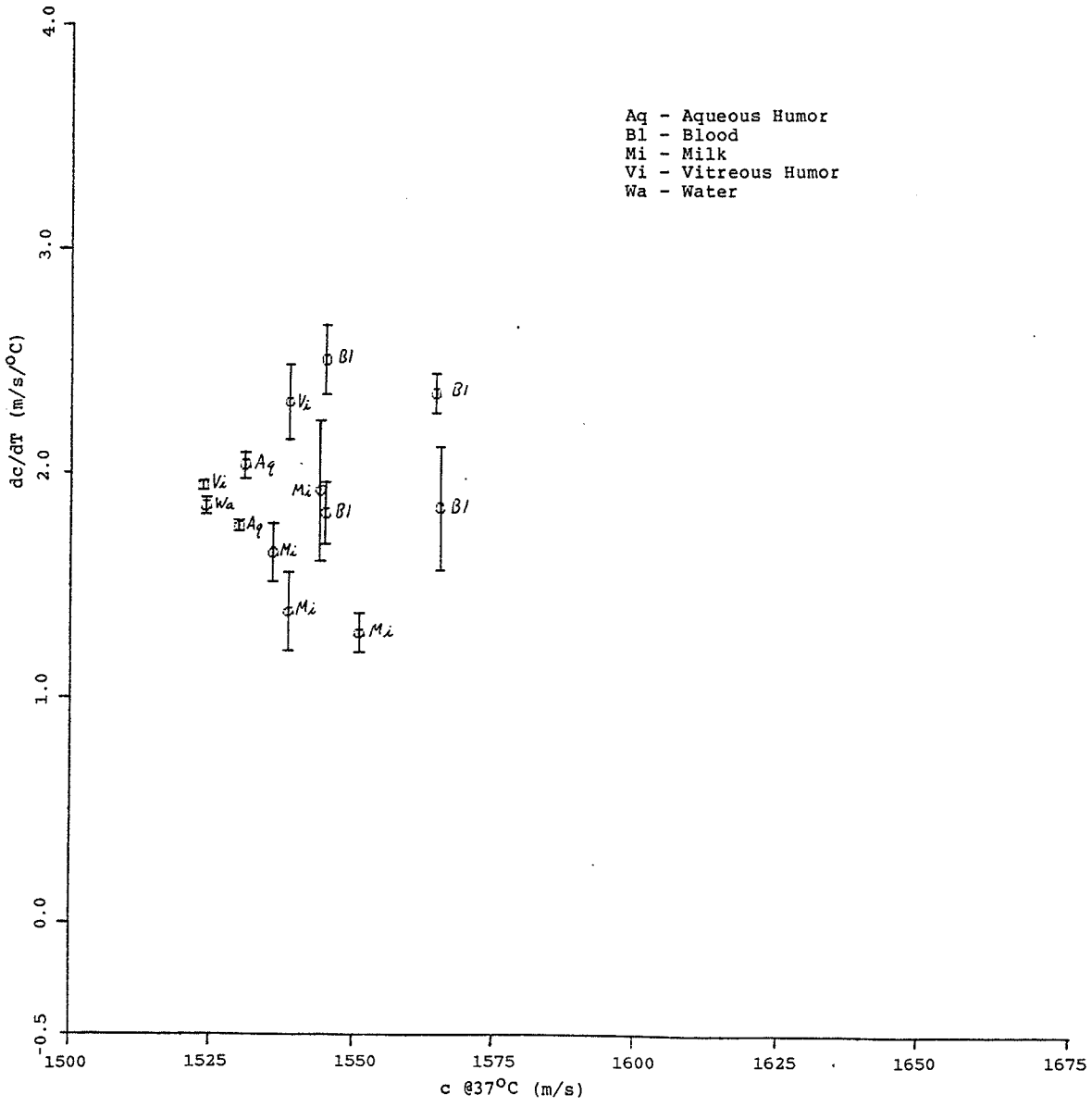

Figure 5.1. Speed thermal coefficient (dc/dT) vs speed at 37°C for various fluids. The error bars represent ± one standard deviation.

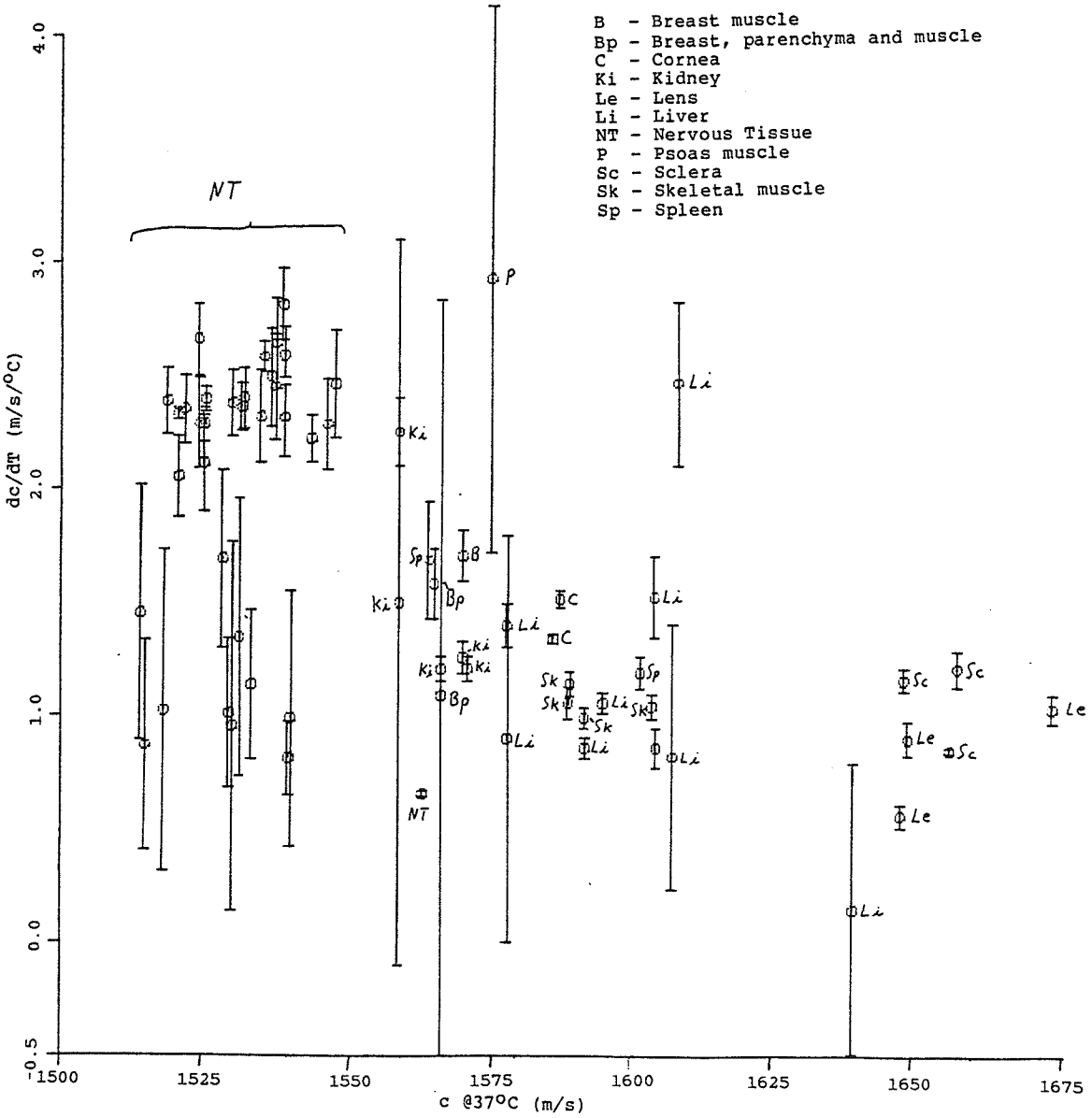

Figure 5.2. Speed thermal coefficient (dc/dT) vs speed at 37°C for various nonfatty tissues. The error bars represent ± one standard deviation.

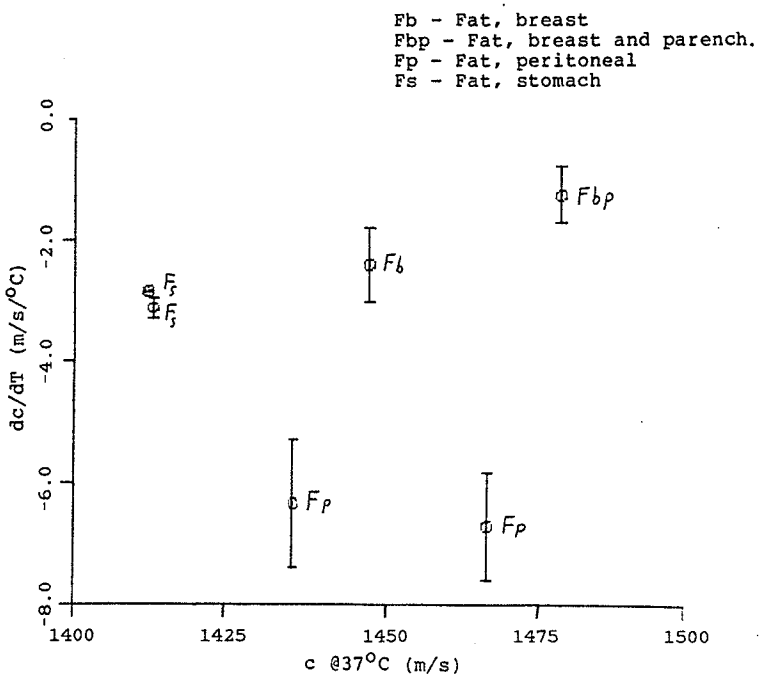

Figure 5.3. Speed thermal coefficient (dc/dT) vs speed at 37°C for various fatty tissues. The error bars represent ± one standard deviation.

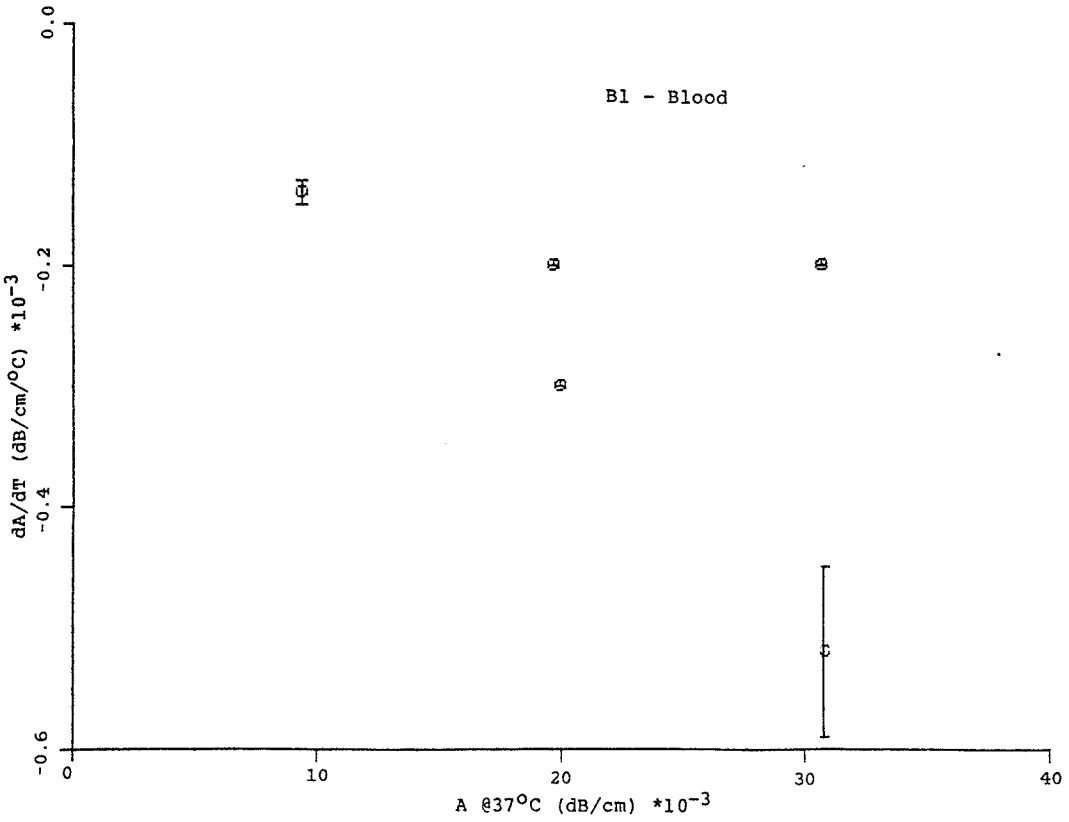

Figure 5.4. Attenuation coefficient thermal coefficient (dA/dT) vs attenuation coefficient at 37°C for blood. The error bars represent ± one standard deviation.

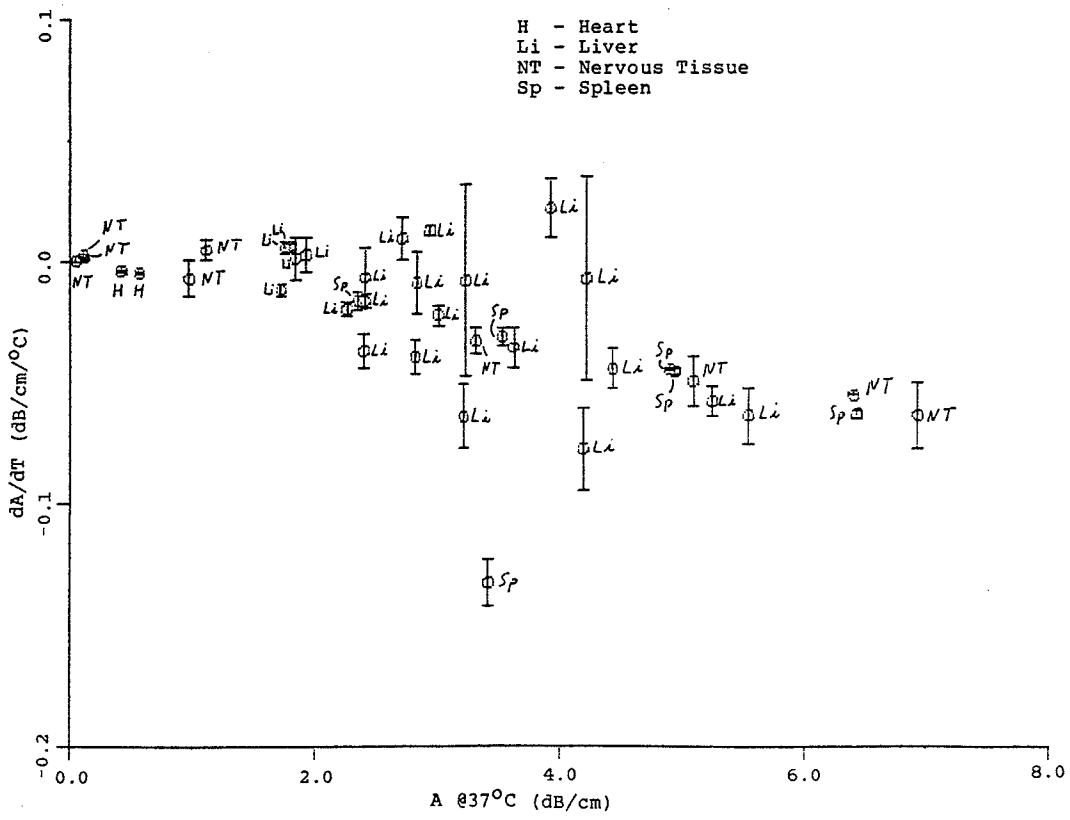

Figure 5.5. Attenuation coefficient thermal coefficient (dA/dT) vs attenuation coefficient at 37°C for various nonfatty tissues. The error bars represent ± one standard deviation.

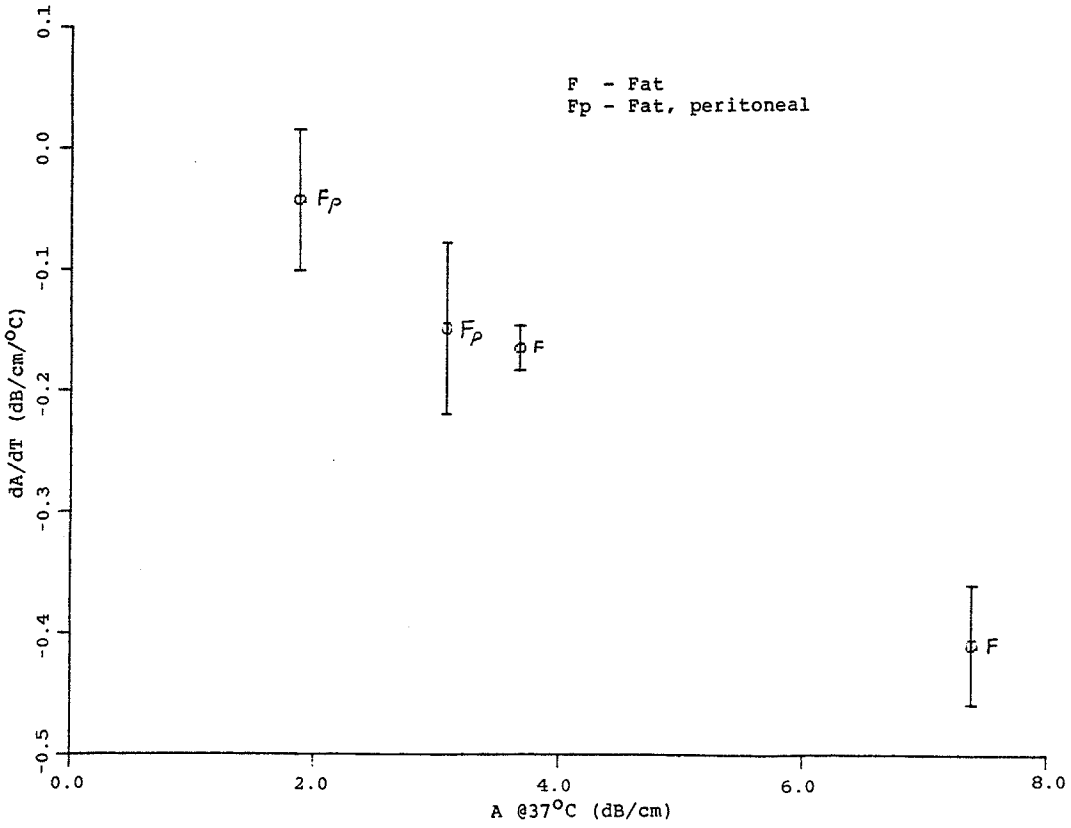

Figure 5.6. Attenuation coefficient thermal coefficient (dA/dT) vs attenuation coefficient at 37°C for various fatty tissues. The error bars represent ± one standard deviation.

Figure 5.7. Reconstructed speed images of excised rat liver, showing typical (rat T-1033, above) and best (rat T-1026, below) results available.

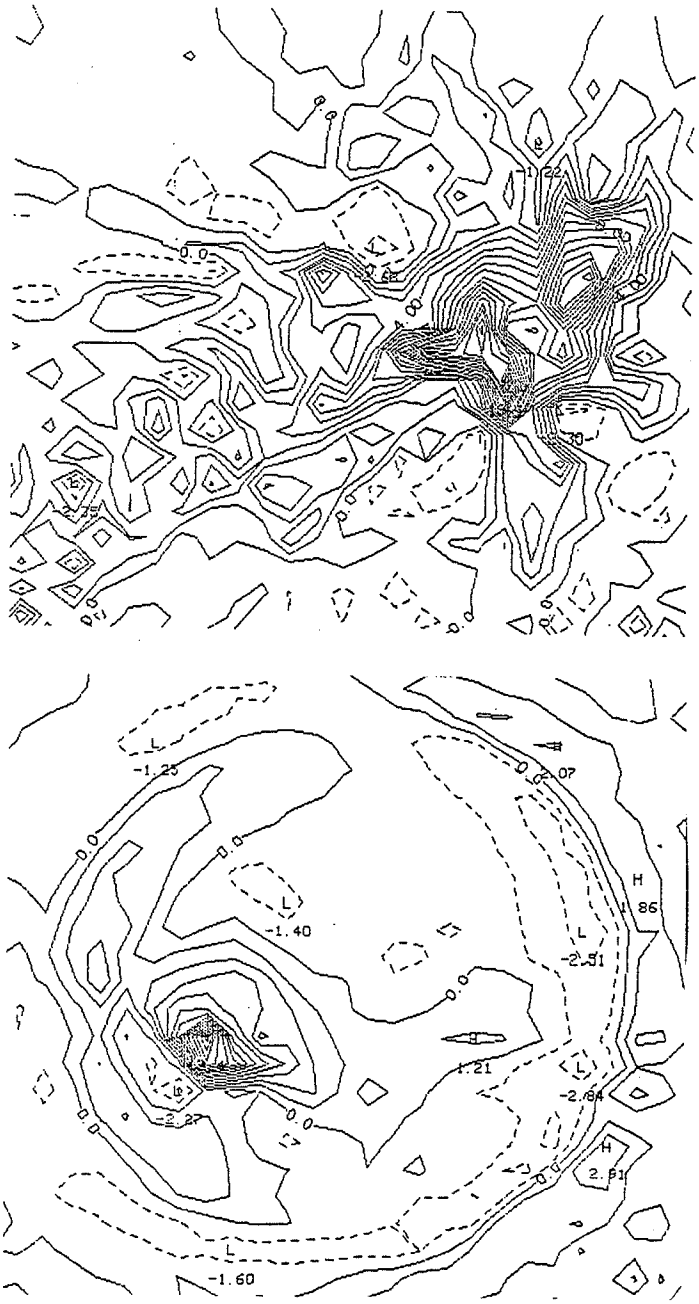

Figure 5.8. Reconstructed attenuation coefficient images of excised rat liver at 4.1 MHz, showing typical (rat T-1033, above) and best (rat T-1026, below) results available.

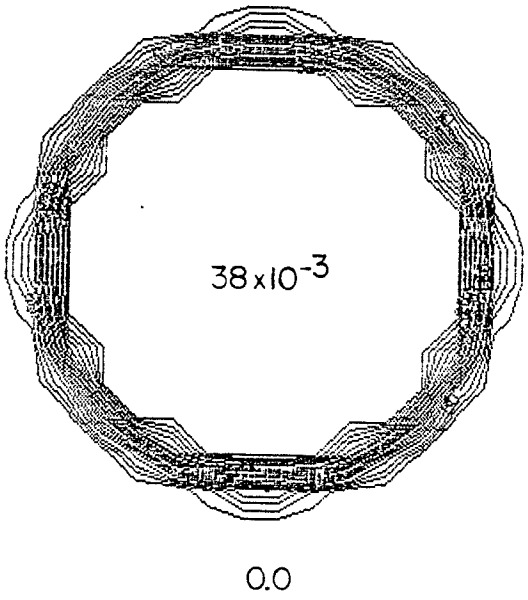

Figure 5.9. Inverse speed image model used for reconstruction analysis. The background values are 0.0 μs/mm; the foreground values are 0.03823 μs/mm.

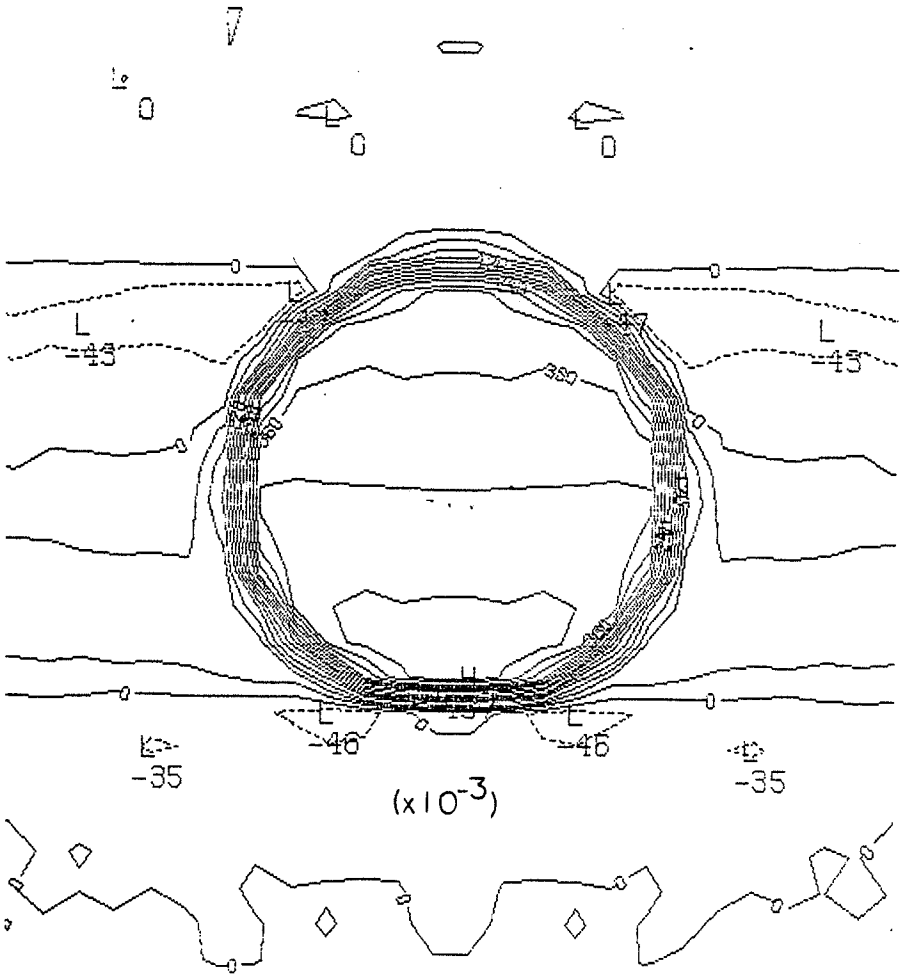

Figure 5.10. Reconstructed inverse speed image produced by convolution backprojection, based on 57 points over 33.6° of fan angle, and 51 views over 180° of view angle, for the model shown in Figure 5.9. The mean background value is 0.000357 μs/mm, and the mean foreground value is 0.03863 μs/mm.

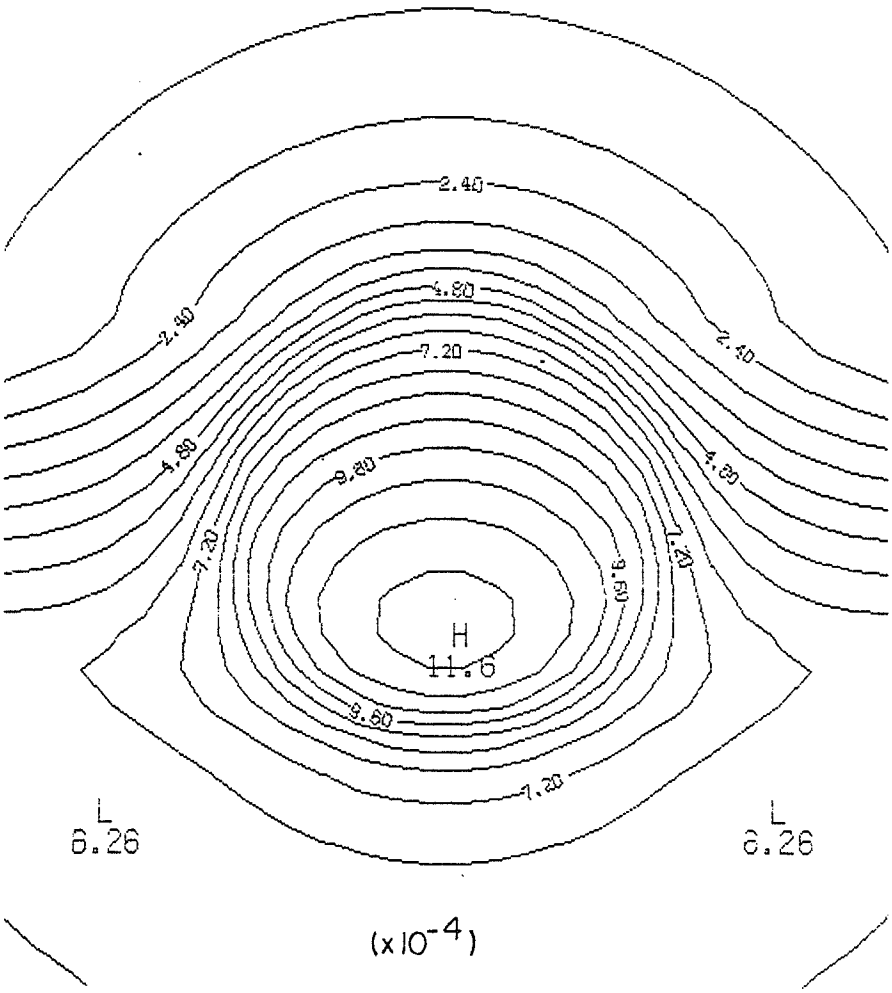

Figure 5.11. Reconstructed variance image, assuming a background variance of 10^{-6} $\mu s^2/mm^2$, and a foreground variance of 10^{-4} $\mu s^2/mm^2$ (similar in appearance to Figure 5.9). The mean background value in this image is 4.16 $*10^{-4}$ $\mu s^2/mm^2$, and the mean foreground value is 9.51 $*10^{-4}$ $\mu s^2/mm^2$.

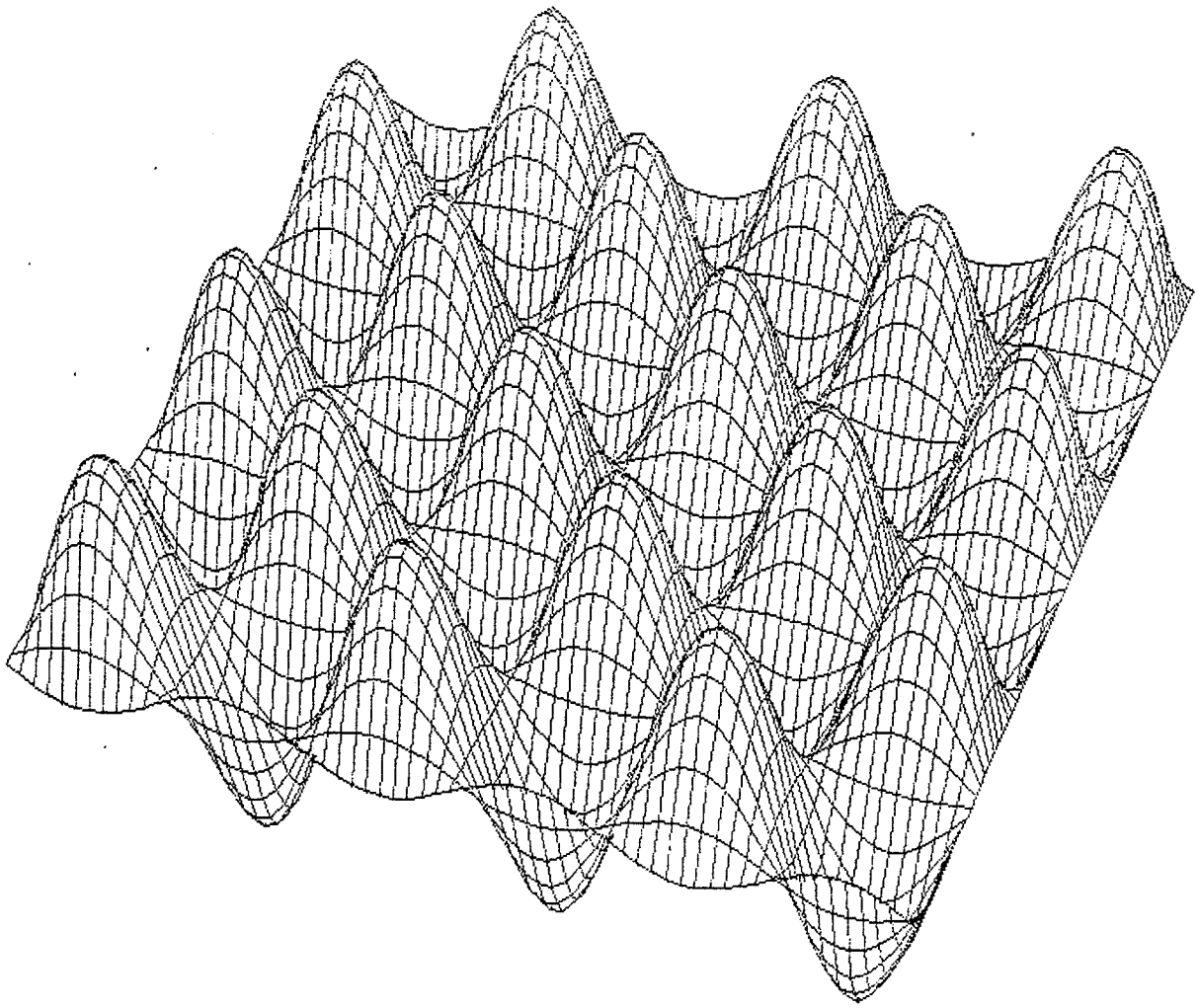

Figure 5.12. Simulated continuous wave field, with three cycles (n=3), and a phase offset (ϕ) of /10.

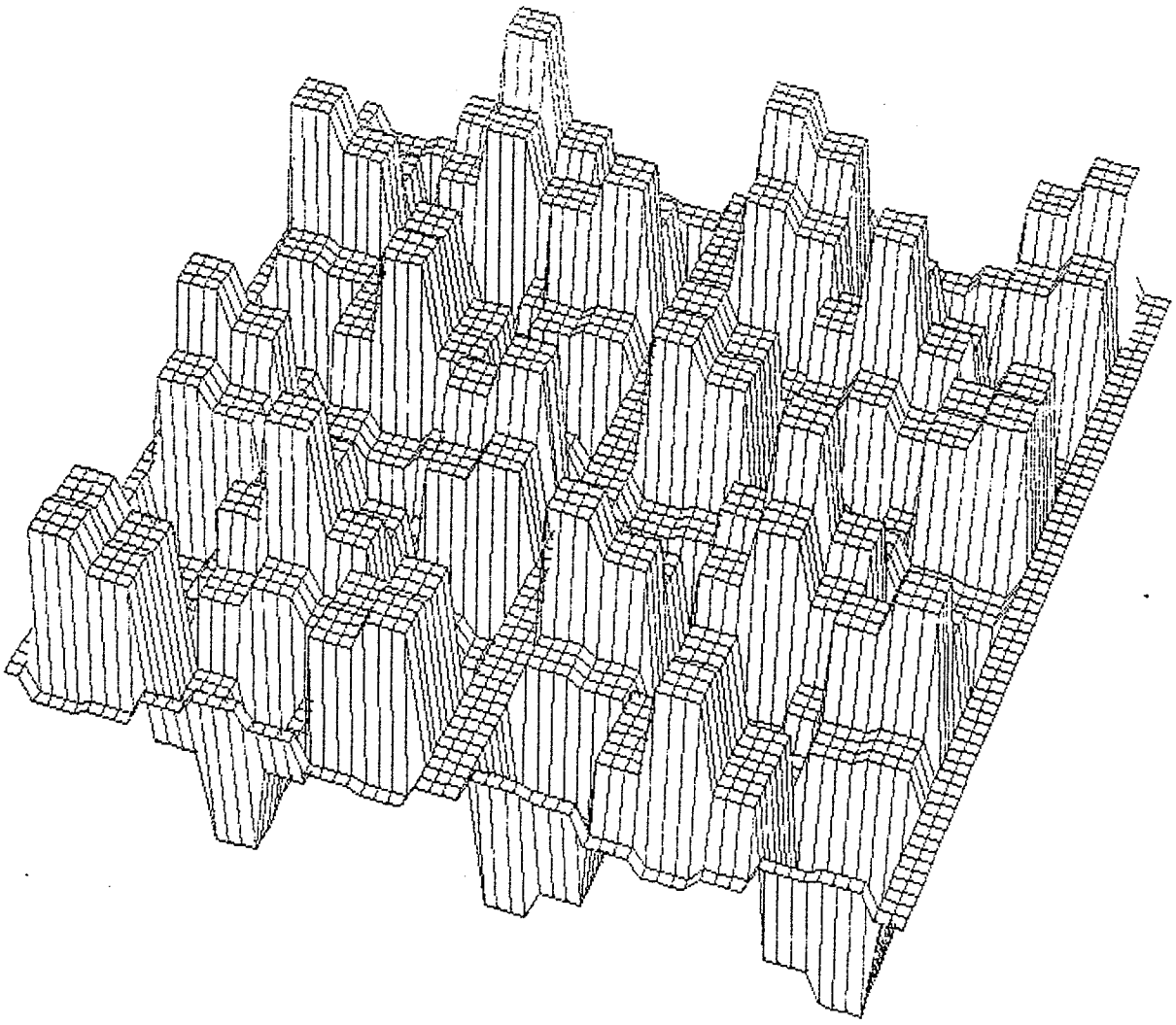

Figure 5.13. Simulated nearest neighbor wave field, with three cycles (n=3), and a phase offset (ϕ) of /10, on a 16x16 point array.

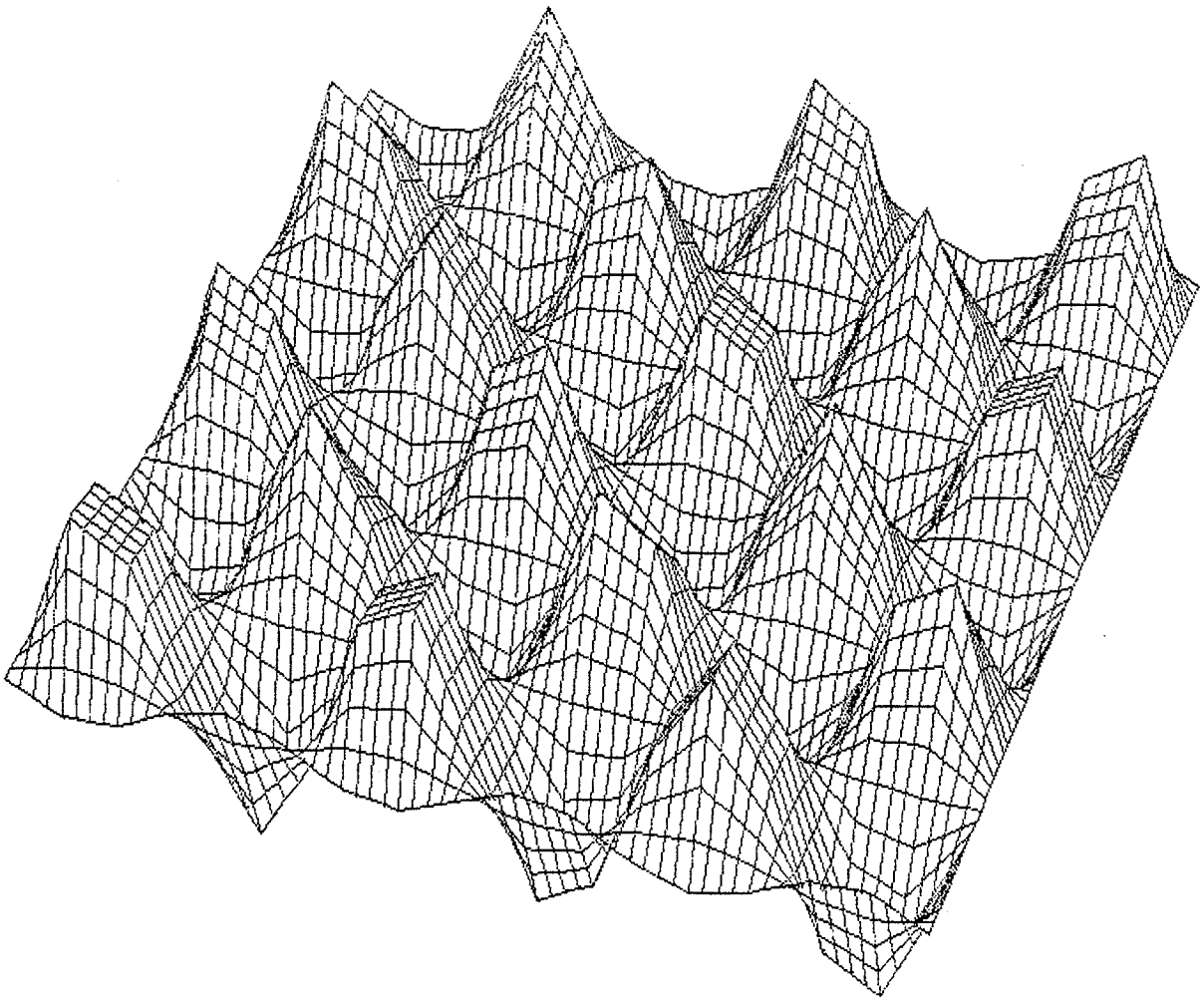

Figure 5.14. Simulated linear interpolated wave field, with three cycles (n=3), and a phase offset (ϕ) of /10, on a 16x16 point array.

APPENDIX A

ULTRASOUND SPEED

Ultrasound speed as a function of temperature for biological material. NR indicates data not reported. Values marked with an (*) were interpolated from graphes. Values marked with a (#) were estimated by the author (see text for details). Following each block of data are linear and quadratic (if 3 or more data points are available) least squares fits. The correlation coefficient (r=...), the estimated variance of the data with respect to the fit (var=...), the probability that random data could have produced such a linear fit (P_r=...), and the probability that noise could have accounted for the change in χ^2 between the linear and the quadratic fits (P_F=...) are provided. See Chapter 5 for a more detailed explanation of these statistical parameters. The standard deviations of the coefficients of the fits are included in parentheses under the coefficients. References marked m*1 or m*2 were measurements made by m, but the data were taken from Goss et al. (1978) or Goss et al. (1980), respectively.

Tissue/Material

species state/age	freq MHz	temp °C	speed m/s	(dev)	thermal coef m/s/°C	ref
Blood						
human						
fresh,	5	25	1565 *		2.20 #	Kikuchi
heparinized,		30	1576 *		1.40 #	et al.
whole, 40% hct		40	1590 *			(1972)*1
= 1525.42859 + 1.62857*T					r=0.993	P_r=0.077
(6.38877) (0.19795)					var=4.57143	
= 1470.00000 + 5.13333*T - 0.05333*T^2					r=1.000	
(0.00000) (0.00000) (0.00000)					var=0.00000	

Blood

human						
fresh, heparinized	5	26.8 40.5	1569.3 1587.1 #		1.3	Bakke et al. (1975)*1
= 1534.47974 + 1.29926*T (0.00000) (0.00000)					r=1.000 var=0.00000	
human						
< 21 days	1-15	27 44	1557 * 1582.2 #		1.48	Bradley & Sacerio (1972)*1
= 1516.97656 + 1.48235*T (0.00000) (0.00000)					r=1.000 var=0.00000	
human						
heparinized	2	22.4 22.6 23.2 24.2	1565 1570 1549.6 1556.4	(8%) (1.5%) (0.7%) (0.3%)	25.0 # 6.80 #	van Venrooij (1971)*1
= 1719.35681 - 6.88774*T (144.32841) (6.24512)					r=0.615 var=76.44297	P_r=0.385
= 9317.34473 - 659.15070*T + 13.98481*T^2 (6952.74707) (596.78369) (12.79467)					r=0.847 var=69.66178	P_F=0.50
human						
fresh, plasma	5	25 30 35 40	1522 * 1534 * 1541 * 1550 *		2.40 # 1.40 # 1.80 #	Kikuchi et al. (1972)*1
= 1477.59998 + 1.82000*T (4.52161) (0.13711)					r=0.994 var=2.35000	P_r=0.006
= 1446.84998 + 3.77000*T - 0.03000*T^2 (32.41801) (2.03963) (0.03130)					r=0.997 var=2.45000	P_F>0.50
human						
NR, albumen 12.5 %	NR	10 20 30 40	1500 * 1525 * 1550 * 1570 *		2.50 # 2.50 # 2.00 #	Carstensen et al. (1953).
= 1477.50000 + 2.35000*T (2.37171) (0.08660)					r=0.999 var=3.75000	P_r=0.001
= 1471.25000 + 2.97500*T - 0.01250*T^2 (3.11247) (0.28395) (0.00559)					r=1.000 var=1.25000	P_F=0.50

Blood

NR, albumen 6.2 %	NR	10	1475 *		3.00 #	"
		20	1505 *		2.50 #	
		30	1530 *		2.00 #	
		40	1550 *			

$= 1452.50000 + 2.50000*T$ r=0.996 $P_r=0.004$
(4.33013) (0.15811) var=12.50000
$= 1440.00000 + 3.75000*T - 0.02500*T^2$ r=1.000
(0.00000) (0.00000) (0.00000) var=0.00000 $P_F=0.000$

canine fresh, heparinized, 26% hct	5	25	1541 *		3.00 #	Kikuchi
		30	1556 *		1.00 #	et al.
		35	1561 *		1.80 #	(1972)*1
		40	1570 *			

$= 1497.19995 + 1.84000*T$ r=0.979 $P_r=0.021$
(9.04323) (0.27423) var=9.40000
$= 1435.69995 + 5.74000*T - 0.06000*T^2$ r=0.989
(64.83602) (4.07926) (0.06261) var=9.80000 $P_F>0.50$

Breast, fat with parenchyma

human excised	NR	22.5	1494.7	(4.1)	-2.18 #	Rajagopalan
		25.8	1487.5	(5.5)	2.00 #	et al.
		27.8	1491.5	(5.5)	2.63 #	(1979).
		30.2	1497.8	(5.7)	1.55 #	
		32.2	1500.9	(6.2)	-10.2 #	
		35.1	1471.3	(9.7)	0.00 #	
		38.0	1471.3	(13.1)	1.38 #	
		40.1	1474.2	(13.4)	0.71 #	
		42.5	1475.9	(12.8)		

$= 1526.23474 - 1.26109*T$ r=0.717 $P_r=0.030$
(15.42494) (0.46312) var=78.67373
$= 1475.94836 + 1.93783*T - 0.04893*T^2$ r=0.734
(89.75390) (5.63661) (0.08590) var=87.07650 $P_F>0.50$

Breast, parenchyma

Breast, parenchyma
---

human							
excised	NR	22.5	1539.4	(4.5)	1.91	#	Rajagopalan
		25.8	1545.7	(4.0)	2.65	#	et al.
		27.8	1551	(4.6)	2.96	#	(1979).
		30.2	1558.1	(3.9)	2.00	#	
		32.2	1562.1	(4.1)	0.83	#	
		35.1	1564.5	(7.6)	-0.07	#	
		38.0	1564.3	(6.4)	2.52	#	
		40.1	1569.6	(6.3)	0.96	#	
		42.5	1571.9	(6.4)			

= 1507.02905 + 1.57491*T r=0.968 P_r=0.000
(5.11747) (0.15365) var=8.65950
= 1448.29797 + 5.31104*T - 0.05715*T^2 r=0.989
(18.44787) (1.15854) (0.01766) var=3.67864 P_F=0.025

Cerebrospinal Fluid
---

human							
fresh	2	24.4	1515	(3.0%)	-9.17	#	van Venrooij
		25.0	1509.5	(0.5%)			(1971)*1

= 1738.66650 - 9.16666*T r=1.000
(0.00000) (0.00000) var=0.00000

Eye
---

human							
p. m.	2.5	29	1560		1.50	#	Tschewnenko
		37	1572	(5)			(1965)*1

= 1516.50000 + 1.50000*T r=1.000
(0.00000) (0.00000) var=0.00000

Eye, aqueous humor
---

porcine							
8 hrs.	4	4	1462.51	(2.13)	2.22	#	Rivara &
p. m.		15	1486.94	(2.48)	2.03	#	Sanna
		25	1507.25	(2.86)	1.87	#	(1962)*1
		37	1529.63	(3.08)			

= 1455.43494 + 2.03198*T r=0.999 P_r=0.001
(1.39917) (0.05919) var=2.08381
= 1453.17261 + 2.37152*T - 0.00826*T^2 r=1.000
(0.11157) (0.01299) (0.00031) var=0.00574 P_F=0.025

Eye, cornea

Eye, cornea

human					
24-48 hrs.	4	4	1542.03 (4.05)	1.42 #	Rivara &
p. m.		15	1557.64 (4.13)	1.23 #	Sanna
		25	1569.91 (3.76)	1.37 #	(1962)*1
		37	1586.38 (3.87)		
$= 1536.97852 + 1.33390*T$				r=1.000	$P_r=0.000$
(0.56616)	(0.02395)			var=0.34119	
$= 1536.73975 + 1.36973*T - 0.00087*T^2$				r=1.000	
(1.17462)	(0.13671)	(0.00323)		var=0.63605	$P_F>0.50$
porcine					
8 hrs.	4	4	1537.68 (4.02)	1.56 #	Rivara &
p. m.		15	1554.86 (3.88)	1.36 #	Sanna
		25	1568.43 (4.10)	1.62 #	(1962)*1
		37	1587.92 (3.53)		
$= 1531.66833 + 1.50885*T$				r=0.999	$P_r=0.001$
(0.81488)	(0.03447)			var=0.70681	
$= 1532.14648 + 1.43708*T + 0.00175*T^2$				r=1.000	
(1.63192)	(0.18993)	(0.00448)		var=1.22769	$P_F>0.50$

Eye, lens

human					
24-48 hrs.	4	4	1617.51 (4.01)	1.13 #	Rivara &
p. m.		15	1629.98 (2.98)	0.89 #	Sanna
		25	1638.84 (3.17)	0.69 #	(1962)*1
		37	1647.11 (3.53)		
$= 1615.25842 + 0.89390*T$				r=0.993	$P_r=0.007$
(1.74670)	(0.07389)			var=3.24754	
$= 1612.43677 + 1.31740*T - 0.01030*T^2$				r=1.000	
(0.21206)	(0.02468)	(0.00058)		var=0.02073	$P_F=0.05$
human					
30-40 hrs.	2.5	29	1638.2	1.10 #	Tschewnenko
p. m.		37	1647		(1965)*1
$= 1606.29980 + 1.10001*T$				r=1.000	
(0.00000)	(0.00000)			var=0.00000	
porcine					
fresh,	4	23	1642.61	1.00	Jansson &
within 2.5 hrs.		37	1656.61 #		Sundmark
					(1961)*1
$= 1619.60999 + 1.00000*T$				r=1.000	
(0.00000)	(0.00000)			var=0.00000	

Eye, lens

porcine					
8 hrs.	4	4	1638.71 (3.65)	1.25 #	Rivara &
p. m.		15	1652.42 (3.5)	0.98 #	Sanna
		25	1662.20 (3.72)	0.88 #	(1962)*1
		37	1672.75 (3.12)		

$= 1635.75854 + 1.02525*T$ (1.45586) (0.06159) — r=0.996, var=2.25610, $P_r=0.004$

$= 1633.44934 + 1.37184*T - 0.00843*T^2$ (0.61772) (0.07189) (0.00170) — r=1.000, var=0.17590, $P_F=0.25$

Eye, sclera

human					
24-48 hrs.	4	4	1609.12 (3.76)	1.18 #	Rivara &
p. m.		15	1622.06 (4.25)	1.31 #	Sanna
		25	1635.12 (3.71)	0.97 #	(1962)*1
		37	1646.75 (3.94)		

$= 1604.91016 + 1.15320*T$ (1.14167) (0.04830) — r=0.998, var=1.38739, $P_r=0.002$

$= 1603.51050 + 1.36327*T - 0.00511*T^2$ (1.60112) (0.18634) (0.00440) — r=0.999, var=1.18178, $P_F=0.50$

porcine					
8 hrs.	4	4	1616.07 (4.14)	1.44 #	Rivara &
p. m.		15	1631.92 (4.01)	1.22 #	Sanna
		25	1644.12 (3.92)	0.97 #	(1962)*1
		37	1655.76 (3.86)		

$= 1612.62891 + 1.20191*T$ (1.85673) (0.07855) — r=0.996, var=3.66957, $P_r=0.004$

$= 1609.62500 + 1.65274*T - 0.01096*T^2$ (0.06285) (0.00731) (0.00017) — r=1.000, var=0.00182, $P_F=0.025$

Eye, vitreous humor

human					
24-48 hrs.	4	4	1458.91 (1.95)	2.01 #	Rivara &
p. m.		15	1481.02 (1.86)	1.87 #	Sanna
		25	1499.76 (2.05)	1.95 #	(1962)*1
		37	1523.20 (2.14)		

$= 1451.40344 + 1.94168*T$ (0.40291) (0.01704) — r=1.000, var=0.17279, $P_r=0.000$

$= 1451.07959 + 1.99029*T - 0.00118*T^2$ (0.75141) (0.08745) (0.00206) — r=1.000, var=0.26029, $P_F>0.50$

Eye, vitreous humor

bovine							
< 10 days	5	27.0	1495		-5.00	#	Begui (1954)
stored @ 0-5°C		27.4	1493	(0.5%)	52.5	#	
		27.8	1514	(0.4%)	11.7	#	
		29.6	1535	(2%)			

$= 1054.62036 + 16.26582*T$ r=0.952 $P_r=0.048$
(103.25042) (3.69178) var=53.83549
$=-1237.58313 + 177.99014*T - 2.84840*T^2$ r=0.957
(6734.42334) (475.06668) (8.36675) var=96.48791 $P_F>0.50$

porcine						
fresh,	4	23	1468.95	1.81	Jansson &	
within 2.5 hrs.		37	1494.29 #		Sundmark	
					(1961)*1	

$= 1427.31982 + 1.81001*T$ r=1.000
(0.00000) (0.00000) var=0.00000

porcine							
8 hrs.	4	4	1463.88	(2.27)	2.19	#	Rivara &
p. m.		15	1487.94	(2.56)	1.82	#	Sanna
		25	1506.12	(3.10)	2.95	#	(1962)*1
		37	1541.53	(2.94)			

$= 1453.05286 + 2.31183*T$ r=0.995 $P_r=0.005$
(3.96925) (0.16792) var=16.77001
$= 1458.17346 + 1.54331*T + 0.01869*T^2$ r=0.998
(5.14824) (0.59917) (0.01415) var=12.21825 $P_F=0.50$

Fat
---

bovine						
fresh	1-7	20	1581	(1%)	-10.1	Bamber & Hill
		37	1430		-7.4	(1979).

$= 1758.64709 - 8.88235*T$ r=1.000
(0.00000) (0.00000) var=0.00000

Fat, breast

Fat, breast

human

excised	NR	22.5	1480.7	(2.5)	-4.18 #	Rajagopalan
		25.8	1466.9	(9.9)	2.60 #	et al.
		27.8	1472.1	(9.8)	2.21 #	(1979).
		30.2	1477.4	(9.9)	0.35 #	
		32.2	1478.1	(11.4)	-14.4 #	
		35.1	1436.3	(15.6)	-0.24 #	
		38.0	1435.6	(18.4)	1.48 #	
		40.1	1438.7	(18.1)	1.29 #	
		42.5	1441.8	(17.5)		

= 1538.19543 - 2.43426*T r=0.827 P_r=0.006
(20.82912) (0.62538) var=143.45807
= 1506.05652 - 0.38977*T - 0.03127*T^2 r=0.829
(123.71671) (7.76950) (0.11840) var=165.4440 P_F>0.50

Fat, orbital

human

< 2 days	6-14	20	1582	(20.4)	-7.06 #	Buschmann
p. m.		37	1462	(23.7)		et al.
						(1970)*1

= 1723.17651 - 7.05882*T r=1.000
(0.00000) (0.00000) var=0.00000

Fat, peritoneal

bovine

fresh	10	10	1680 *	(1%)	-10.5 #	Bamber & Hill
		20	1575 *		-8.50 #	(1979)*2
		30	1490 *		-7.14 #	
		44	1390 *		-2.81 #	
		60	1345 *			

= 1716.88586 - 6.73433*T r=0.976 P_r=0.005
(32.55093) (0.87396) var=1189.10583
= 1810.73828 - 13.89282*T + 0.10160*T^2 r=1.000
(10.87792) (0.72854) (0.01012) var=34.70859 P_F=0.01

Fat, stomach

canine

fresh	5	35	1455 *		-2.56 #	Nasoni et al.
		44	1432 *			(1979).

= 1544.44446 - 2.55556*T r=1.000
(0.00000) (0.00000) var=0.00000

Fat, stomach

canine						
fresh	5	37	1411.9		-2.89	Bowen et al.
		40	1403.2 #		-2.85	(1979).
		43	1394.7 #		-2.86	

$= 1517.93384 - 2.86668*T$ (0.77152) (0.01925) r=1.000 var=0.00667 $P_r=0.004$

$= 1535.65137 - 3.75589*T + 0.01112*T^2$ (0.00000) (0.00000) (0.00000) r=1.000 var=0.00000

refrig.	5	37	1412.9		-3.43	"
5 hrs.		40	1402.6 #		-2.86	
		43	1394.0 #		-2.91	

$= 1529.16687 - 3.15000*T$ (6.55584) (0.16359) r=0.999 var=0.48171 $P_r=0.033$

$= 1679.71777 - 10.70588*T + 0.09445*T^2$ (0.00000) (0.00000) (0.00000) r=1.000 var=0.00000

Heart

canine						
fresh	5	35	1592 *		1.25 #	Nasoni et al.
		43	1602 *			(1979).

$= 1548.25000 + 1.25000*T$ (0.00000) (0.00000) r=1.000 var=0.00000

Kidney

human						
excised	NR	17.0	1508.5	(4.3)	3.06 #	Rajagopalan
		22.0	1523.8	(4.6)	8.20 #	et al.
		23.5	1536.1	(2.1)	0.07 #	(1979).
		26.2	1536.3	(5.2)	2.23 #	
		30.2	1545.2	(2.7)	2.07 #	
		33.2	1551.4	(1.4)	2.20 #	
		35.2	1555.8	(1.8)	2.20 #	
		37.2	1560.2	(1.8)	1.33 #	
		39.0	1562.6	(1.2)	0.94 #	
		40.8	1564.3	(0.9)		

$= 1476.08374 + 2.24569*T$ (4.76592) (0.15197) r=0.982 var=13.27208 $P_r=0.000$

$= 1436.70422 + 5.12553*T - 0.04907*T^2$ (13.97224) (0.99656) (0.01688) r=0.992 var=6.87112 $P_F=0.025$

canine						
in vivo	5	38.5	1566.6		1.27	Nasoni et al.
			1580.7		1.18	(1979).
			1569.9		1.17	
			1568.6		1.14	

Kidney

canine						
fresh	5	37	1570.2		1.35	Bowen et al.
		40	1574.3	#	1.16	(1979).
		43	1577.7	#	0.98	

$= 1524.06665 + 1.25000*T$ r=0.999 $P_r=0.034$
(2.70010) (0.06738) var=0.08171
$= 1462.06042 + 4.36198*T - 0.03890*T^2$ r=1.000
(0.00000) (0.00000) (0.00000) var=0.00000

37	1566.5		1.29	"	
40	1570.4	#	1.11		
43	1573.7	#	0.93		

$= 1522.20032 + 1.19999*T$ r=0.999 $P_r=0.031$
(2.31410) (0.05774) var=0.06002
$= 1469.05835 + 3.86709*T - 0.03334*T^2$ r=1.000
(0.00000) (0.00000) (0.00000) var=0.00000

37	1571.1		1.29	"	
40	1575.0	#	1.11		
43	1578.3	#	0.94		

$= 1526.79956 + 1.20001*T$ r=0.999 $P_r=0.031$
(2.31363) (0.05773) var=0.06000
$= 1473.66833 + 3.86657*T - 0.03333*T^2$ r=1.000
(0.00000) (0.00000) (0.00000) var=0.00000

canine						
fresh	5	38.5	1588.4		1.30	Nasoni et al.
5-30 min.			1579.6		1.30	(1979).
			1580.2		1.28	
			1584.5		1.05	
		35	1576	*	1.22 #	"
		44	1587	*		

$= 1533.22217 + 1.22222*T$ r=1.000
(0.00000) (0.00000) var=0.00000

Liver

human						
p. m.	1-7	20	1584	(1%)	1.86	Bamber & Hill
		37	1607		0.96	(1979).

$= 1556.94116 + 1.35294*T$ r=1.000
(0.00000) (0.00000) var=0.00000

Liver

human						
p. m.	10	5	1550 *	(1%)	1.71 #	Bamber & Hill
		12	1562 *		2.89 #	(1979)*2
		21	1588 *		1.33 #	
		30	1600 *		1.14 #	
		37	1608 *		0.33 #	
		43	1610 *		0.50 #	
		47	1612 *			

$= 1547.75684 + 1.51642*T$ (5.56956) (0.17692) r=0.968 $P_r=0.000$ var=47.10454

$= 1532.47546 + 3.22491*T - 0.03261*T^2$ (3.74734) (0.34138) (0.00637) r=0.996 var=7.79571 $P_F=0.01$

human						
excised	NR	17.0	1547.0	(2.5)	1.70 #	Rajagopalan
		22.0	1555.5	(1.8)	5.07 #	et al.
		23.5	1563.1	(3.0)	0.56 #	(1979).
		26.2	1564.6	(2.8)	1.63 #	
		30.2	1571.1	(2.5)	0.80 #	
		33.2	1573.5	(1.8)	0.90 #	
		35.2	1575.3	(2.5)	1.40 #	
		37.2	1578.1	(2.9)	1.06 #	
		39.0	1580.0	(2.2)	0.94 #	
		40.8	1581.7	(1.5)		

$= 1526.71228 + 1.38934*T$ (2.94912) (0.09404) r=0.982 $P_r=0.000$ var=5.08193

$= 1500.59631 + 3.29922*T - 0.03254*T^2$ (7.83169) (0.55859) (0.00946) r=0.993 var=2.15877 $P_F=0.025$

bovine						
fresh	1-7	20	1575	(1%)	1.83	Bamber & Hill
		37	1597		0.56	(1979).

$= 1549.11768 + 1.29412*T$ (0.00000) (0.00000) r=1.000 var=0.00000

		20	1627		1.01	"
		37	1639		0.31	

$= 1612.88232 + 0.70588*T$ (0.00000) (0.00000) r=1.000 var=0.00000

Liver

bovine						
fresh	10	8	1610 *	(1%)	1.15 #	Bamber & Hill
<30 min.		21	1625 *		0.94 #	(1979)*2
		37	1640 *		0.20 #	
		42	1641 *		-0.85 #	
		55	1630 *			
$= 1612.34912 + 0.51690*T$					r=0.749	$P_r=0.145$
(9.64091) (0.26410)					var=94.10490	
$= 1590.85632 + 2.45095*T - 0.03119*T^2$					r=0.982	
(5.65571) (0.41858) (0.00658)					var=11.54875	$P_F=0.05$
		9	1545 *		2.27 #	"
		20	1570 *		2.00 #	
		30	1590 *		0.77 #	
		43	1600 *		4.09 #	
		65	1690 *			
$= 1516.76331 + 2.46218*T$					r=0.969	$P_r=0.007$
(13.99537) (0.36245)					var=246.60487	
$= 1544.70532 + 0.39705*T + 0.02752*T^2$					r=0.987	
(20.38579) (1.29215) (0.01678)					var=157.7544	$P_F=0.25$
canine						
fresh	5	38.5	1598.3		1.26	Nasoni et al.
5-30 minutes			1604.3		1.15	(1979).
			1603.3		1.06	
		35	1599 *		1.13 #	"
		43	1608 *			
$= 1559.62500 + 1.12500*T$					r=1.000	
(0.00000) (0.00000)					var=0.00000	
fresh	5	37	1591.7		0.93	Bowen et al.
		40	1594.5 #		0.78	(1979).
		43	1596.8 #		0.62	
$= 1560.33264 + 0.85002*T$					r=0.998	$P_r=0.036$
(1.92811) (0.04811)					var=0.04167	
$= 1516.05493 + 3.07224*T - 0.02778*T^2$					r=1.000	
(0.00000) (0.00000) (0.00000)					var=0.00000	
		37	1594.8		1.13	"
		40	1598.2 #		0.96	
		43	1601.1 #		0.80	
$= 1556.03381 + 1.04999*T$					r=0.999	$P_r=0.029$
(1.92764) (0.04810)					var=0.04165	
$= 1511.76685 + 3.27167*T - 0.02777*T^2$					r=1.000	
(0.00000) (0.00000) (0.00000)					var=0.00000	

Liver

			37	1604.0	0.99	"
			40	1607.0 #	0.72	
			43	1609.1 #	0.46	
= 1572.70020 + 0.85000*T					r=0.995	P_r=0.065
(3.47068) (0.08660)					var=0.13501	
= 1492.99805 + 4.85010*T - 0.05000*T^2					r=1.000	
(0.00000) (0.00000) (0.00000)					var=0.00000	
porcine						
homogenate	4	5.5	1490	(.2%)	4.33 #	Danckwerts
		8.5	1503		5.43 #	(1974)*1
		12.0	1522		1.71 #	
		15.5	1528		2.00 #	
		16.5	1530		3.33 #	
		18.0	1535		3.75 #	
		18.8	1538		1.48 #	
		21.5	1542		2.78 #	
		23.3	1547		2.00 #	
		25.8	1552		5.71 #	
		27.2	1560		37.5 #	
		28.8	1620		33.3 #	
		30.0	1660			
= 1450.55554 + 5.05083*T					r=0.854	P_r=0.000
(19.18531) (0.92632)					var=613.35309	
= 1518.47864 - 3.88037*T + 0.24429*T^2					r=0.906	
(34.40061) (4.05404) (0.10875)					var=448.4181	P_F=0.05
Milk						
bovine						
whole,	NR	10	1488 *		2.10 #	Fitzgerald
8% non-fat		20	1509 *		1.90 #	et al.
solids,		30	1528 *		1.50 #	(1961)*2
4% butter fat		40	1543 *		1.00 #	
		50	1553 *			
= 1475.00000 + 1.64000*T					r=0.991	P_r=0.001
(4.24735) (0.12806)					var=16.40000	
= 1462.00000 + 2.75429*T - 0.01857*T^2					r=1.000	
(1.45012) (0.11051) (0.00181)					var=0.45714	P_F=0.01
skimmed,	NR	10	1483 *		3.30 #	"
8% non-fat		20	1516 *		2.40 #	
solids		30	1540 *		1.40 #	
		40	1554 *		0.60 #	
		50	1560 *			
= 1473.00000 + 1.92000*T					r=0.963	P_r=0.009
(10.36147) (0.31241)					var=97.60000	
= 1441.00000 + 4.66286*T - 0.04571*T^2					r=1.000	
(0.72506) (0.05525) (0.00090)					var=0.11429	P_F=0.001

Muscle, breast

Muscle, breast

human						
excised	NR	22.5	1543.1	(5.2)	2.52 #	Rajagopalan
		25.8	1551.4	(6.2)	1.40 #	et al.
		27.8	1554.2	(6.5)	3.42 #	(1979).
		30.2	1562.4	(7.1)	1.55 #	
		32.2	1565.5	(6.4)	0.48 #	
		35.1	1566.9	(4.5)	1.31 #	
		38.0	1570.7	(6.9)	1.86 #	
		40.1	1574.6	(6.7)	2.04 #	
		42.5	1579.5	(5.4)		

= 1507.52527 + 1.70147*T r=0.984 P_r=0.000
(3.82308) (0.11479) var=4.83293
= 1471.42529 + 3.99794*T - 0.03513*T^2 r=0.991
(17.23627) (1.08245) (0.01650) var=3.21130 P_F=0.10

Muscle, external to eye

human						
< 2 days	6-14	20	1612	(12.5)	1.12 #	Buschmann
p. m.		37	1631	(15.3)		et al. (1970)*1

= 1589.64709 + 1.11765*T r=1.000
(0.00000) (0.00000) var=0.00000

Muscle, psoas

human						
excised	NR	17.0	1542.5	(3.0)	-16.6 #	Rajagopalan
		22.0	1459.5	(3.0)	63.5 #	et al.
		23.5	1554.8	(1.1)	2.00 #	(1979).
		26.2	1560.2	(1.7)	1.55 #	
		30.2	1566.4	(2.2)	1.73 #	
		33.2	1571.6	(1.8)	0.95 #	
		35.2	1573.5	(1.8)	1.05 #	
		37.2	1575.6	(1.1)	1.11 #	
		39.0	1577.6	(2.1)	1.50 #	
		40.8	1580.3	(1.8)		

= 1467.26563 + 2.92259*T r=0.650 P_r=0.042
(37.86994) (1.20759) var=837.98065
= 1462.79175 + 3.24977*T - 0.00557*T^2 r=0.650
(164.94563) (11.76465) (0.19923) var=957.5851 P_F>0.50

Muscle, skeletal

Muscle, skeletal
---

canine						
fresh	5	38.5	1608.7	0.88	Nasoni et al.	
5-30 min.			1629.3	0.56	(1979).	
		35	1606 *	1.00 #	"	
		41	1612 *			
= 1571.00000 + 1.00000*T				r=1.000		
(0.00000) (0.00000)				var=0.00000		
canine						
fresh	5	37	1589.1	1.23	Bowen et al.	
		40	1592.8 #	1.03	(1979).	
		43	1595.9 #	0.82		
= 1547.26636 + 1.13334*T				r=0.999		P_r=0.032
(2.31410) (0.05774)				var=0.06002		
= 1494.12439 + 3.80044*T - 0.03334*T^2				r=1.000		
(0.00000) (0.00000) (0.00000)				var=0.00000		
		37	1603.3	1.13	"	
		40	1606.7 #	0.92		
		43	1609.5 #	0.71		
= 1565.16699 + 1.03333*T				r=0.998		P_r=0.036
(2.31316) (0.05772)				var=0.05997		
= 1512.04663 + 3.69934*T - 0.03333*T^2				r=1.000		
(0.00000) (0.00000) (0.00000)				var=0.00000		
		37	1588.8	1.16	"	
		40	1592.3 #	0.95		
		43	1595.1 #	0.78		
= 1550.06714 + 1.04999*T				r=0.998		P_r=0.041
(2.69963) (0.06736)				var=0.08168		
= 1488.07178 + 4.16142*T - 0.03889*T^2				r=1.000		
(0.00000) (0.00000) (0.00000)				var=0.00000		
		37	1591.6	1.08	"	
		40	1594.8 #	0.87		
		43	1597.5 #	0.65		
= 1555.29980 + 0.98334*T				r=0.999		P_r=0.031
(1.92858) (0.04812)				var=0.04169		
= 1511.01123 + 3.20610*T - 0.02778*T^2				r=1.000		
(0.00000) (0.00000) (0.00000)				var=0.00000		

Nervous Tissue, brain

Nervous Tissue, brain

---

human

fetal, spontaneous labor, gest.: 17 weeks	5	0	1435	2.13 #	Wladimiroff et al. (1975)*1
		8	1452	2.38 #	
		16	1471	2.38 #	
		24	1490	2.50 #	
		30	1505	2.14 #	
		37	1520		

$= 1434.22632 + 2.32732*T$ (0.59251) (0.02580) — r=1.000, var=0.63946, $P_r=0.000$

$= 1434.51428 + 2.26807*T + 0.00161*T^2$ (0.79797) (0.10070) (0.00262) — r=1.000, var=0.75779, $P_F>0.50$

fetal, 17 weeks	0	1435	2.75 #	"
	8	1457	2.25 #	
	16	1475	2.50 #	
	24	1495	2.50 #	
	30	1510	1.86 #	
	37	1523		

$= 1436.62964 + 2.39323*T$ (1.29698) (0.05647) — r=0.999, var=3.06401, $P_r=0.000$

$= 1435.11414 + 2.70518*T - 0.00846*T^2$ (1.10648) (0.13963) (0.00364) — r=1.000, var=1.45700, $P_F=0.25$

fetal, 18 weeks	0	1430	3.13 #	"
	8	1455	2.88 #	
	16	1478	1.50 #	
	24	1490	3.00 #	
	30	1508	1.29 #	
	37	1517		

$= 1434.67737 + 2.34727*T$ (3.46470) (0.15085) — r=0.992, var=21.86539, $P_r=0.000$

$= 1430.46509 + 3.21431*T - 0.02352*T^2$ (2.72681) (0.34411) (0.00896) — r=0.998, var=8.84874, $P_F=0.10$

fetal, 19 weeks	0	1433	3.25 #	"
	8	1459	3.25 #	
	16	1485	1.38 #	
	24	1496	2.00 #	
	30	1508	1.57 #	
	37	1519		

$= 1439.53430 + 2.28517*T$ (4.56546) (0.19878) — r=0.985, var=37.96592, $P_r=0.000$

$= 1433.43005 + 3.54163*T - 0.03408*T^2$ (2.58960) (0.32680) (0.00851) — r=0.998, var=7.98067, $P_F=0.05$

Nervous Tissue, brain

fetal,	0	1438	2.75 # "	
24 weeks	8	1460	2.50 #	
	16	1480	1.88 #	
	24	1495	2.50 #	
	30	1510	1.86 #	
	37	1523		

$= 1440.59412 + 2.28205*T$ (1.72042) (0.07491) r=0.998 var=5.39133 $P_r=0.000$

$= 1438.44116 + 2.72519*T - 0.01202*T^2$ (1.25829) (0.15879) (0.00414) r=0.999 var=1.88424 $P_F=0.10$

fetal,	0	1437	3.25 # "	
28 weeks	8	1463	3.00 #	
	16	1487	1.38 #	
	24	1498	2.33 #	
	30	1512	2.29 #	
	37	1528		

$= 1441.98877 + 2.37450*T$ (3.39697) (0.14790) r=0.992 var=21.01882 $P_r=0.000$

$= 1438.30627 + 3.13247*T - 0.02056*T^2$ (3.24187) (0.40911) (0.01066) r=0.997 var=12.50731 $P_F=0.25$

fetal,	0	1440	3.25 # "	
28 weeks	8	1466	2.38 #	
	16	1485	2.13 #	
	24	1502	2.17 #	
	30	1515	2.00 #	
	37	1529		

$= 1444.28796 + 2.35889*T$ (2.43151) (0.10587) r=0.996 var=10.76904 $P_r=0.000$

$= 1441.05432 + 3.02447*T - 0.01805*T^2$ (1.41814) (0.17896) (0.00466) r=0.999 var=2.39336 $P_F=0.05$

fetal,	0	1438	3.50 # "	
29 weeks	8	1466	2.50 #	
	16	1486	1.75 #	
	24	1500	2.67 #	
	30	1516	1.86 #	
	37	1529		

$= 1443.22986 + 2.39670*T$ (3.09124) (0.13459) r=0.994 var=17.40572 $P_r=0.000$

$= 1439.54016 + 3.15618*T - 0.02060*T^2$ (2.53179) (0.31950) (0.00832) r=0.998 var=7.62833 $P_F=0.10$

Nervous Tissue, brain

fetal,	0	1459	2.75 # "		
38 weeks	8	1481	2.25 #		
	16	1499	1.88 #		
	24	1514	3.00 #		
	30	1532	1.14 #		
	37	1540			

$= 1461.70081 + 2.21561*T$ (2.40568) (0.10474) r=0.996 var=10.54146 $P_r=0.000$

$= 1459.23206 + 2.72377*T - 0.01378*T^2$ (2.43924) (0.30782) (0.00802) r=0.998 var=7.08076 $P_F=0.25$

fetal,	0	1449	3.75 # "		
40 weeks	8	1479	3.13 #		
	16	1504	2.13 #		
	24	1521	1.83 #		
	30	1532	1.14 #		
	37	1540			

$= 1457.07288 + 2.45707*T$ (5.47128) (0.23822) r=0.982 var=54.52602 $P_r=0.000$

$= 1449.12500 + 4.09301*T - 0.04437*T^2$ (0.59024) (0.07449) (0.00194) r=1.000 var=0.41461 $P_F=0.001$

fetal,	0	1457	2.88 # "		
40 weeks	8	1480	3.00 #		
	16	1504	2.50 #		
	24	1524	1.00 #		
	30	1530	1.43 #		
	37	1540			

$= 1462.16394 + 2.27840*T$ (4.52261) (0.19691) r=0.985 var=37.25672 $P_r=0.000$

$= 1455.91675 + 3.56428*T - 0.03488*T^2$ (2.05286) (0.25906) (0.00675) r=0.999 var=5.01526 $P_F=0.025$

fetal, 5	0	1424	2.38 # "		
induced labor	8	1443	3.75 #		
gest.: 17 weeks	16	1473	2.50 #		
	24	1493	2.50 #		
	30	1508	1.43 #		
	37	1518			

$= 1425.58289 + 2.65655*T$ (3.64236) (0.15859) r=0.993 var=24.16522 $P_r=0.000$

$= 1421.55920 + 3.48475*T - 0.02247*T^2$ (3.39213) (0.42807) (0.01115) r=0.997 var=13.69357 $P_F=0.25$

Nervous Tissue, brain

fetal,	0	1435	3.13 #	"
17 weeks	8	1460	3.63 #	
	16	1489	2.25 #	
	24	1507	2.50 #	
	30	1522	1.14 #	
	37	1530		

$= 1439.94189 + 2.63781*T$ (4.56689) (0.19884) r=0.989 var=37.98985 $P_r=0.000$

$= 1433.68958 + 3.92477*T - 0.03491*T^2$ (2.23000) (0.28142) (0.00733) r=0.999 var=5.91811 $P_F=0.025$

fetal,	0	1433	3.00 #	"
17 weeks	8	1457	2.75 #	
	16	1479	3.38 #	
	24	1506	3.17 #	
	30	1525	1.00 #	
	37	1532		

$= 1434.78052 + 2.81145*T$ (3.68009) (0.16023) r=0.994 var=24.66852 $P_r=0.000$

$= 1431.39368 + 3.50858*T - 0.01891*T^2$ (4.07529) (0.51429) (0.01340) r=0.996 var=19.76467 $P_F=0.50$

fetal,	0	1441	3.25 #	"
18 weeks	8	1467	2.75 #	
	16	1489	3.13 #	
	24	1514	1.50 #	
	30	1523	0.71 #	
	37	1528		

$= 1446.78235 + 2.44614*T$ (5.36979) (0.23380) r=0.982 var=52.52194 $P_r=0.000$

$= 1439.56897 + 3.93091*T - 0.04027*T^2$ (2.96823) (0.37458) (0.00976) r=0.997 var=10.48495 $P_F=0.05$

fetal,	0	1443	3.63 #	"
18 weeks	8	1472	1.13 #	
	16	1481	1.00 #	
	24	1489	3.33 #	
	30	1509	2.86 #	
	37	1529		

$= 1446.73547 + 2.10945*T$ (4.87736) (0.21236) r=0.980 var=43.33062 $P_r=0.001$

$= 1447.88098 + 1.87366*T + 0.00640*T^2$ (6.87641) (0.86777) (0.02260) r=0.981 var=56.27245 $P_F>0.50$

Nervous Tissue, brain

fetal,	0	1447	3.50 #	"
18 weeks	8	1475	2.63 #	
	16	1496	2.00 #	
	24	1512	1.83 #	
	30	1523	1.57 #	
	37	1534		

$= 1453.52563 + 2.31171*T$ r=0.989 $P_r=0.000$
(3.99259) (0.17384) var=29.03582
$= 1447.84155 + 3.48167*T - 0.03174*T^2$ r=1.000
(1.21022) (0.15272) (0.00398) var=1.74301 $P_F=0.005$

fetal,	0	1441	4.25 #	"
19 weeks	8	1475	1.75 #	
	16	1489	2.38 #	
	24	1508	1.83 #	
	30	1519	1.57 #	
	37	1530		

$= 1449.29578 + 2.31500*T$ r=0.985 $P_r=0.000$
(4.71524) (0.20530) var=40.49800
$= 1443.44714 + 3.51886*T - 0.03265*T^2$ r=0.996
(3.53280) (0.44583) (0.01161) var=14.85291 $P_F=0.10$

fetal,	0	1437	3.75 #	"
20 weeks	8	1467	3.13 #	
	16	1492	2.00 #	
	24	1508	2.00 #	
	30	1520	1.43 #	
	37	1530		

$= 1444.62451 + 2.48916*T$ r=0.985 $P_r=0.000$
(4.97174) (0.21647) var=45.02385
$= 1437.48621 + 3.95847*T - 0.03985*T^2$ r=1.000
(1.20260) (0.15176) (0.00395) var=1.72114 $P_F=0.005$

fetal,	0	1440	2.38 #	"
21 weeks	8	1459	2.88 #	
	16	1482	2.75 #	
	24	1504	2.50 #	
	30	1519	2.00 #	
	37	1533		

$= 1440.05896 + 2.57953*T$ r=0.999 $P_r=0.000$
(1.48794) (0.06478) var=4.03270
$= 1438.77100 + 2.84464*T - 0.00719*T^2$ r=0.999
(1.70968) (0.21575) (0.00562) var=3.47857 $P_F=0.50$

Nervous Tissue, brain

fetal, induced labor, gest.: 21 weeks	5	0	1441	2.63 # "	
		8	1462	3.38 #	
		16	1489	2.38 #	
		24	1508	2.50 #	
		30	1523	1.57 #	
		37	1534		
$= 1443.27930 + 2.58543*T$				r=0.995	$P_r=0.000$
(2.96832)	(0.12924)			var=16.04900	
$= 1439.54871 + 3.35331*T - 0.02083*T^2$				r=0.999	
(2.14441)	(0.27062)	(0.00705)		var=5.47255	$P_F=0.10$
fetal, induced labor, gest.: 16 weeks	5	0	1427	2.63 # "	
		8	1448	3.25 #	
		16	1474	2.00 #	
		24	1490	2.33 #	
		30	1504	1.29 #	
		37	1513		
$= 1430.33911 + 2.38231*T$				r=0.992	$P_r=0.000$
(3.41357)	(0.14863)			var=21.22480	
$= 1425.82727 + 3.31100*T - 0.02519*T^2$				r=0.999	
(2.05063)	(0.25878)	(0.00674)		var=5.00435	$P_F=0.05$
fetal, 18 weeks	5	0	1440	2.50 # "	
		8	1460	2.88 #	
		16	1483	2.00 #	
		24	1499	1.33 #	
		30	1507	1.00 #	
		37	1514		
$= 1444.51257 + 2.05152*T$				r=0.985	$P_r=0.000$
(4.10791)	(0.17886)			var=30.73747	
$= 1438.78076 + 3.23132*T - 0.03200*T^2$				r=0.999	
(1.68713)	(0.21291)	(0.00555)		var=3.38744	$P_F=0.025$
canine fresh	5	35	1565 *	0.56 # Nasoni et al.	
		44	1570 *	(1979).	
$= 1545.55554 + 0.55556*T$				r=1.000	
(0.00000)	(0.00000)			var=0.00000	
canine fresh, white matter	5	37	1563.2	0.67 Bowen et al.	
		40	1565.2 #	0.62 (1979).	
		43	1567.1 #	0.26 ?62	
$= 1539.16650 + 0.65000*T$				r=1.000	$P_r=0.009$
(0.38553)	(0.00962)			var=0.00167	
$= 1530.31311 + 1.09434*T - 0.00555*T^2$				r=1.000	
(0.00000)	(0.00000)	(0.00000)		var=0.00000	

Nervous Tissue, brain

feline							
fresh	4.2	25	1558	*		0.80	# Robinson &
		30	1562	*		1.86	# Lele
		37	1575	*		-5.00	# (1972)*1
		40	1560	*		2.86	#
		47	1580	*		-2.25	#
		51	1571	*			

$= 1543.85913 + 0.62107*T$ r=0.684 $P_r=0.134$
(13.02776) (0.33083) var=53.33926
$= 1519.74707 + 1.96334*T - 0.01763*T^2$ r=0.700
(68.96774) (3.76931) (0.04927) var=68.20718 $P_F>0.50$

fresh	4.2	38	1568	*		-1.00	# "
		42	1564	*		1.80	#
		47	1573	*		1.00	#
		52	1578	*		0.00	#
		57	1578	*		-2.80	#
		62	1564	*		0.20	#
		67	1565	*			

$= 1571.70996 - 0.03279*T$ r=0.055 $P_r=0.907$
(14.11063) (0.26597) var=47.45571
$= 1430.65601 + 5.54592*T - 0.05323*T^2$ r=0.738
(65.45407) (2.56208) (0.02437) var=27.05433 $P_F=0.10$

Nervous Tissue, optic nerve

human						
< 2 days	6-14	20	1644	(25.4)	-1.71	# Buschmann
p. m.		37	1615	(3.1)		# et al. (1970)*1

$= 1678.11768 - 1.70588*T$ r=1.000
(0.00000) (0.00000) var=0.00000

Nervous Tissue, spinal cord

human						
excised	NR	17.0	1509.0	(4.5)	2.80	# Rajagopalan
		22.0	1523.0	(4.6)	0.00	# et al.
		23.5	1523.0	(5.3)	1.11	# (1979).
		26.2	1526.0	(3.0)	1.65	#
		30.2	1532.6	(3.2)	1.80	#
		33.2	1538.0	(2.6)	0.00	#
		35.2	1538.0	(3.5)	2.20	#
		37.2	1542.4	(3.3)	0.78	#
		39.0	1543.8	(3.0)	-48.5	#
		40.8	1456.5	(2.0)		

$= 1528.19653 - 0.16321*T$ r=0.051 $P_r=0.890$
(35.71491) (1.13887) var=745.32202
$= 1292.51050 + 17.07262*T - 0.29366*T^2$ r=0.592
(125.52821) (8.95323) (0.15162) var=554.5982 $P_F=0.10$

Spleen

Spleen

human						
excised	NR	17.0	1528.0	(1.8)	2.16 #	Rajagopalan
		22.0	1538.8	(1.8)	3.67 #	et al.
		23.5	1544.3	(1.8)	1.78 #	(1979).
		26.2	1549.1	(1.6)	1.83 #	
		30.2	1556.4	(2.0)	1.83 #	
		33.2	1561.9	(1.7)	-7.95 #	
		35.2	1546.0	(2.1)	10.6 #	
		37.2	1567.1	(2.3)	1.22 #	
		39.0	1569.3	(2.6)	2.06 #	
		40.8	1573.0	(2.1)		

$= 1502.27417 + 1.67978*T$ r=0.919 $P_r=0.000$
(7.99560) (0.25496) var=37.35487
$= 1494.45959 + 2.25127*T - 0.00974*T^2$ r=0.920
(34.69392) (2.47452) (0.04191) var=42.36454 $P_F>0.50$

canine						
fresh	5	37	1601.3		1.31	Bowen et al.
		40	1605.2 #		1.07	(1979).
		43	1608.4 #		0.84	

$= 1557.63354 + 1.18333*T$ r=0.998 $P_r=0.036$
(2.69869) (0.06734) var=0.08163
$= 1495.65979 + 4.29368*T - 0.03888*T^2$ r=1.000
(0.00000) (0.00000) (0.00000) var=0.00000

Water

-						
distilled	60	23.41	1492.27	(.1)	2.79 #	McSkimin
		23.79	1493.33		2.81 #	(1965).
		24.20	1494.48		2.56 #	
		24.63	1495.58		2.74 #	
		25.02	1496.65		2.69 #	
		25.41	1497.70		2.55 #	
		25.83	1498.77		2.54 #	
		28.00	1504.29		2.43 #	
		29.00	1506.72		2.46 #	
		29.93	1509.01		2.54 #	
		30.06	1509.34		2.12 #	
		31.00	1511.33		2.13 #	
		34.99	1519.81		1.80 #	
		40.00	1528.83		1.51 #	
		45.00	1536.36			

$= 1444.66577 + 2.09981*T$ r=0.995 $P_r=0.000$
(1.79421) (0.05985) var=1.99646
$= 1408.70215 + 4.36714*T - 0.03403*T^2$ r=1.000
(0.42018) (0.02619) (0.00039) var=0.00343 $P_F=0.001$

APPENDIX B

ULTRASOUND ATTENUATION COEFFICIENT

Ultrasound attenuation coefficient as a function of temperature for biological material. NR indicates data not reported. Values marked with an (*) were interpolated from graphes. Values marked with a (#) were estimated by the author (see text for details). Following each block of data are linear and quadratic (if 3 or more data points are available) least squares fits, as well as log-linear and log-quadratic fits. The correlation coefficient (r=...), the estimated variance of the data with respect to the fit (var=...), the probability that random data could have produced such a linear fit (P_r=...), and the probability that noise could have accounted for the change in χ^2 between the linear and the quadratic fits (P_F=...) are provided. See Chapter 5 for a more detailed explanation of these statistical parameters. The standard deviations of the coefficients of the fits are included in parentheses under the coefficients. References marked m*1 or m*2 were measurements made by m, but the data were taken from Goss et al. (1978) or Goss et al. (1980), respectively.

Tissue/Material species state/age	freq MHz	temp °C	atten coef dB/cm	(dev)	thermal coef dB/cm/°C *10^{-3}	ref
Blood						
human						
NR,	1	10	0.012 *		0.00 #	Carstensen
average of		20	0.012 *		-0.20 #	et al.
red cells,		30	0.01 *		-0.10 #	(1953).
HGB, albumin		40	0.009 *		#	/gm protein /100 cc
$= 0.01350 - 0.00011*T$					r=0.947	P_r=0.053
(0.00072) (0.00003)					var=0.00000	
$= 0.01225 + 0.00002*T + 0.00000*T^2$					r=0.966	
(0.00187) (0.00017) (0.00000)					var=0.00000	P_F>0.50
$\ln=-4.27901 - 0.01045*T$					r=0.948	P_r=0.052
(0.06784) (0.00248)					var=0.00307	
$\ln=-4.41071 + 0.00272*T - 0.00026*T^2$					r=0.972	
(0.16140) (0.01472) (0.00029)					var=0.00336	P_F>0.50
	2	10	0.025 *		-0.20 #	"
		20	0.023 *		-0.20 #	
		30	0.021 *		-0.20 #	
		40	0.019 *			
$= 0.02700 - 0.00020*T$					r=1.000	P_r=0.000
(0.00000) (0.00000)					var=0.00000	
$= 0.02700 - 0.00020*T + 0.00000*T^2$					r=1.000	
(0.00000) (0.00000) (0.00000)					var=0.00000	P_F>0.50
$\ln=-3.59335 - 0.00914*T$					r=0.999	P_r=0.001
(0.00724) (0.00026)					var=0.00003	
$\ln=-3.61423 - 0.00706*T - 0.00004*T^2$					r=1.000	
(0.00095) (0.00009) (0.00000)					var=0.00000	P_F=0.05
	3	10	0.036 *		-0.20 #	"
		20	0.034 *		-0.20 #	
		30	0.032 *		-0.20 #	
		40	0.03 *			
$= 0.03800 - 0.00020*T$					r=1.000	P_r=0.000
(0.00000) (0.00000)					var=0.00000	
$= 0.03800 - 0.00020*T + 0.00000*T^2$					r=1.000	
(0.00000) (0.00000) (0.00000)					var=0.00000	P_F=0.10
$\ln=-3.26165 - 0.00608*T$					r=1.000	P_r=0.000
(0.00320) (0.00012)					var=0.00001	
$\ln=-3.27088 - 0.00515*T - 0.00002*T^2$					r=1.000	
(0.00028) (0.00003) (0.00000)					var=0.00000	P_F=0.025

Blood

human						
NR,	1	10	0.013 *		-0.10 #	Carstensen
plasma		20	0.012 *		-0.20 #	et al.
		30	0.01 *		-0.10 #	(1953).
		40	0.009 *			
$= 0.01450 - 0.00014*T$					r=0.990	$P_r=0.010$
(0.00039) (0.00001)					var=0.00000	
$= 0.01450 - 0.00014*T + 0.00000*T^2$					r=0.990	
(0.00124) (0.00011) (0.00000)					var=0.00000	$P_F>0.50$
$\ln=-4.19896 - 0.01285*T$					r=0.989	$P_r=0.011$
(0.03640) (0.00133)					var=0.00088	
$\ln=-4.23061 - 0.00969*T - 0.00006*T^2$					r=0.990	
(0.11158) (0.01018) (0.00020)					var=0.00161	$P_F>0.50$
	2	10	0.028 *		-0.30 #	"
		20	0.025 *		-0.30 #	
		30	0.022 *		-0.30 #	
		40	0.019 *			
$= 0.03100 - 0.00030*T$					r=1.000	$P_r=0.000$
(0.00000) (0.00000)					var=0.00000	
$= 0.03100 - 0.00030*T + 0.00000*T^2$					r=1.000	
(0.00000) (0.00000) (0.00000)					var=0.00000	$P_F>0.50$
$\ln=-3.43833 - 0.01291*T$					r=0.998	$P_r=0.002$
(0.01443) (0.00053)					var=0.00014	
$\ln=-3.47993 - 0.00875*T - 0.00008*T^2$					r=1.000	
(0.00266) (0.00024) (0.00000)					var=0.00000	$P_F=0.05$
	3	10	0.046 *		-0.80 #	"
		20	0.038 *		-0.40 #	
		30	0.034 *		-0.40 #	
		40	0.03 *			
$= 0.05000 - 0.00052*T$					r=0.983	$P_r=0.017$
(0.00190) (0.00007)					var=0.00000	
$= 0.05500 - 0.00102*T + 0.00001*T^2$					r=0.997	
(0.00249) (0.00023) (0.00000)					var=0.00000	$P_F=0.50$
$\ln=-2.96092 - 0.01394*T$					r=0.992	$P_r=0.008$
(0.03382) (0.00123)					var=0.00076	
$\ln=-2.87855 - 0.02217*T + 0.00016*T^2$					r=0.998	
(0.05837) (0.00532) (0.00010)					var=0.00044	$P_F=0.50$

Blood

canine							
fresh,	0.58	30	0.11	*	-2.00	#	Yosioka
citrated		40	0.09	*			et al. (1969)*1

= 0.17000 - 0.00200*T r=1.000
(0.00000) (0.00000) var=0.00000

ln=-1.60526 - 0.02007*T r=1.000
(0.00000) (0.00000) var=0.00000

0.97	30	0.165	*	-0.50	#	"
	40	0.16	*			

= 0.18000 - 0.00050*T r=1.000
(0.00000) (0.00000) var=0.00000

ln=-1.70949 - 0.00308*T r=1.000
(0.00000) (0.00000) var=0.00000

1.8	30	0.3	*	-1.00	#	"
	40	0.29	*			

= 0.33000 - 0.00100*T r=1.000
(0.00000) (0.00000) var=0.00000

ln=-1.10227 - 0.00339*T r=1.000
(0.00000) (0.00000) var=0.00000

3.0	30	0.6	*	-2.00	#	"
	40	0.58	*			

= 0.66000 - 0.00200*T r=1.000
(0.00000) (0.00000) var=0.00000

ln=-0.40912 - 0.00339*T r=1.000
(0.00000) (0.00000) var=0.00000

4.8	30	1.15	*	-5.00	#	"
	40	1.1	*			

= 1.30000 - 0.00500*T r=1.000
(0.00000) (0.00000) var=0.00000

ln= 0.27312 - 0.00445*T r=1.000
(0.00000) (0.00000) var=0.00000

Blood

NR							
plasma	1.2	20	0.08		-0.50	#	Schwan & Carstensen (1952)*1
		40	0.07				
= 0.09000 - 0.00050*T					r=1.000		
(0.00000) (0.00000)					var=0.00000		
ln=-2.39220 - 0.00668*T					r=1.000		
(0.00000) (0.00000)					var=0.00000		
	2.4	20	0.16		-1.50	#	"
		40	0.13				
= 0.19000 - 0.00150*T					r=1.000		
(0.00000) (0.00000)					var=0.00000		
ln=-1.62494 - 0.01038*T					r=1.000		
(0.00000) (0.00000)					var=0.00000		

Bone

equine							
NR	1.43	10	28.5	*	150.0	#	Kishimoto (1958)*1
		20	30	*	100.0	#	
		30	31	*	200.0	#	
		40	33	*	200.0	#	
		50	35	*			
=26.70000 + 0.16000*T					r=0.992		P_r=0.001
(0.38297) (0.01155)					var=0.13333		
=27.70000 + 0.07429*T + 0.00143*T^2					r=0.998		
(0.51270) (0.03907) (0.00064)					var=0.05714		P_F=0.25
ln= 3.29553 + 0.00506*T					r=0.995		P_r=0.000
(0.00978) (0.00029)					var=0.00009		
ln= 3.31794 + 0.00314*T + 0.00003*T^2					r=0.998		
(0.01642) (0.00125) (0.00002)					var=0.00006		P_F=0.50

Bone

	2.86	5	41 *	200.0 # "	
		10	42 *	220.0 #	
		20	44.2 *	180.0 #	
		30	46 *	200.0 #	
		40	48 *	200.0 #	
		50	50 *		
=40.05315 + 0.19923*T				r=1.000	P_r=0.000
(0.07007) (0.00231)				var=0.00811	
=39.97109 + 0.20852*T - 0.00017*T^2				r=1.000	
(0.11514) (0.01047) (0.00019)				var=0.00847	P_F=0.50
ln= 3.69503 + 0.00440*T				r=0.999	P_r=0.000
(0.00296) (0.00010)				var=0.00001	
ln= 3.68852 + 0.00513*T - 0.00001*T^2				r=1.000	
(0.00268) (0.00024) (0.00000)				var=0.00000	P_F=0.10
	4.5	10	72 *	300.0 # "	
		20	75 *	150.0 #	
		30	76.5 *	150.0 #	
		40	78 *	120.0 #	
		50	79.2 *	180.0 #	
		60	81 *		
=71.04000 + 0.16886*T				r=0.988	P_r=0.000
(0.50515) (0.01297)				var=0.29443	
=69.84000 + 0.25886*T - 0.00129*T^2				r=0.994	
(0.77327) (0.05059) (0.00071)				var=0.18686	P_F=0.25
ln= 4.26525 + 0.00221*T				r=0.986	P_r=0.000
(0.00731) (0.00019)				var=0.00006	
ln= 4.24694 + 0.00358*T - 0.00002*T^2				r=0.994	
(0.01048) (0.00069) (0.00001)				var=0.00003	P_F=0.25

Fat

Fat
---

porcine							
fresh,	2	4	9.0	*	(1.5)	-125.0 #	Gammell
stored @ 5°C,		20	7.0	*		-235.3 #	et al.
backfat		37	3.0	*		-83.33 #	(1979)*2
		49	2.0	*			

$= 9.80965 - 0.16581*T$ r=0.987 P_r=0.013
(0.61252) (0.01893) var=0.41624
$= 9.87931 - 0.17489*T + 0.00017*T^2$ r=0.987
(1.21149) (0.11406) (0.00210) var=0.82692 P_F>0.50

$\ln= 2.45225 - 0.03522*T$ r=0.981 P_r=0.019
(0.15875) (0.00491) var=0.02796
$\ln= 2.29695 - 0.01496*T - 0.00038*T^2$ r=0.990
(0.22415) (0.02110) (0.00039) var=0.02831 P_F>0.50

4	4	20.8	*		-343.8 #	"
	20	15.3	*		-576.5 #	
	37	5.5	*		-166.7 #	
	49	3.5	*			

$=22.55095 - 0.41003*T$ r=0.986 P_r=0.014
(1.57879) (0.04880) var=2.76530
$=23.20702 - 0.49564*T + 0.00162*T^2$ r=0.987
(2.99027) (0.28154) (0.00519) var=5.03785 P_F>0.50

$\ln= 3.33244 - 0.04190*T$ r=0.981 P_r=0.019
(0.18755) (0.00580) var=0.03902
$\ln= 3.16446 - 0.01999*T - 0.00042*T^2$ r=0.989
(0.28494) (0.02683) (0.00049) var=0.04574 P_F>0.50

6	37	8.5	*		-208.3 #	"
	49	6.0	*			

$=16.20833 - 0.20833*T$ r=1.000
(0.00000) (0.00000) var=0.00000

$\ln= 3.21401 - 0.02903*T$ r=1.000
(0.00000) (0.00000) var=0.00000

8	37	12.5	*		-291.7 #	"
	49	9.0	*			

$=23.29167 - 0.29167*T$ r=1.000
(0.00000) (0.00000) var=0.00000

$\ln= 3.53862 - 0.02738*T$ r=1.000
(0.00000) (0.00000) var=0.00000

Fat

		9.9	37	17.5	*	-333.3 #	"
			49	13.5	*		

=29.83333 - 0.33333*T r=1.000
(0.00000) (0.00000) var=0.00000

ln= 3.66236 - 0.02163*T r=1.000
(0.00000) (0.00000) var=0.00000

Fat, peritoneal

bovine

fresh, peritoneal	1	10	* 6.0	*	(10%)	-200.0 #	Bamber & Hill
		20	4.0	*		-200.0 #	(1979)*2
		30	2.0	*		14.29 #	
		37	2.1	*		39.13 #	
		60	3.0	*			

= 5.14883 - 0.05506*T r=0.632 P_r=0.253
(1.39172) (0.03899) var=2.18839
= 9.10395 - 0.34709*T + 0.00409*T^2 r=0.989
(0.63217) (0.04107) (0.00056) var=0.11903 P_F=0.025

ln= 1.56873 - 0.01358*T r=0.560 P_r=0.326
(0.41362) (0.01159) var=0.19330
ln= 2.71185 - 0.09798*T + 0.00118*T^2 r=0.969
(0.29366) (0.01908) (0.00026) var=0.02568 P_F=0.05

	2	20	6.6	*		-340.0 #	"
		30	3.2	*		-85.71 #	
		37	2.6	*		60.87 #	
		60	4.0	*			

= 5.73239 - 0.04442*T r=0.428 P_r=0.572
(2.62299) (0.06626) var=3.80494
=17.22541 - 0.69414*T + 0.00790*T^2 r=0.991
(1.79860) (0.09784) (0.00118) var=0.16546 P_F=0.10

ln= 1.64436 - 0.00806*T r=0.343 P_r=0.657
(0.61908) (0.01564) var=0.21196
ln= 4.38265 - 0.16286*T + 0.00188*T^2 r=0.999
(0.16079) (0.00875) (0.00011) var=0.00132 P_F=0.05

Fat, peritoneal

	3	20	9.5	*	-490.0 # "
		30	4.6	*	-200.0 #
		37	3.2	*	147.8 #
		60	6.6	*	

$= 7.49821 - 0.04145*T$ r=0.258 $P_r=0.742$
(4.34883) (0.10985) var=10.45924
$=26.74143 - 1.12930*T + 0.01323*T^2$ r=0.999
(0.97586) (0.05309) (0.00064) var=0.04871 $P_F=0.05$

$\ln= 1.86991 - 0.00444*T$ r=0.161 $P_r=0.839$
(0.76075) (0.01922) var=0.32007
$\ln= 5.22963 - 0.19437*T + 0.00231*T^2$ r=0.997
(0.27873) (0.01516) (0.00018) var=0.00397 $P_F=0.10$

	4	30	7.2	*	-428.6 # "
		37	4.2	*	134.8 #
		60	7.3	*	

$= 4.70670 + 0.03606*T$ r=0.321 $P_r=0.792$
(4.70127) (0.10629) var=5.56596
$=40.90124 - 1.68673*T + 0.01878*T^2$ r=1.000
(0.00000) (0.00000) (0.00000) var=0.00000

$\ln= 1.53106 + 0.00633*T$ r=0.315 $P_r=0.796$
(0.84314) (0.01906) var=0.17902
$\ln= 8.02232 - 0.30264*T + 0.00337*T^2$ r=1.000
(0.00000) (0.00000) (0.00000) var=0.00000

	5	30	10.0	*	-571.4 # "
		37	6.0	*	95.65 #
		60	8.2	*	

$= 8.96604 - 0.02124*T$ r=0.166 $P_r=0.894$
(5.56688) (0.12586) var=7.80430
$=51.82484 - 2.06124*T + 0.02224*T^2$ r=1.000
(0.00000) (0.00000) (0.00000) var=0.00000

$\ln= 2.13332 - 0.00159*T$ r=0.097 $P_r=0.938$
(0.72233) (0.01633) var=0.13139
$\ln= 7.69443 - 0.26628*T + 0.00289*T^2$ r=1.000
(0.00000) (0.00000) (0.00000) var=0.00000

Fat, peritoneal

	6	30	12.5	*	-785.7 #	"
		37	7.0	*	86.96 #	
		60	9.0	*		

$=12.29263 - 0.06597*T$ $r=0.372$ $P_r=0.757$
(7.28256) (0.16465) $var=13.35606$
$=68.36024 - 2.73468*T + 0.02909*T^2$ $r=1.000$
(0.00000) (0.00000) (0.00000) $var=0.00000$

$\ln= 2.45592 - 0.00550*T$ $r=0.297$ $P_r=0.808$
(0.78242) (0.01769) $var=0.15417$
$\ln= 8.47971 - 0.29222*T + 0.00313*T^2$ $r=1.000$
(0.00000) (0.00000) (0.00000) $var=0.00000$

	7	30	16.0	*	-1143. #	"
		37	8.0	*	65.22 #	
		60	9.5	*		

$=17.36773 - 0.14648*T$ $r=0.541$ $P_r=0.636$
(10.08155) (0.22793) $var=25.59557$
$=94.98447 - 3.84089*T + 0.04027*T^2$ $r=1.000$
(0.00000) (0.00000) (0.00000) $var=0.00000$

$\ln= 2.84147 - 0.01119*T$ $r=0.487$ $P_r=0.677$
(0.88870) (0.02009) $var=0.19889$
$\ln= 9.68345 - 0.33685*T + 0.00355*T^2$ $r=1.000$
(0.00000) (0.00000) (0.00000) $var=0.00000$

Heart

---

canine		cm^{-1}				
fresh,	2	19.5	0.10	(0.02)	-0.65 #	O'Donnell
15 min.,		35	0.09	(0.02)		et al.
left ventrical						(1977).

$= 0.11258 - 0.00065*T$ $r=1.000$
(0.00000) (0.00000) $var=0.00000$

$\ln=-2.17003 - 0.00680*T$ $r=1.000$
(0.00000) (0.00000) $var=0.00000$

	4	19.5	0.19	(0.03)	-1.29 #	"
		35	0.17	(0.02)		

$= 0.21516 - 0.00129*T$ $r=1.000$
(0.00000) (0.00000) $var=0.00000$

$\ln=-1.52080 - 0.00718*T$ $r=1.000$
(0.00000) (0.00000) $var=0.00000$

Heart

	6	19.5	0.34	(0.02) -2.58 # "
		35	0.30	(0.03)

= 0.39032 - 0.00258*T r=1.000
(0.00000) (0.00000) var=0.00000

ln=-0.92135 - 0.00808*T r=1.000
(0.00000) (0.00000) var=0.00000

	8	19.5	0.48	(0.03) -3.23 # "
		35	0.43	(0.03)

= 0.54290 - 0.00323*T r=1.000
(0.00000) (0.00000) var=0.00000

ln=-0.59558 - 0.00710*T r=1.000
(0.00000) (0.00000) var=0.00000

	10	19.5	0.65	(0.03) -5.81 # "
		35	0.56	(0.03)

= 0.76323 - 0.00581*T r=1.000
(0.00000) (0.00000) var=0.00000

ln=-0.24329 - 0.00962*T r=1.000
(0.00000) (0.00000) var=0.00000

fresh,	2	19.5	0.10	(0.02) -0.65 # "
2 hrs.		35	0.09	(0.02)
left ventrical				

= 0.11258 - 0.00065*T r=1.000
(0.00000) (0.00000) var=0.00000

ln=-2.17003 - 0.00680*T r=1.000
(0.00000) (0.00000) var=0.00000

	4	19.5	0.20	(0.02) -0.65 # "
		35	0.19	(0.03)

= 0.21258 - 0.00065*T r=1.000
(0.00000) (0.00000) var=0.00000

ln=-1.54491 - 0.00331*T r=1.000
(0.00000) (0.00000) var=0.00000

Heart

```
                6      19.5 0.36     (0.02) -1.29 # "
                       35   0.34     (0.03)

  = 0.38516 - 0.00129*T                    r=1.000
   (0.00000) (0.00000)                   var=0.00000

ln=-0.94974 - 0.00369*T                    r=1.000
   (0.00000) (0.00000)                   var=0.00000

                8      19.5 0.50     (0.03) -1.94 # "
                       35   0.47     (0.03)

  = 0.53774 - 0.00194*T                    r=1.000
   (0.00000) (0.00000)                   var=0.00000

ln=-0.61530 - 0.00399*T                    r=1.000
   (0.00000) (0.00000)                   var=0.00000

               10      19.5 0.70     (0.03) -5.81 # "
                       35   0.61     (0.04)

  = 0.81323 - 0.00581*T                    r=1.000
   (0.00000) (0.00000)                   var=0.00000

ln=-0.18354 - 0.00888*T                    r=1.000
   (0.00000) (0.00000)                   var=0.00000

    fresh,       2      19.5 0.10     (0.02)  0.65 # "
    4 hrs.,             35   0.11     (0.02)
    left ventrical

  = 0.08742 + 0.00065*T                    r=1.000
   (0.00000) (0.00000)                   var=0.00000

ln=-2.42249 + 0.00615*T                    r=1.000
   (0.00000) (0.00000)                   var=0.00000

                4      19.5 0.20     (0.02)  1.29 # "
                       35   0.22     (0.03)

  = 0.17484 + 0.00129*T                    r=1.000
   (0.00000) (0.00000)                   var=0.00000

ln=-1.72934 + 0.00615*T                    r=1.000
   (0.00000) (0.00000)                   var=0.00000
```

Heart

	6	19.5	0.35	(0.02)	1.29 # "
		35	0.37	(0.03)	

= 0.32484 + 0.00129*T r=1.000
(0.00000) (0.00000) var=0.00000

ln=-1.11973 + 0.00359*T r=1.000
(0.00000) (0.00000) var=0.00000

	8	19.5	0.49	(0.03)	1.94 # "
		35	0.52	(0.03)	

= 0.45226 + 0.00194*T r=1.000
(0.00000) (0.00000) var=0.00000

ln=-0.78811 + 0.00383*T r=1.000
(0.00000) (0.00000) var=0.00000

	10	19.5	0.69	(0.03)	-3.23 # "
		35	0.64	(0.04)	

= 0.75290 - 0.00323*T r=1.000
(0.00000) (0.00000) var=0.00000

ln=-0.27643 - 0.00485*T r=1.000
(0.00000) (0.00000) var=0.00000

fresh,	2	20.5	0.10	(0.02)	0.00 # "
left ventrical		25	0.10	(0.02)	0.00 #
		30	0.10	(0.02)	1.43 #
		37	0.11	(0.02)	

= 0.08588 + 0.00059*T r=0.836 P_r=0.164
(0.00789) (0.00027) var=0.00001
= 0.14523 - 0.00371*T + 0.00007*T^2 r=0.986
(0.01911) (0.00137) (0.00002) var=0.00000 P_F=0.25

ln=-2.43716 + 0.00563*T r=0.836 P_r=0.164
(0.07518) (0.00261) var=0.00102
ln=-1.87150 - 0.03539*T + 0.00071*T^2 r=0.986
(0.18210) (0.01305) (0.00022) var=0.00019 P_F=0.25

Heart

	4	20.5	0.19	(0.02) 0.00 #	"
		25	0.19	(0.02) -4.00 #	
		30	0.17	(0.02) 2.86 #	
		37	0.19	(0.02)	

$= 0.19202 - 0.00025*T$ (0.02831) (0.00098) r=0.177 var=0.00015 $P_r=0.823$

$= 0.35128 - 0.01180*T + 0.00020*T^2$ (0.15928) (0.01141) (0.00020) r=0.723 var=0.00014 $P_F=0.50$

$\ln=-1.64948 - 0.00139*T$ (0.15746) (0.00547) r=0.177 var=0.00449 $P_r=0.823$

$\ln=-0.76381 - 0.06562*T + 0.00111*T^2$ (0.88582) (0.06347) (0.00109) r=0.723 var=0.00442 $P_F=0.50$

	6	20.5	0.34	(0.03) -2.22 #	"
		25	0.33	(0.03) -4.00 #	
		30	0.31	(0.03) 0.00 #	
		37	0.31	(0.03)	

$= 0.37704 - 0.00194*T$ (0.01743) (0.00061) r=0.915 var=0.00006 $P_r=0.085$

$= 0.48739 - 0.00994*T + 0.00014*T^2$ (0.08353) (0.00598) (0.00010) r=0.970 var=0.00004 $P_F=0.50$

$\ln=-0.96397 - 0.00599*T$ (0.05391) (0.00187) r=0.915 var=0.00053 $P_r=0.085$

$\ln=-0.62885 - 0.03030*T + 0.00042*T^2$ (0.26640) (0.01909) (0.00033) r=0.968 var=0.00040 $P_F=0.50$

	8	20.5	0.48	(0.03) -6.67 #	"
		25	0.45	(0.03) -4.00 #	
		30	0.43	(0.03) -2.86 #	
		37	0.41	(0.03)	

$= 0.55884 - 0.00414*T$ (0.01704) (0.00059) r=0.980 var=0.00005 $P_r=0.020$

$= 0.69006 - 0.01365*T + 0.00016*T^2$ (0.02977) (0.00213) (0.00004) r=0.999 var=0.00000 $P_F=0.25$

$\ln=-0.55418 - 0.00935*T$ (0.03372) (0.00117) r=0.985 var=0.00021 $P_r=0.015$

$\ln=-0.29425 - 0.02820*T + 0.00033*T^2$ (0.05808) (0.00416) (0.00007) r=0.999 var=0.00002 $P_F=0.25$

Heart

	10	20.5	0.64	(0.03) -6.67 #	"
		25	0.61	(0.03) -6.00 #	
		30	0.58	(0.03) -2.86 #	
		37	0.56	(0.03)	

= 0.73397 - 0.00485*T (0.01957) (0.00068) r=0.981 var=0.00007 P_r=0.019

= 0.88547 - 0.01584*T + 0.00019*T^2 (0.03077) (0.00220) (0.00004) r=0.999 var=0.00001 P_F=0.25

ln=-0.28789 - 0.00812*T (0.02991) (0.00104) r=0.984 var=0.00016 P_r=0.016

ln=-0.05883 - 0.02473*T + 0.00029*T^2 (0.05801) (0.00416) (0.00007) r=0.999 var=0.00002 P_F=0.25

---

canine		cm^{-1}/MHz			
fresh, 15 min., left ventrical	2-10	19.5	0.072	(0.002)-0.71 #	O'Donnell et al. (1977)*1
		35	0.061	(0.003)	

= 0.08584 - 0.00071*T (0.00000) (0.00000) r=1.000 var=0.00000

ln=-2.42251 - 0.01070*T (0.00000) (0.00000) r=1.000 var=0.00000

fresh, 2 hrs., left ventrical	2-10	19.5	0.075	(0.002)-0.45 #	"
		35	0.068	(0.003)	

= 0.08381 - 0.00045*T (0.00000) (0.00000) r=1.000 var=0.00000

ln=-2.46700 - 0.00632*T (0.00000) (0.00000) r=1.000 var=0.00000

fresh, 4 hrs., left ventrical	2-10	19.5	0.075	(0.002)-0.26 #	"
		35	0.071	(0.003)	

= 0.08003 - 0.00026*T (0.00000) (0.00000) r=1.000 var=0.00000

ln=-2.52132 - 0.00354*T (0.00000) (0.00000) r=1.000 var=0.00000

Heart

fresh, left ventrical	2-10	10.5	0.071	(0.002)	-0.21 #	"
		25	0.068	(0.002)	-0.80 #	
		30	0.064	(0.002)	-0.86 #	
		37	0.058	(0.002)		

$= 0.07723 - 0.00047*T$ (0.00348) (0.00013) r=0.934 var=0.00001 $P_r=0.066$

$= 0.06763 + 0.00056*T - 0.00002*T^2$ (0.00157) (0.00015) (0.00000) r=0.999 var=0.00000 $P_F=0.10$

$\ln=-2.54732 - 0.00722*T$ (0.05774) (0.00211) r=0.924 var=0.00168 $P_r=0.076$

$\ln=-2.70770 + 0.00989*T - 0.00037*T^2$ (0.01887) (0.00182) (0.00004) r=0.999 var=0.00004 $P_F=0.10$

Kidney

porcine fresh, <1 hr. p.m. stored @ 5°C	2	4	1.3	* (1.5)	-50.0 #	Gammell
		20	0.5	*	88.2 #	et al.
		37	2.0		#	(1979)*2

$= 0.82117 + 0.02191*T$ (0.97220) (0.03986) r=0.482 var=0.86521 $P_r=0.680$

$= 1.83512 - 0.15053*T + 0.00419*T^2$ (0.00000) (0.00000) (0.00000) r=1.000 var=0.00000

$\ln=-0.19247 + 0.01377*T$ (0.99351) (0.04073) r=0.320 var=0.90357 $P_r=0.792$

$\ln= 0.84371 - 0.16246*T + 0.00428*T^2$ (0.00000) (0.00000) (0.00000) r=1.000 var=0.00000

	4	4	3.2	*	-43.8 #	"
		20	2.5	*	70.6 #	
		37	3.7			

$= 2.81353 + 0.01573*T$ (0.80413) (0.03297) r=0.431 var=0.59193 $P_r=0.717$

$= 3.65218 - 0.12691*T + 0.00346*T^2$ (0.00000) (0.00000) (0.00000) r=1.000 var=0.00000

$\ln= 1.03585 + 0.00459*T$ (0.27070) (0.01110) r=0.382 var=0.06708 $P_r=0.750$

$\ln= 1.31817 - 0.04342*T + 0.00117*T^2$ (0.00000) (0.00000) (0.00000) r=1.000 var=0.00000

Kidney

	6	4	5.5	*	-93.8 # "
		20	4.0	*	58.8 #
		37	5.0		

$= 5.12576 - 0.01438*T$ (1.07304) (0.04399) — r=0.311, var=1.05401, P_r=0.799

$= 6.24488 - 0.20471*T + 0.00462*T^2$ (0.00000) (0.00000) (0.00000) — r=1.000, var=0.00000

$\ln = 1.62217 - 0.00272*T$ (0.23229) (0.00952) — r=0.275, var=0.04940, P_r=0.823

$\ln = 1.86443 - 0.04392*T + 0.00100*T^2$ (0.00000) (0.00000) (0.00000) — r=1.000, var=0.00000

	8	4	8.5	*	-156.3 # "
		20	6.0	*	52.9 #
		37	6.9		

$= 8.09774 - 0.04743*T$ (1.47123) (0.06031) — r=0.618, var=1.98140, P_r=0.576

$= 9.63213 - 0.30839*T + 0.00634*T^2$ (0.00000) (0.00000) (0.00000) — r=1.000, var=0.00000

$\ln = 2.07987 - 0.00617*T$ (0.21092) (0.00865) — r=0.581, var=0.04072, P_r=0.606

$\ln = 2.29985 - 0.04358*T + 0.00091*T^2$ (0.00000) (0.00000) (0.00000) — r=1.000, var=0.00000

	9.9	4	12.6	*	-300.0 # "
		20	7.8	*	70.6 #
		37	9.0	*	

$=11.98017 - 0.10722*T$ (2.60632) (0.10685) — r=0.708, var=6.21826, P_r=0.499

$=14.69840 - 0.56952*T + 0.01123*T^2$ (0.00000) (0.00000) (0.00000) — r=1.000, var=0.00000

$\ln = 2.46507 - 0.01000*T$ (0.27000) (0.01107) — r=0.670, var=0.06673, P_r=0.532

$\ln = 2.74666 - 0.05789*T + 0.00116*T^2$ (0.00000) (0.00000) (0.00000) — r=1.000, var=0.00000

Liver

Liver

human

p. m.	1	5	1.2	* (10%)	50.0 #	Bamber & Hill
		11	1.5	*	9.09 #	(1979)*2
		22	1.6	*	0.00 #	
		30	1.6	*	0.00 #	
		42	1.6	*		

$= 1.30114 + 0.00904*T$ (0.11050) (0.00430) — r=0.771, var=0.01620, $P_r=0.127$

$= 1.08617 + 0.03638*T - 0.00059*T^2$ (0.11500) (0.01194) (0.00025) — r=0.945, var=0.00645, $P_F=0.25$

$\ln= 0.25859 + 0.00641*T$ (0.08118) (0.00316) — r=0.760, var=0.00874, $P_r=0.136$

$\ln= 0.10332 + 0.02616*T - 0.00042*T^2$ (0.08830) (0.00917) (0.00019) — r=0.937, var=0.00381, $P_F=0.25$

	2	5	2.1	*	0.00 #	"
		11	2.1	*	-27.3 #	
		22	1.8	*	0.00 #	
		30	1.8	*	-8.33 #	
		42	1.7	*		

$= 2.16178 - 0.01190*T$ (0.06389) (0.00249) — r=0.940, var=0.00542, $P_r=0.017$

$= 2.24165 - 0.02206*T + 0.00022*T^2$ (0.10770) (0.01119) (0.00023) — r=0.959, var=0.00566, $P_F=0.50$

$\ln= 0.77544 - 0.00625*T$ (0.03200) (0.00125) — r=0.945, var=0.00136, $P_r=0.015$

$\ln= 0.81293 - 0.01102*T + 0.00010*T^2$ (0.05534) (0.00575) (0.00012) — r=0.960, var=0.00149, $P_F=0.50$

	3	5	3.0	*	-50.0 #	"
		11	2.7	*	-18.2 #	
		22	2.5	*	-12.5 #	
		30	2.4	*	-16.7 #	
		42	2.2	*		

$= 3.00050 - 0.02002*T$ (0.07367) (0.00287) — r=0.971, var=0.00720, $P_r=0.006$

$= 3.12521 - 0.03589*T + 0.00034*T^2$ (0.09912) (0.01029) (0.00022) — r=0.987, var=0.00480, $P_F=0.50$

$\ln= 1.10632 - 0.00781*T$ (0.02333) (0.00091) — r=0.980, var=0.00072, $P_r=0.003$

$\ln= 1.14216 - 0.01237*T + 0.00010*T^2$ (0.03469) (0.00360) (0.00008) — r=0.989, var=0.00059, $P_F=0.50$

Liver

	4	5	3.8	*	-83.3 # "
		11	3.3	*	-45.5 #
		22	2.8	*	-37.5 #
		30	2.5	*	-8.33 #
		42	2.4	*	

$= 3.78815 - 0.03764*T$ (0.18318) (0.00714) — r=0.950, var=0.04451, $P_r=0.013$

$= 4.19770 - 0.08974*T + 0.00112*T^2$ (0.06424) (0.00667) (0.00014) — r=0.999, var=0.00201, $P_F=0.025$

$\ln= 1.34666 - 0.01257*T$ (0.05143) (0.00200) — r=0.964, var=0.00351, $P_r=0.008$

$\ln= 1.46119 - 0.02714*T + 0.00031*T^2$ (0.02025) (0.00210) (0.00004) — r=0.999, var=0.00020, $P_F=0.025$

	5	5	4.3	*	-83.3 # "
		11	3.8	*	-54.5 #
		22	3.2	*	-25.0 #
		30	3.0	*	-16.7 #
		42	2.8	*	

$= 4.29849 - 0.03993*T$ (0.18376) (0.00716) — r=0.955, var=0.04480, $P_r=0.011$

$= 4.70858 - 0.09210*T + 0.00112*T^2$ (0.06822) (0.00709) (0.00015) — r=0.999, var=0.00227, $P_F=0.025$

$\ln= 1.47124 - 0.01156*T$ (0.04372) (0.00170) — r=0.969, var=0.00254, $P_r=0.007$

$\ln= 1.56948 - 0.02405*T + 0.00027*T^2$ (0.01265) (0.00131) (0.00003) — r=0.999, var=0.00008, $P_F=0.025$

	6	5	5.7	*	-166.7 # "
		11	4.7	*	-81.8 #
		22	3.8	*	-37.5 #
		30	3.5	*	-25.0 #
		42	3.2	*	

$= 5.60471 - 0.06476*T$ (0.34822) (0.01357) — r=0.940, var=0.16087, $P_r=0.017$

$= 6.35978 - 0.16081*T + 0.00206*T^2$ (0.20836) (0.02164) (0.00045) — r=0.995, var=0.02119, $P_F=0.05$

$\ln= 1.74323 - 0.01525*T$ (0.06381) (0.00249) — r=0.962, var=0.00540, $P_r=0.009$

$\ln= 1.88416 - 0.03317*T + 0.00038*T^2$ (0.02985) (0.00310) (0.00006) — r=0.998, var=0.00044, $P_F=0.05$

Liver

	7	5	7.2	*		-200.0 #	"
		11	6.0	*		-100.0 #	
		22	4.9	*		-50.0 #	
		30	4.5	*		-25.0 #	
		42	4.2	*			

$= 7.08174 - 0.07826*T$ (0.43089) (0.01679) r=0.937 var=0.24632 $P_r=0.019$

$= 8.02809 - 0.19864*T + 0.00258*T^2$ (0.22045) (0.02290) (0.00048) r=0.996 var=0.02372 $P_F=0.05$

$\ln= 1.97436 - 0.01434*T$ (0.06369) (0.00248) r=0.958 var=0.00538 $P_r=0.010$

$\ln= 2.11685 - 0.03247*T + 0.00039*T^2$ (0.02190) (0.00227) (0.00005) r=0.999 var=0.00023 $P_F=0.025$

human autopsy, refrig 60 hrs., micronodular cirrhosis	2	4	4.2	*	(1.5)	-100.0 #	Gammell
		20	2.6	*		-35.3 #	et al.
		37	2.0	*		#	(1979)*2

$= 4.28225 - 0.06634*T$ (0.45507) (0.01866) r=0.963 var=0.18957 $P_r=0.175$

$= 4.75686 - 0.14706*T + 0.00196*T^2$ (0.00000) (0.00000) (0.00000) r=1.000 var=0.00000

$\ln= 1.48358 - 0.02241*T$ (0.10226) (0.00419) r=0.983 var=0.00957 $P_r=0.118$

$\ln= 1.59023 - 0.04055*T + 0.00044*T^2$ (0.00000) (0.00000) (0.00000) r=1.000 var=0.00000

	4	4	8.0	*		-125.0 #	"
		20	6.0	*		-88.2 #	
		37	4.5	*			

$= 8.31946 - 0.10588*T$ (0.25856) (0.01060) r=0.995 var=0.06120 $P_r=0.063$

$= 8.58913 - 0.15174*T + 0.00111*T^2$ (0.00000) (0.00000) (0.00000) r=1.000 var=0.00000

$\ln= 2.14617 - 0.01743*T$ (0.00744) (0.00030) r=1.000 var=0.00005 $P_r=0.011$

$\ln= 2.15393 - 0.01875*T + 0.00003*T^2$ (0.00000) (0.00000) (0.00000) r=1.000 var=0.00000

Liver

	6	4	13.0	*	-218.8 # "
		20	9.5	*	-88.2 #
		37	8.0	*	

$=13.23409 - 0.15086*T$ r=0.970 $P_r=0.156$
(0.91790) (0.03763) var=0.77127
$=14.19140 - 0.31367*T + 0.00395*T^2$ r=1.000
(0.00000) (0.00000) (0.00000) var=0.00000

$\ln= 2.59674 - 0.01466*T$ r=0.983 $P_r=0.117$
(0.06678) (0.00274) var=0.00408
$\ln= 2.66638 - 0.02651*T + 0.00029*T^2$ r=1.000
(0.00000) (0.00000) (0.00000) var=0.00000

	8	4	18.6	*	-312.5 # "
		20	13.6	*	-123.5 #
		37	11.5	*	

$=18.92203 - 0.21420*T$ r=0.969 $P_r=0.159$
(1.32902) (0.05448) var=1.61687
$=20.30811 - 0.44993*T + 0.00573*T^2$ r=1.000
(0.00000) (0.00000) (0.00000) var=0.00000

$\ln= 2.95379 - 0.01452*T$ r=0.982 $P_r=0.121$
(0.06823) (0.00280) var=0.00426
$\ln= 3.02495 - 0.02662*T + 0.00029*T^2$ r=1.000
(0.00000) (0.00000) (0.00000) var=0.00000

	9.9	4	24.0	*	-381.3 # "
		20	17.9	*	-141.2 #
		37	15.5	*	

$=24.34608 - 0.25636*T$ r=0.965 $P_r=0.168$
(1.68842) (0.06922) var=2.60960
$=26.10700 - 0.55585*T + 0.00727*T^2$ r=1.000
(0.00000) (0.00000) (0.00000) var=0.00000

$\ln= 3.20295 - 0.01320*T$ r=0.978 $P_r=0.135$
(0.06934) (0.00284) var=0.00440
$\ln= 3.27527 - 0.02550*T + 0.00030*T^2$ r=1.000
(0.00000) (0.00000) (0.00000) var=0.00000

Liver

bovine							
fresh,	1	8	2.0	* (10%)	0.00 #	Bamber & Hill	
<30 min.		21	2.0	*	6.25 #	(1979)*2	
		37	2.1	*	137.5 #	sample #1	
		45	3.2	*	0.00 #		
		58	3.2	*			

$= 1.56717 + 0.02760*T$ r=0.849 $P_r=0.069$
(0.37847) (0.00993) var=0.15293
$= 1.96648 - 0.00702*T + 0.00053*T^2$ r=0.882
(0.68809) (0.04896) (0.00073) var=0.18164 $P_F>0.50$

$\ln= 0.52487 + 0.01083*T$ r=0.855 $P_r=0.065$
(0.14439) (0.00379) var=0.02226
$\ln= 0.67503 - 0.00219*T + 0.00020*T^2$ r=0.886
(0.26349) (0.01875) (0.00028) var=0.02663 $P_F>0.50$

2	8	2.9	*	-38.5 #	"
	21	2.4	*	6.25 #	
	37	2.5	*	162.5 #	
	45	3.8	*	0.00 #	
	58	3.8	*		

$= 2.27401 + 0.02385*T$ r=0.687 $P_r=0.200$
(0.55490) (0.01456) var=0.32873
$= 3.07755 - 0.04582*T + 0.00107*T^2$ r=0.824
(0.88394) (0.06289) (0.00094) var=0.29976 $P_F=0.50$

$\ln= 0.85431 + 0.00743*T$ r=0.661 $P_r=0.225$
(0.18550) (0.00487) var=0.03674
$\ln= 1.12930 - 0.01641*T + 0.00037*T^2$ r=0.817
(0.29089) (0.02070) (0.00031) var=0.03246 $P_F=0.50$

3	8	4.7	*	-92.3 #	"
	21	3.5	*	-12.5 #	
	37	3.3	*	150.0 #	
	45	4.5	*	0.00 #	
	58	4.5	*		

$= 4.01718 + 0.00245*T$ r=0.074 $P_r=0.905$
(0.72224) (0.01895) var=0.55690
$= 5.31822 - 0.11035*T + 0.00173*T^2$ r=0.780
(0.92535) (0.06584) (0.00098) var=0.32851 $P_F=0.25$

$\ln= 1.37645 + 0.00071*T$ r=0.085 $P_r=0.891$
(0.18261) (0.00479) var=0.03560
$\ln= 1.70456 - 0.02774*T + 0.00044*T^2$ r=0.779
(0.23489) (0.01671) (0.00025) var=0.02117 $P_F=0.25$

Liver

	4	8	4.7	*	-92.3 # "
		21	3.5	*	-18.8 #
		37	3.2	*	212.5 #
		45	4.9	*	7.69 #
		58	5.0	*	

$= 3.82279 + 0.01294*T$ (0.89970) (0.02361) — r=0.302, var=0.86417, $P_r=0.622$

$= 5.41725 - 0.12530*T + 0.00212*T^2$ (1.18093) (0.08403) (0.00126) — r=0.790, var=0.53503, $P_F=0.25$

$\ln= 1.33419 + 0.00291*T$ (0.22411) (0.00588) — r=0.274, var=0.05362, $P_r=0.655$

$\ln= 1.73011 - 0.03142*T + 0.00053*T^2$ (0.29549) (0.02102) (0.00031) — r=0.784, var=0.03350, $P_F=0.25$

	5	8	5.8	*	-123.1 # "
		21	4.2	*	-37.5 #
		37	3.6	*	212.5 #
		45	5.3	*	46.2 #
		58	5.9	*	

$= 4.73638 + 0.00662*T$ (1.12647) (0.02956) — r=0.128, var=1.35471, $P_r=0.837$

$= 7.03996 - 0.19310*T + 0.00306*T^2$ (1.07479) (0.07647) (0.00114) — r=0.886, var=0.44318, $P_F=0.25$

$\ln= 1.53951 + 0.00130*T$ (0.24041) (0.00631) — r=0.118, var=0.06171, $P_r=0.850$

$\ln= 2.01967 - 0.04033*T + 0.00064*T^2$ (0.24763) (0.01762) (0.00026) — r=0.866, var=0.02353, $P_F=0.25$

	6	8	6.9	*	-138.5 # "
		21	5.1	*	-56.3 #
		37	4.2	*	225.0 #
		45	6.0	*	53.8 #
		58	6.7	*	

$= 5.79133 - 0.00034*T$ (1.26285) (0.03313) — r=0.006, var=1.70261, $P_r=0.993$

$= 8.41674 - 0.22795*T + 0.00349*T^2$ (1.13022) (0.08042) (0.00120) — r=0.899, var=0.49007, $P_F=0.25$

$\ln= 1.73787 + 0.00000*T$ (0.23097) (0.00606) — r=0.000, var=0.05695, $P_r=1.000$

$\ln= 2.20575 - 0.04056*T + 0.00062*T^2$ (0.22764) (0.01620) (0.00024) — r=0.876, var=0.01988, $P_F=0.25$

Liver

7	8	8.7	*	-184.6 #	"
	21	6.3	*	-62.5 #	
	37	5.3	*	212.5 #	
	45	7.0	*	66.7 #	
	57	7.8	*		

$= 7.50639 - 0.01448*T$ r=0.214 $P_r=0.730$
(1.44571) (0.03824) var=2.19767
$=10.66266 - 0.29263*T + 0.00433*T^2$ r=0.937
(1.06674) (0.07739) (0.00118) var=0.42381 $P_F=0.10$

$\ln= 1.99360 - 0.00176*T$ r=0.179 $P_r=0.774$
(0.21226) (0.00561) var=0.04738
$\ln= 2.44878 - 0.04188*T + 0.00062*T^2$ r=0.920
(0.17431) (0.01265) (0.00019) var=0.01132 $P_F=0.10$

1	9	1.7	*	0.00 #	" sample #2
	20	1.7	*	0.00 #	
	30	1.7	*	7.69 #	
	43	1.8	*	9.09 #	
	65	2.0	*		

$= 1.59425 + 0.00556*T$ r=0.924 $P_r=0.025$
(0.05130) (0.00133) var=0.00331
$= 1.72580 - 0.00416*T + 0.00013*T^2$ r=0.996
(0.02650) (0.00168) (0.00002) var=0.00027 $P_F=0.05$

$\ln= 0.47343 + 0.00303*T$ r=0.927 $P_r=0.023$
(0.02730) (0.00071) var=0.00094
$\ln= 0.54273 - 0.00209*T + 0.00007*T^2$ r=0.995
(0.01643) (0.00104) (0.00001) var=0.00010 $P_F=0.05$

2	9	2.2	*	-18.2 #	"
	20	2.0	*	-10.0 #	
	30	1.9	*	-7.69 #	
	43	1.8	*	22.7 #	
	65	2.3			

$= 1.98627 + 0.00161*T$ r=0.168 $P_r=0.787$
(0.21036) (0.00545) var=0.05571
$= 2.52830 - 0.03845*T + 0.00053*T^2$ r=0.978
(0.09923) (0.00629) (0.00008) var=0.00374 $P_F=0.025$

$\ln= 0.68652 + 0.00067*T$ r=0.143 $P_r=0.819$
(0.10327) (0.00267) var=0.01343
$\ln= 0.95154 - 0.01892*T + 0.00026*T^2$ r=0.974
(0.05276) (0.00334) (0.00004) var=0.00106 $P_F=0.05$

Liver

	3	9	2.9	*	-63.6 # "
		20	2.2	*	-20.0 #
		30	2.0	*	0.00 #
		43	2.0	*	45.5 #
		65	3.0	*	

$= 2.29616 + 0.00371*T$ (0.49945) (0.01293) — r=0.163, var=0.31406, $P_r=0.793$

$= 3.60924 - 0.09334*T + 0.00129*T^2$ (0.08268) (0.00524) (0.00007) — r=0.997, var=0.00259, $P_F=0.005$

$\ln= 0.82368 + 0.00132*T$ (0.20330) (0.00526) — r=0.143, var=0.05203, $P_r=0.819$

$\ln= 1.35895 - 0.03825*T + 0.00053*T^2$ (0.02275) (0.00144) (0.00002) — r=0.999, var=0.00020, $P_F=0.005$

	4	9	3.3	*	-72.7 # "
		20	2.5	*	20.0 #
		30	2.7	*	0.00 #
		43	2.7	*	45.5 #
		65	3.7	*	

$= 2.63056 + 0.01046*T$ (0.46095) (0.01194) — r=0.451, var=0.26751, $P_r=0.445$

$= 3.77672 - 0.07425*T + 0.00113*T^2$ (0.34160) (0.02165) (0.00028) — r=0.955, var=0.04430, $P_F=0.10$

$\ln= 0.97263 + 0.00324*T$ (0.15194) (0.00393) — r=0.430, var=0.02906, $P_r=0.470$

$\ln= 1.34479 - 0.02426*T + 0.00037*T^2$ (0.12532) (0.00794) (0.00010) — r=0.943, var=0.00596, $P_F=0.10$

	5	9	3.8	*	-72.7 # "
		20	3.0	*	-20.0 #
		30	2.8	*	0.00 #
		43	2.8	*	68.2 #
		65	4.3	*	

$= 2.97846 + 0.01082*T$ (0.65330) (0.01692) — r=0.347, var=0.53735, $P_r=0.568$

$= 4.69654 - 0.11615*T + 0.00169*T^2$ (0.10184) (0.00646) (0.00008) — r=0.998, var=0.00394, $P_F=0.005$

$\ln= 1.09812 + 0.00276*T$ (0.19161) (0.00496) — r=0.306, var=0.04623, $P_r=0.617$

$\ln= 1.60245 - 0.03451*T + 0.00050*T^2$ (0.02441) (0.00155) (0.00002) — r=0.999, var=0.00023, $P_F=0.005$

Liver

	6	9	4.7	*	-109.1 #	"
		20	3.5	*	-50.0 #	
		30	3.0	*	7.69 #	
		43	3.1	*	104.5 #	
		65	5.4	*		

$= 3.43078 + 0.01525*T$ (1.03622) (0.02684) — r=0.312, var=1.35189, $P_r=0.610$

$= 6.16244 - 0.18664*T + 0.00269*T^2$ (0.02317) (0.00147) (0.00002) — r=1.000, var=0.00020, $P_F=0.001$

$\ln= 1.23893 + 0.00313*T$ (0.25935) (0.00672) — r=0.260, var=0.08469, $P_r=0.673$

$\ln= 1.92245 - 0.04739*T + 0.00067*T^2$ (0.01427) (0.00090) (0.00001) — r=1.000, var=0.00008, $P_F=0.001$

	7	9	5.5	*	-109.1 #	"
		20	4.3	*	-30.0 #	
		30	4.0	*	7.69 #	
		43	4.1	*	118.2 #	
		65	6.7	*		

$= 4.10760 + 0.02432*T$ (1.06666) (0.02762) — r=0.453, var=1.43246, $P_r=0.443$

$= 6.91489 - 0.18316*T + 0.00276*T^2$ (0.13819) (0.00876) (0.00011) — r=0.999, var=0.00725, $P_F=0.005$

$\ln= 1.43382 + 0.00415*T$ (0.21057) (0.00545) — r=0.403, var=0.05582, $P_r=0.502$

$\ln= 1.98846 - 0.03684*T + 0.00055*T^2$ (0.01947) (0.00123) (0.00002) — r=0.999, var=0.00014, $P_F=0.001$

bovine

formalin fixed, 2 months 4%	3	18	2.4	* (10 %)	-40.0 #	Bamber & Hill
		28	2.0	*	0.00 #	(1979)*2
		40	2.0	*	0.00 #	sample #1
		58	2.0	*		

$= 2.39189 - 0.00811*T$ (0.22950) (0.00589) — r=0.697, var=0.03081, $P_r=0.303$

$= 3.15494 - 0.05502*T + 0.00061*T^2$ (0.46418) (0.02709) (0.00035) — r=0.935, var=0.01514, $P_F=0.50$

$\ln= 0.87177 - 0.00370*T$ (0.10461) (0.00268) — r=0.697, var=0.00640, $P_r=0.303$

$\ln= 1.21958 - 0.02508*T + 0.00028*T^2$ (0.21158) (0.01235) (0.00016) — r=0.935, var=0.00314, $P_F=0.50$

Liver

	4	18	3.4	*	-50.0 # "
		28	2.9	*	-16.7 #
		40	2.7	*	-11.1 #
		58	2.5	*	

$= 3.62905 - 0.02095*T$ (0.22247) (0.00571) r=0.933 $P_r=0.067$ var=0.02895

$= 4.41889 - 0.06951*T + 0.00063*T^2$ (0.33954) (0.01981) (0.00025) r=0.991 var=0.00810 $P_F=0.25$

$\ln= 1.30954 - 0.00722*T$ (0.06654) (0.00171) r=0.948 $P_r=0.052$ var=0.00259

$\ln= 1.54592 - 0.02176*T + 0.00019*T^2$ (0.10119) (0.00590) (0.00008) r=0.993 var=0.00072 $P_F=0.25$

	5	18	4.3	*	-70.0 # "
		28	3.6	*	-25.0 #
		40	3.3	*	-16.7 #
		58	3.0	*	

$= 4.64459 - 0.03041*T$ (0.30531) (0.00784) r=0.940 $P_r=0.060$ var=0.05453

$= 5.73397 - 0.09738*T + 0.00087*T^2$ (0.45129) (0.02633) (0.00034) r=0.992 var=0.01431 $P_F=0.25$

$\ln= 1.56440 - 0.00851*T$ (0.07140) (0.00183) r=0.957 $P_r=0.043$ var=0.00298

$\ln= 1.81924 - 0.02418*T + 0.00020*T^2$ (0.10540) (0.00615) (0.00008) r=0.994 var=0.00078 $P_F=0.25$

	6	18	5.5	*	-90.0 # "
		28	4.6	*	-33.3 #
		40	4.2	*	-33.3 #
		58	3.6	*	

$= 6.08851 - 0.04482*T$ (0.32512) (0.00834) r=0.967 $P_r=0.033$ var=0.06184

$= 7.16950 - 0.11128*T + 0.00086*T^2$ (0.65759) (0.03837) (0.00049) r=0.992 var=0.03038 $P_F=0.50$

$\ln= 1.85048 - 0.01010*T$ (0.05412) (0.00139) r=0.982 $P_r=0.018$ var=0.00171

$\ln= 2.01950 - 0.02050*T + 0.00014*T^2$ (0.12775) (0.00745) (0.00010) r=0.994 var=0.00115 $P_F=0.50$

Liver

	7	18	7.0	*	-110.0 # "
		28	5.9	*	-66.7 #
		40	5.1	*	-16.7 #
		58	4.8	*	

$= 7.61351 - 0.05315*T$ (0.57823) (0.01484) r=0.930 var=0.19559 $P_r=0.070$

$= 9.82582 - 0.18917*T + 0.00177*T^2$ (0.07736) (0.00451) (0.00006) r=1.000 var=0.00042 $P_F=0.025$

$\ln= 2.06209 - 0.00923*T$ (0.08831) (0.00227) r=0.945 var=0.00456 $P_r=0.055$

$\ln= 2.39975 - 0.02999*T + 0.00027*T^2$ (0.01719) (0.00100) (0.00001) r=1.000 var=0.00002 $P_F=0.05$

	3	18	2.8	*	-30.0 # " sample #2
		28	2.5	*	-16.7 #
		40	2.3	*	-11.1 #
		58	2.1	*	

$= 3.03311 - 0.01689*T$ (0.10986) (0.00282) r=0.973 var=0.00706 $P_r=0.027$

$= 3.44142 - 0.04200*T + 0.00033*T^2$ (0.10745) (0.00627) (0.00008) r=0.998 var=0.00081 $P_F=0.25$

$\ln= 1.13191 - 0.00699*T$ (0.03657) (0.00094) r=0.982 var=0.00078 $P_r=0.018$

$\ln= 1.26805 - 0.01536*T + 0.00011*T^2$ (0.03476) (0.00203) (0.00003) r=0.999 var=0.00008 $P_F=0.25$

	4	18	3.5	*	-30.0 # "
		28	3.2	*	-33.3 #
		40	2.8	*	-11.1 #
		58	2.6	*	

$= 3.84392 - 0.02275*T$ (0.15469) (0.00397) r=0.971 var=0.01400 $P_r=0.029$

$= 4.39618 - 0.05670*T + 0.00044*T^2$ (0.22779) (0.01329) (0.00017) r=0.996 var=0.00365 $P_F=0.25$

$\ln= 1.37250 - 0.00756*T$ (0.04504) (0.00116) r=0.977 var=0.00119 $P_r=0.023$

$\ln= 1.52546 - 0.01697*T + 0.00012*T^2$ (0.08480) (0.00495) (0.00006) r=0.995 var=0.00051 $P_F=0.50$

Liver

	5	18	4.5	*	-70.0 # "
		28	3.8	*	-41.7 #
		40	3.3	*	-16.7 #
		58	3.0	*	

$= 4.95541 - 0.03626*T$ (0.32343) (0.00830) r=0.951 var=0.06119 $P_r=0.049$

$= 6.18874 - 0.11209*T + 0.00099*T^2$ (0.11604) (0.00677) (0.00009) r=1.000 var=0.00095 $P_F=0.10$

$\ln= 1.63999 - 0.00992*T$ (0.07246) (0.00186) r=0.967 var=0.00307 $P_r=0.033$

$\ln= 1.91733 - 0.02697*T + 0.00022*T^2$ (0.00479) (0.00028) (0.00000) r=1.000 var=0.00000 $P_F=0.025$

	6	18	5.6	*	-80.0 # "
		28	4.8	*	-66.7 #
		40	4.0	*	-11.1 #
		58	3.8	*	

$= 6.15541 - 0.04459*T$ (0.47507) (0.01219) r=0.933 var=0.13203 $P_r=0.067$

$= 7.94939 - 0.15489*T + 0.00143*T^2$ (0.31805) (0.01856) (0.00024) r=0.998 var=0.00711 $P_F=0.25$

$\ln= 1.85358 - 0.00973*T$ (0.09389) (0.00241) r=0.944 var=0.00516 $P_r=0.056$

$\ln= 2.19990 - 0.03103*T + 0.00028*T^2$ (0.10247) (0.00598) (0.00008) r=0.996 var=0.00074 $P_F=0.25$

	7	18	7.0	*	-100.0 # "
		28	6.0	*	-83.3 #
		40	5.0	*	-33.3 #
		58	4.4	*	

$= 7.91892 - 0.06441*T$ (0.44865) (0.01152) r=0.969 var=0.11775 $P_r=0.030$

$= 9.62253 - 0.16916*T + 0.00136*T^2$ (0.23209) (0.01354) (0.00017) r=1.000 var=0.00378 $P_F=0.10$

$\ln= 2.12586 - 0.01163*T$ (0.06185) (0.00159) r=0.982 var=0.00224 $P_r=0.018$

$\ln= 2.35433 - 0.02568*T + 0.00018*T^2$ (0.06629) (0.00387) (0.00005) r=0.999 var=0.00031 $P_F=0.25$

Liver

porcine							
fresh	2	4	3.3	* (1.5)	-6.25	#	Gammell
< 1 hr.,		20	3.2	*	47.1	#	et al.
stored @ 5°C		37	4.0	*		#	(1979)*2

$= 3.06322 + 0.02148*T$ r=0.813 $P_r=0.395$
(0.37492) (0.01537) var=0.12867
$= 3.45423 - 0.04502*T + 0.00162*T^2$ r=1.000
(0.00000) (0.00000) (0.00000) var=0.00000

$\ln= 1.12771 + 0.00591*T$ r=0.806 $P_r=0.403$
(0.10584) (0.00434) var=0.01025
$\ln= 1.23810 - 0.01287*T + 0.00046*T^2$ r=1.000
(0.00000) (0.00000) (0.00000) var=0.00000

4	4	7.2	*	-43.8	#	"
	20	6.5	*	-29.4	#	
	37	6.0	*			

$= 7.30459 - 0.03629*T$ r=0.994 $P_r=0.072$
(0.10084) (0.00413) var=0.00931
$= 7.40976 - 0.05418*T + 0.00043*T^2$ r=1.000
(0.00000) (0.00000) (0.00000) var=0.00000

$\ln= 1.99138 - 0.00552*T$ r=0.996 $P_r=0.056$
(0.01184) (0.00049) var=0.00013
$\ln= 2.00373 - 0.00762*T + 0.00005*T^2$ r=1.000
(0.00000) (0.00000) (0.00000) var=0.00000

6	4	12.0	*	-106.3	#	"
	20	10.3	*	-76.5	#	
	37	9.0	*			

$=12.27876 - 0.09076*T$ r=0.996 $P_r=0.060$
(0.20944) (0.00859) var=0.04015
$=12.49719 - 0.12791*T + 0.00090*T^2$ r=1.000
(0.00000) (0.00000) (0.00000) var=0.00000

$\ln= 2.51519 - 0.00871*T$ r=0.999 $P_r=0.034$
(0.01133) (0.00046) var=0.00012
$\ln= 2.52700 - 0.01072*T + 0.00005*T^2$ r=1.000
(0.00000) (0.00000) (0.00000) var=0.00000

Liver

	8	4	17.3 *	-162.5 #	"
		20	14.7 *	-158.8 #	
		37	12.0 *		

=17.93195 - 0.16059*T	r=1.000	P_r=0.004
(0.02586) (0.00106)	var=0.00061	
=17.95891 - 0.16517*T + 0.00011*T^2	r=1.000	
(0.00000) (0.00000) (0.00000)	var=0.00000	
ln= 2.90006 - 0.01109*T	r=0.999	P_r=0.029
(0.01237) (0.00051)	var=0.00014	
ln= 2.88716 - 0.00890*T - 0.00005*T^2	r=1.000	
(0.00000) (0.00000) (0.00000)	var=0.00000	

	9.9	4	23.3 *	-143.8 #	"
		20	21.0 *	-294.1 #	
		37	16.0 *		

=24.61340 - 0.22197*T	r=0.981	P_r=0.123
(1.05752) (0.04335)	var=1.02375	
=23.51047 - 0.03439*T - 0.00456*T^2	r=1.000	
(0.00000) (0.00000) (0.00000)	var=0.00000	
ln= 3.22109 - 0.01144*T	r=0.973	P_r=0.150
(0.06682) (0.00274)	var=0.00409	
ln= 3.15140 + 0.00041*T - 0.00029*T^2	r=1.000	
(0.00000) (0.00000) (0.00000)	var=0.00000	

Liver

porcine						
homogenate	4.0	4.0	1.32	(5%)	-33.3 #	Danckwerts
		5.2	1.28		-75.0 #	(1974)*1
		6.0	1.22		-20.0 #	
		7.0	1.20		-7.90 #	
		10.8	1.17		-28.1 #	
		14.0	1.08		30.0 #	
		15.0	1.11		-16.7 #	
		18.0	1.06		-50.0 #	
		18.8	1.02		-46.7 #	
		20.0	0.964		2.67 #	
		23.0	0.972		-18.9 #	
		24.8	0.938		3.75 #	
		28.0	0.95		-13.3 #	
		28.9	0.938		-47.3 #	
		30.0	0.886			

$= 1.32567 - 0.01490*T$ r=0.971 $P_r=0.000$
(0.01918) (0.00101) var=0.00115
$= 1.39529 - 0.02615*T + 0.00033*T^2$ r=0.984
(0.02723) (0.00376) (0.00011) var=0.00070 $P_F=0.01$

$\ln= 0.29622 - 0.01375*T$ r=0.976 $P_r=0.000$
(0.01600) (0.00084) var=0.00080
$\ln= 0.34213 - 0.02117*T + 0.00022*T^2$ r=0.983
(0.02584) (0.00357) (0.00010) var=0.00063 $P_F=0.10$

Nervous Tissue, brain

bovine						
formalin	1	10	0.30	*	50.00 #	Bamber & Hill
fixed,		18	0.70	*	21.05 #	(1979)*2
2 months,		37	1.1	*	-14.29 #	
10 %		58	0.8	*		

$= 0.42248 + 0.00984*T$ r=0.637 $P_r=0.363$
(0.30195) (0.00841) var=0.09722
$=-0.33001 + 0.07308*T - 0.00092*T^2$ r=0.999
(0.03615) (0.00269) (0.00004) var=0.00034 $P_F=0.05$

$\ln=-0.95995 + 0.01749*T$ r=0.675 $P_r=0.325$
(0.48533) (0.01352) var=0.25117
$\ln=-2.12043 + 0.11502*T - 0.00143*T^2$ r=0.978
(0.39615) (0.02947) (0.00042) var=0.04071 $P_F=0.25$

Nervous Tissue, brain

	2	10	2.3	*	-62.50 # "
		18	1.8	*	-5.26 #
		37	1.7	*	-14.29 #
		58	1.4	*	

$= 2.28985 - 0.01593*T$ (0.18263) (0.00509) — r=0.911, var=0.03556, $P_r=0.089$

$= 2.52375 - 0.03559*T + 0.00029*T^2$ (0.44935) (0.03343) (0.00048) — r=0.936, var=0.05238, $P_F>0.50$

$\ln= 0.84689 - 0.00894*T$ (0.08554) (0.00238) — r=0.936, var=0.00780, $P_r=0.064$

$\ln= 0.92990 - 0.01592*T + 0.00010*T^2$ (0.22594) (0.01681) (0.00024) — r=0.946, var=0.01324, $P_F>0.50$

	3	10	4.4	*	-75.00 # "
		18	3.8	*	-31.58 #
		37	3.2	*	-23.81 #
		58	2.7	*	

$= 4.55783 - 0.03359*T$ (0.18949) (0.00528) — r=0.976, var=0.03829, $P_r=0.024$

$= 4.96754 - 0.06802*T + 0.00050*T^2$ (0.27089) (0.02015) (0.00029) — r=0.994, var=0.01904, $P_F=0.50$

$\ln= 1.54362 - 0.00977*T$ (0.03733) (0.00104) — r=0.989, var=0.00149, $P_r=0.011$

$\ln= 1.61997 - 0.01618*T + 0.00009*T^2$ (0.06128) (0.00456) (0.00007) — r=0.996, var=0.00097, $P_F=0.50$

	4	10	6.8	*	-137.5 # "
		18	5.7	*	-42.11 #
		37	4.9	*	-33.33 #
		58	4.2	*	

$= 6.93666 - 0.04997*T$ (0.37933) (0.01056) — r=0.958, var=0.15344, $P_r=0.042$

$= 7.70491 - 0.11454*T + 0.00094*T^2$ (0.63488) (0.04723) (0.00068) — r=0.986, var=0.10456, $P_F=0.50$

$\ln= 1.95960 - 0.00940*T$ (0.05333) (0.00149) — r=0.976, var=0.00303, $P_r=0.024$

$\ln= 2.06237 - 0.01804*T + 0.00013*T^2$ (0.09707) (0.00722) (0.00010) — r=0.990, var=0.00244, $P_F=0.50$

Nervous Tissue, brain

	5	10	9.0	*	-125.0 #	"
		18	8.0	*	-84.21 #	
		37	6.4	*	-23.81 #	
		58	5.9	*		

= 9.29280 - 0.06399*T r=0.957 P_r=0.043
(0.49269) (0.01372) var=0.25884
=10.52170 - 0.16727*T + 0.00151*T^2 r=1.000
(0.00013) (0.00001) (0.00000) var=0.00000 P_F=0.001

ln= 2.24843 - 0.00883*T r=0.968 P_r=0.032
(0.05831) (0.00162) var=0.00363
ln= 2.39317 - 0.02099*T + 0.00018*T^2 r=1.000
(0.01656) (0.00123) (0.00002) var=0.00007 P_F=0.10

feline					
in vivo	1.0	25	0.85		Hasegawa
			0.97		et al.
		27	0.88		(1966)*1
		28	1.04		
			0.81		
		29	0.73		

=-3.44000 + 0.16000*T r=1.000
(0.00000) (0.00000) var=0.00000

ln=-4.63829 + 0.16705*T r=1.000
(0.00000) (0.00000) var=0.00000

feline					
p. m.	1.0	25	0.84		Hasegawa
			0.91		et al.
		27	0.85		(1966)*1
		28	1.07		
			0.80		
		29	0.74		

=-5.09000 + 0.22000*T r=1.000
(0.00000) (0.00000) var=0.00000

ln=-6.37731 + 0.23018*T r=1.000
(0.00000) (0.00000) var=0.00000

Nervous Tissue, spinal cord

Nervous Tissue, spinal cord

---

murine			cm^{-1}			
neonatal,	0.26	2	0.048	*	-0.21	# Johnston
24 hrs.,		10	0.0463	*	-0.17	# <u>et al.</u>
3rd lumbar		20	0.0446	*	-0.27	# (1979).
vertebra		30	0.0419	*	-0.13	# absorption
		40	0.0406	*		

$= 0.04836 - 0.00020*T$ (0.00027) (0.00001) — $r=0.996$, $var=0.00000$, $P_r=0.000$

$= 0.04849 - 0.00022*T + 0.00000*T^2$ (0.00043) (0.00005) (0.00000) — $r=0.996$, $var=0.00000$, $P_F>0.50$

$\ln=-3.02672 - 0.00453*T$ (0.00601) (0.00025) — $r=0.996$, $var=0.00006$, $P_r=0.000$

$\ln=-3.02608 - 0.00463*T + 0.00000*T^2$ (0.01014) (0.00119) (0.00003) — $r=0.996$, $var=0.00008$, $P_F>0.50$

---

murine						
neonatal,	0.5	2	1.13	(10%)	-32.5	# Dunn & Brady
24 hrs.,		10	0.87		-17.0	# (1974a)*1
3rd lumbar		20	0.7		-2.50	# absorption
vertebra		40	0.65			

$= 1.04557 - 0.01156*T$ (0.10318) (0.00450) — $r=0.876$, $var=0.01636$, $P_r=0.124$

$= 1.19509 - 0.03689*T + 0.00058*T^2$ (0.02153) (0.00270) (0.00006) — $r=0.999$, $var=0.00035$, $P_F=0.10$

$\ln= 0.04464 - 0.01365*T$ (0.10626) (0.00463) — $r=0.902$, $var=0.01735$, $P_r=0.098$

$\ln= 0.19944 - 0.03987*T + 0.00060*T^2$ (0.00039) (0.00005) (0.00000) — $r=1.000$, $var=0.00000$, $P_F=0.005$

Nervous Tissue, spinal cord

neonatal	0.7	2	0.77	17.5 #	"
		10	0.91	5.00 #	
		30	1.01	-10.0 #	
		40	0.91	0.00 #	
		45	0.91		

$= 0.83437 + 0.00266*T$ r=0.583 $P_r=0.302$
(0.06521) (0.00214) var=0.00644
$= 0.73964 + 0.01963*T - 0.00036*T^2$ r=0.967
(0.03318) (0.00402) (0.00008) var=0.00094 $P_F=0.05$

$\ln=-0.18631 + 0.00313*T$ r=0.601 $P_r=0.284$
(0.07305) (0.00240) var=0.00809
$\ln=-0.29221 + 0.02209*T - 0.00041*T^2$ r=0.967
(0.03792) (0.00459) (0.00010) var=0.00122 $P_F=0.10$

neonatal	1.0	40	0.100	1.80 #	"
		45	0.109		

$= 0.02800 + 0.00180*T$ r=1.000
(0.00000) (0.00000) var=0.00000

$\ln=-2.99201 + 0.01724*T$ r=1.000
(0.00000) (0.00000) var=0.00000

---

murine			cm^{-1}		
neonatal,	1.0	2	0.02 *	3.75 #	Johnston
24 hrs.,		10	0.05 *	2.65 #	et al.
3rd lumbar		27	0.095 *	1.54 #	(1979).
vertebra		40	0.115 *	1.00 #	absorption
		45	0.12 *		

$= 0.02288 + 0.00230*T$ r=0.986 $P_r=0.002$
(0.00678) (0.00023) var=0.00007
$= 0.01228 + 0.00410*T - 0.00004*T^2$ r=1.000
(0.00063) (0.00007) (0.00000) var=0.00000 $P_F=0.005$

$\ln=-3.65317 + 0.03807*T$ r=0.933 $P_r=0.020$
(0.25223) (0.00845) var=0.09867
$\ln=-4.01821 + 0.09987*T - 0.00131*T^2$ r=0.991
(0.15829) (0.01839) (0.00038) var=0.02140 $P_F=0.10$

Spleen

Spleen

bovine							
formalin	1	10	1.2	* (10%)	25.0 #	Bamber & Hill	
fixed, 2 months		18	1.4	*	26.3 #	(1979)*2	
4%		37	1.9	*	-23.8 #		
		58	1.4	*			

$= 1.31227 + 0.00529*T$ r=0.379 $P_r=0.621$
(0.32769) (0.00913) var=0.11450
$= 0.52425 + 0.07152*T - 0.00097*T^2$ r=0.969
(0.24942) (0.01855) (0.00027) var=0.01614 $P_F=0.25$

$\ln= 0.26004 + 0.00372*T$ r=0.413 $P_r=0.587$
(0.20807) (0.00579) var=0.04616
$\ln=-0.24762 + 0.04638*T - 0.00062*T^2$ r=0.982
(0.12395) (0.00922) (0.00013) var=0.00399 $P_F=0.25$

2	10	2.9	*	-50.0 #	"	
	18	2.5	*	-5.26 #		
	37	2.4	*	-19.0 #		
	58	2.0	*			

$= 2.95439 - 0.01640*T$ r=0.950 $P_r=0.050$
(0.13715) (0.00382) var=0.02006
$= 3.03020 - 0.02277*T + 0.00009*T^2$ r=0.952
(0.38346) (0.02853) (0.00041) var=0.03814 $P_F>0.50$

$\ln= 1.09801 - 0.00685*T$ r=0.959 $P_r=0.041$
(0.05154) (0.00144) var=0.00283
$\ln= 1.10230 - 0.00721*T + 0.00001*T^2$ r=0.959
(0.14769) (0.01099) (0.00016) var=0.00566 $P_F>0.50$

3	10	4.5	*	-62.5 #	"	
	18	4.0	*	-26.3 #		
	37	3.5	*	-28.6 #		
	58	2.9	*			

$= 4.69744 - 0.03162*T$ r=0.988 $P_r=0.012$
(0.12373) (0.00345) var=0.01632
$= 4.90011 - 0.04866*T + 0.00025*T^2$ r=0.993
(0.26756) (0.01990) (0.00029) var=0.01857 $P_F>0.50$

$\ln= 1.57131 - 0.00876*T$ r=0.994 $P_r=0.006$
(0.02367) (0.00066) var=0.00060
$\ln= 1.59140 - 0.01045*T + 0.00002*T^2$ r=0.995
(0.06383) (0.00475) (0.00007) var=0.00106 $P_F>0.50$

Spleen

	4	10	6.2	*		-50.0 #	"
		18	5.8	*		-47.4 #	
		37	4.9	*		-42.9 #	
		58	4.0	*			

$= 6.63361 - 0.04581*T$ (0.03572) (0.00099) — r=1.000, var=0.00136, $P_r=0.000$

$= 6.72266 - 0.05329*T + 0.00011*T^2$ (0.00293) (0.00022) (0.00000) — r=1.000, var=0.00000, $P_F=0.025$

$\ln= 1.92049 - 0.00914*T$ (0.00645) (0.00018) — r=1.000, var=0.00004, $P_r=0.000$

$\ln= 1.90440 - 0.00779*T - 0.00002*T^2$ (0.00004) (0.00000) (0.00000) — r=1.000, var=0.00000, $P_F=0.005$

	5	10	8.1	*		-50.0 #	"
		18	7.7	*		-68.4 #	
		37	6.4	*		-61.9 #	
		58	5.1	*			

$= 8.77714 - 0.06348*T$ (0.05692) (0.00159) — r=0.999, var=0.00346, $P_r=0.001$

$= 8.75928 - 0.06198*T - 0.00002*T^2$ (0.16192) (0.01205) (0.00017) — r=0.999, var=0.00680, $P_F>0.50$

$\ln= 2.20512 - 0.00977*T$ (0.01719) (0.00048) — r=0.998, var=0.00032, $P_r=0.002$

$\ln= 2.16554 - 0.00644*T - 0.00005*T^2$ (0.01897) (0.00141) (0.00002) — r=1.000, var=0.00009, $P_F=0.50$

porcine							
fresh,	2	4	2.0	*	(1.5)	-6.25 #	Gammell
< 1 hr.,		20	1.9	*		-52.9 #	<u>et al.</u>
stored @ 5°C		37	1.0	*		#	(1979)*2

$= 2.25428 - 0.03054*T$ (0.32838) (0.01346) — r=0.915, var=0.09871, $P_r=0.264$

$= 1.91181 + 0.02771*T - 0.00141*T^2$ (0.00000) (0.00000) (0.00000) — r=1.000, var=0.00000

$\ln= 0.87563 - 0.02118*T$ (0.24299) (0.00996) — r=0.905, var=0.05405, $P_r=0.280$

$\ln= 0.62221 + 0.02192*T - 0.00105*T^2$ (0.00000) (0.00000) (0.00000) — r=1.000, var=0.00000

Spleen

	4	4	7.9	*	-150.0 # "
		20	5.5	*	-117.6 #
		37	3.5	*	

$= 8.34113 - 0.13317*T$ r=0.998 $P_r=0.044$
(0.22754) (0.00933) var=0.04739
$= 8.57843 - 0.17353*T + 0.00098*T^2$ r=1.000
(0.00000) (0.00000) (0.00000) var=0.00000

$\ln= 2.17681 - 0.02469*T$ r=0.999 $P_r=0.029$
(0.02782) (0.00114) var=0.00071
$\ln= 2.14780 - 0.01976*T - 0.00012*T^2$ r=1.000
(0.00000) (0.00000) (0.00000) var=0.00000

	6	4	14.0	*	-318.8 # "
		20	8.9	*	-170.6 #
		37	6.0	*	

$=14.54743 - 0.24168*T$ r=0.985 $P_r=0.111$
(1.04201) (0.04272) var=0.99394
$=15.63418 - 0.42650*T + 0.00449*T^2$ r=1.000
(0.00000) (0.00000) (0.00000) var=0.00000

$\ln= 2.72717 - 0.02565*T$ r=0.998 $P_r=0.037$
(0.03600) (0.00148) var=0.00119
$\ln= 2.76472 - 0.03204*T + 0.00016*T^2$ r=1.000
(0.00000) (0.00000) (0.00000) var=0.00000

	8	4	21.5	*	-475.0 # "
		20	13.9	*	-347.1 #
		37	8.0	*	

$=22.77173 - 0.40845*T$ r=0.996 $P_r=0.057$
(0.89980) (0.03689) var=0.74115
$=23.71016 - 0.56805*T + 0.00388*T^2$ r=1.000
(0.00000) (0.00000) (0.00000) var=0.00000

$\ln= 3.20281 - 0.02998*T$ r=0.999 $P_r=0.032$
(0.03683) (0.00151) var=0.00124
$\ln= 3.16440 - 0.02345*T - 0.00016*T^2$ r=1.000
(0.00000) (0.00000) (0.00000) var=0.00000

Spleen

	9.9	4	31.8	*	-768.8 # "
		20	19.5	*	-464.7 #
		37	11.6	*	

=33.38195 - 0.61059*T	r=0.990	P_r=0.091
(2.13832) (0.08766)	var=4.18561	
=35.61208 - 0.98987*T + 0.00921*T^2	r=1.000	
(0.00000) (0.00000) (0.00000)	var=0.00000	
ln= 3.58167 - 0.03056*T	r=1.000	P_r=0.000
(0.00009) (0.00000)	var=0.00000	
ln= 3.58176 - 0.03057*T + 0.00000*T^2	r=1.000	
(0.00000) (0.00000) (0.00000)	var=0.00000	

REFERENCES

Altman, P. L. and Dittmer, D. S., Blood and other body fluids, in Federation of American Societies for Experimental Biology, Washington, D. C., 1961.

American Institute of Ultrasound in Medicine, Safety Considerations for Diagnostic Ultrasound, prepared by the Bioeffects Committee of the AIUM, Publication 316, AIUM Publications, Bethesda, MD., 1984.

Bakke, T., Gytre, T., Haagensen, A., and Giezendanner, L., Ultrasonic measurement of sound velocity in whole blood. A comparison between an ultrasonic method and conventional packed-cell-volume test for hematocrit determination, Scand. J. Clin. Lab. Invest., 35, pp 473-478, 1975.

Bamber, J. C., Fry, M. J., Hill, C. R., and Dunn, F., Ultrasonic attenuation and backscatter by mammalian organs as a function of time after excision, Ultrasound in Medicine and Biology, 3, pp 15-20, 1977.

Bamber, J. C. and Hill, C. R., Ultrasonic attenuation and propagation speed in mammalian tissues as a function of temperature, Ultrasound in Medicine and Biology, 5, No. 2, pp 149-157, 1979.

Begui, Z. E., Acoustic properties of the refractive media of the eye, JASA, 26, No. 3, pp 365-368, 1954.

Berkwits, L., A multiple motor control system for ultrasonic computed axial tomography, Master's thesis, University of Illinois, 1980.

Bevington, P. R., Data Reduction and Error Analysis for the Physical Sciences, McGraw-Hill, New York, 1969.

Bowen, T., Connor, W. G., Nasoni, R. L., Pifer, A. E., and Sholes, R. R., Measurement of temperature dependence of the velocity of ultrasound in soft tissues, in Ultrasonic Tissue Characterization II, M. Linzer, ed., NBS 525, pp 57-61, 1979.

Bradley, J. V., Elementary Microstudies of Human Tissues, Charles C. Thomas, Springfield, IL, 1972.

Bradley, E. L. and Sacerio, J., The velocity of ultrasound in human blood under varying physiologic parameters, J. Surg. Res., 12, pp 290-297, 1972.

Burdic, W. S., Underwater Acoustic System Analysis, Prentice-Hall, Englewood Cliffs, N. J., 1984.

Buschmann, W., Voss, M., and Kemmerling, S., Acoustic properties of normal human orbit tissues, Ophthalmol. Res., 1, pp 354-364, 1970.

Carstensen, E. L., Absorption of sound in tissues, in Ultrasonic Tissue Characterization II, M. Linzer, ed., NBS 525, pp 29-36, 1979.

Carstensen, E. L., Li, K., and Schwan, H. P., Determination of the acoustic properties of blood and its components, JASA, 25, No. 2, pp 286-289, 1953.

Carstensen, E. L. and Schwan, H. P., Acoustic properties of hemoglobin solutions, JASA, 31, No. 3, pp 305-311, 1959.

Chvapil, M., Physiology of Connective Tissue, Butterworths, London, 1967.

Crawford, C. R. and Kak, A. C., Multipath artifacts in ultrasonic transmission tomography, Purdue University technical report, TR-EE 81-33, December, 1981.

Danckwerts, H. J., Discrete relaxation processes as a model of the absorption of ultrasound in liver homogenate, JASA, 55, pp 1098-1099, 1974

Dawson, H., The Physiology of the Eye, Academic Press, New York, 1972.

Dunn, F., Temperature and amplitude dependence of acoustic absorption in tissue, JASA, 34, No. 10, pp 1545-1547, 1962.

Dunn, F., Ultrasonic attenuation, absorption, and velocity in tissues and organs, in Ultrasonic Tissue Characterization I, NBS 453, pp 21-28, 1976.

Dunn, F. and Brady, J. K., Ultrasonic absorption in biological media, Biofizika, 18, pp 1069-1072, 1973 (in Russian, English abstract); translated in Biophysics, 18, pp 1128-1132, 1974a.

Dunn, F. and Brady, J. K., Temperature and frequency dependence of ultrasonic absorption, in Proceedings of the 8th International Congress on Acoustics, Vol. I, Goldcrest Press, Trowbridge, Wilts., p 366c, 1974b.

Dunn, F., Edmonds, P. D., and Fry, W. J., Absorption and dispersion of ultrasound in biological media, in Biological Engineering, H. P. Schwan, ed., McGraw Hill, New York, pp 205-332, 1969.

Edmonds, P. D., Ultrasonic absorption of hemoglobin solutions, Biochim. Biophys. Acta, 63, p 216, 1962.

Edmonds, P. D., Baulk, T. J., III, Dyro, J. F., and Hussey, M., Ultrasonic absorption of aqueous hemoglobin solutions, Biochim. Biophys. Acta, 200, p 174, 1970.

Edmonds, P. D. and Dunn, F., Physical description of ultrasonic fields, Methods of Experimental Physics, Vol. 19, P. D. Edmonds, ed., Academic Press, N. Y., pp 1-28, 1981.

Edwards, C. A. and O'Brien, W. D., Jr., Ultrasonic examination of mammalian tendon with acoustic microscopy in various media, abstract, JASA, 65, Suppl. No. 1, p S4, 1979.

Embree, P. M., Doctoral disseration in progess, University of Illinois, 1986.

Fields, S. and Dunn, F., Correlation of echographic visualizability of tissue with biological composition and physiological state, JASA, 54, pp 809-812, 1973.

Fitzgerald, J. W., Ringo, G. R., and Winder, W. C., An ultrasonic method for measurement of solids-not-fat and butterfat in fluid milk 1. Acoustic properties, in Proceedings of the 56th Annual Meeting of the American Dairy Science Association, American Dairy Science Association, Madison, WI., 1961.

Foster, S. G., A pulsed ultrasonic flowmeter using time domain methods, Doctoral dissertation, University of Illinois, 1985.

Freese, M. and Lyons, E. A., Dependence of ultrasound backscatter from human liver tissue on frequency and protein/lipid composition, in Ultrasonic Tissue Characterization II, M. Linzer, ed., NBS 525, pp 157-163, 1979.

Fry, F. J., Ultrasonically-induced transient thermal gradients: their potential role in acoustic parameter characterization of tissue, in Ultrasonic Tissue Characterization I, NBS 453, pp 143-151, 1975.

Fry, W. J. and Fry, F. J., Ultrasonic visualization of soft-tissue structure, based on gradients in absorption characteristics, JASA, 35, No. 11, pp 1788-1790, 1963.

Fyke, F. E., Greenleaf, J. F., and Johnson, S. A., Continuous wave measurements of acoustic attenuation in an oil/polymer mixture, Ultrasound in Medicine and Biology, 5, pp 87-90, 1979.

Galton, D. J., The Human Adipose Cell, Butterworths, London, 1971.

Gammell, P. M., LeCroisette, D. H., and Heyser, R. C., Temperature and frequency depedence of ultrasonic attenuation in selected tissues, Ultrasound in Medicine and Biology, 5, pp 269-277, 1979.

Ganong, W. F., Review of Medical Physiology, Lange Med. Pub., Los Altos, CA, 1967.

Gordon, R. A., A tutorial on ART, IEEE Trans. Nuclear Science, Vol. NS-21, pp 78-93, 1974.

Goss, S. A., Johnston, R. L., and Dunn, F., Comprehensive compilation of empirical ultrasonic properties of mammalian tissues, JASA, 64, No. 2, pp 423-457, 1978.

Goss, S. A., Johnston, R. L., and Dunn, F., Compilation of empirical ultrasonic properties of mammalian tissues II, JASA, 68, No. 1, pp 93-108, 1980.

Goss, S. A. and Dunn, F., Ultrasonic propagation properties of collagen, Phys. Med. Biol., 25, pp 827-837, 1980.

Goss, S. A. and O'Brien, W. D., Jr., Direct ultrasonic velocity measurements of mammalian collagen threads, JASA, 65, pp 507-511, 1979.

Gramberg, H., Doctoral dissertation, Johann-Wolfgang-Goethe Universitat, Frankfurt, 1956.

Haney, M. J., Segal, L. A., Tervola, K. M. U., Grummer, M. A., Erdman, J. W., Jr., Frizzell, L. A., and O'Brien, W. D., Jr., Comparison of ultrasonic properties measurement in fatty liver using several techniques, abstract, Journal of Ultrasound in Medicine, Vol. 3, No. 9, Supplement, p 130, September, 1984.

Haney, M. J. and O'Brien, W. D., Jr., Ultrasonic tomography for differential tomography, Acoustical Imaging, 12, E. A. Ash and C. R. Hill, eds., Plenum Press, New York, pp 589-597, 1982.

Haney, M. J. and O'Brien, W. D., Jr., Temperature dependency of ultrasonic propagation properties in biological materials, accepted for publication in Characterization of Tissue with Ultrasound, J. F. Greenleaf, ed., CRC Publishing, 1985 (in press).

Hasegawa, H., Watanabe, M., Ito, J., Nakjo, S., Ishitani, K., Ogura, T., and Okawa, M., Study on the ultrasonic attenuation in brain tissue in vivo, Jpn. Med. Ultrasonics, 4, p 8, 1966.

Heffernan, P. B. and Robb, R. A., Image reconstruction from incomplete projection data: iterative reconstruction-reprojection techniques, IEEE Trans. Biomedical Engineering, Vol. BME-30, No. 12, pp 838-841, 1983.

Herman, G. T., Image Reconstruction from Projections, Academic Press, N. Y., 1980.

Herman, G. T., Lakshminarayanan, A. V., and Rowland, S. W., The reconstruction of objects from shadowgraphs with high contrast, Pattern Recognition, 7, No. 4, pp 157-165, 1975.

Horn, B. K. P., Fan-beam reconstruction methods, Proc. IEEE, Vol. 67, No. 12, pp 1616-1623, 1979.

Huang, T. S., Algebraic methods of image restoration, in Digital Image Processing and Analysis, J. C. Simon and A. Rosenfeld, eds., Noordhoff International Publishing, Leyden, 1977, pp 41-46.

Jansson, F. and Sundmark, E., Determination of the velocity of ultrasound in ocular tissues at different temperatures, Acta Ophthalmol., 39, pp 899-910, 1961.

Johnson, S. A., Christensen, D. A., Johnson, C. C., Greenleaf, J. F., and Rajagopalan, B., Non-intrusive measurement of microwave and ultrasound-induced hyperthermia by acoustic temperature tomography, in Proc. IEEE Ultrasonics Symposium, pp 977-982, October, 1977a.

Johnson, S. A., Greenleaf, J. F., Samayoa, W. A., Duck, F. A., and Sjostrand, J., Reconstruction of three-dimensional velocity fields and other parameters by acoustic ray tracing, in Proc. IEEE Ultrasonics Symposium, pp 46-51, September, 1975.

Johnson, S. A., Greenleaf, J. M., Tanaka, M., and Flandro, G., Reconstructing three dimensional temperature and fluid velocity vector fields from acoustic transmission measurements, Instrument Society of America Transactions, 16, No. 3, pp 3-15, 1977b.

Johnston, R. L., Goss, S. A., Maynard, V., Brady, J. K., Frizzell, L. A., O'Brien, W. D., and Dunn, F., Elements of tissue characterization, in Ultrasonic Tissue Charaterization II, M. Linzer, ed., NBS 525, pp 19-27, 1979.

Kak, A. C., Computerized tomography with x-ray, emission, and ultrasound sources, Proc. IEEE, Vol. 67, No. 9, pp 1245-1272, 1979.

Kak, A. C., Notes on Image Processing: Restoration, Compression, and Reconstruction from Projections, Purdue University technical report, TR-EE 80-46, ch. 8, December, 1980.

Katz, M. B., Questions of Uniqueness and Resolution in Reconstruction from Projections, Springer-Verlag, Berlin, 1978.

Kikuchi, Y., Okuyama, D., Kasai, C., and Yoshida, Y., Measurements on the sound velocity and absorption of human blood in 1-10 MHz frequency range, Rec. Elect. Commun. Eng. Convers. Tohoku Univ., 41, pp 152-159, 1972.

Kishimoto, T., Ultrasonic absorption in bones, Acustica, 8, pp 179-180, 1958.

Lambert, J. D., Vibrational and Rotational Relaxation in Gasses, Clarendon Press, Oxford, 1977.

Lang, J., Zana, R., Gairard, B., Dale, G., and Gras, Ch. M., Ultrasonic absorption in the human breast cyst liquids, Ultrasound in Medicine and Biology, 4, No. 2, pp 125-130, 1978.

Lerner, B., Microcomputer-controlled servo system for an ultrasonic computer-assisted tomographic scanner, Master's thesis, University of Illinois, 1979.

Luenberger, D. G., Optimization by Vector Space Methods, John Wiley and Sons, N. Y., 1969.

Madsen, E. L. and Frank, G. R., Interlaboratory comparison of attenuation measurements, abstract, Journal of Ultrasound in Medicine, Vol. 3, No. 9, p 131, 1984.

Mathews, M. B., Connective Tissue: Macromolecular Structure and Evolution, Springer-Verlag, New York, 1975.

McGill, K. C. and Dorfman, L. J., High-resolution alignment of sampled waveforms, IEEE Trans. Biomedical Engineering, Vol. BME-31, No. 6, pp 462-468, 1984.

McSkimin, H. J., Velocity of sound in distilled water for the temperature range 20 - 75°C, JASA, 37, No. 2, pp 325-328, 1965.

Mersereau, R. M. and Oppenheim, A. V., Digital reconstruction of multidimensional signals from their projetions, Proc. IEEE, Vol. 62, pp 1319-1338, 1974.

Millero, F. J. and Kubinski, T., Speed of sound in seawater as a function of temperature and salinity at 1 atm, JASA, 57, No. 2, pp 312-319, 1975.

Morse, P. M. and Ingard, K. U., Theoretical Acoustics, McGraw-Hill, New York, 1968.

Nasoni, R. L., Bowen, T., Connor, W. G., and Sholes, R. R., In vivo temperature dependence of ultrasound speed in tissue and its application to noninvasive temperature monitoring, Ultrasonic Imaging, 1, No. 1, pp 34-43, 1979.

Neufeld, A. H., Canadian J. Research, B15, p 132, 1937.

Nyborg, W. L., Intermediate Biophysical Mechanics, Cummings Publishing Co., Menlo Park, CA, 1975.

O'Brien, W. D., Jr. and Dunn, F., Ultrasonic absorption mechanisms in aqueous solutions of bovine hemoglobin, J. Phys. Chem., 76, p 528, 1972a.

O'Brien, W. D., Jr. and Dunn, F., Ultrasonic absorption in biomacromolecules, in Interaction of Ultrasound and Biological Tissues, J. M. Reid and M. R. Sikov, eds., DHEW Publication (FDA) 73-8008 BRH/DBE 73-1, p 13, 1972b.

O'Donnell, M., Mimbs, J. W., Sobel, B. E., and Miller, J. G., Ultrasonic attenuation of myocardial tissue: dependence on time after excision and on temperature, JASA, 62, No. 4, pp 1054-1057, 1977.

Pan, S. X. and Kak, A. C., A computational study of reconstruction algorithms for diffraction tomography: interpolation versus filtered backpropagation, IEEE Trans. Acoustics, Speech, and Signal Processing, Vol. ASSP-31, No. 5, pp 1262-1275, 1983.

Parker, J. A., Kenyon, R. V., and Troxel, D. E., Comparison of interpolating methods for image resampling, IEEE Trans. Medical Imaging, Vol. MI-2, No. 1, pp 31-39, 1983.

Parry, R. J. and Chivers, R. C., Data of the velocity and attenuation of ultrasound in mammalian tissues - a survey, in Ultrasonic Tissue Characterization II, M. Linzer, ed., NBS 525, pp 343-360, 1979.

Pauly, H. and Schwan, H. P., Mechanism of absorption in liver tissue, JASA, 50, No. 2, pp 692-699, 1971.

Peyrin, F., Odet, C., Fleischmann, P., and Perdrix, M., Mapping of internal material temperature with ultrasonic computed tomography, Ultrasonics International '83, pp 31-36, July, 1983.

Pinkerton, J. M. M., The absorption of ultrasonic waves in liquids and its relation to molecular constitution, in Proc. Physical Society, London, Sec. B, 62, pp 129-141, 1949.

Pohlhammer, J. D. and O'Brien, W. D., Jr., The relationship between ultrasonic attenuation and speed in tissues and constituents: water, collagen, protein, and fat, in Medical Physics of CT Ultrasound: Tissue Imaging and Characterization, G. D. Fullerton and J. A. Zagzebski, eds., pp 409-435, 1980.

Pratt, W. K., Digital Image Processing, John Wiley and Sons, N. Y., 1978.

Rajagopalan, B., Greenleaf, J. F., Thomas, P. J., Johnson, S. A., and Bahn, R. C. Variation of acoustic speed with temperature in various excised human tissues studied by ultrasound computerized tomography, in Ultrasonic Tissue Characterization II, M. Linzer, ed., NBS 525, pp 227-233, 1979.

Rivara, A. and Sanna, G., Determination of the speed of ultrasound in the ocular tissues of humans and swine, Ann. Ottalmol. Clin. Ocul., 88, pp 675-682, 1962 (in Italian).

Robb-Smith, A. H. T., Normal morphology and morphogenesis of connective tissue, in Connective Tissue in Health and Disease, G. Asboe-Hanson, ed., Physiological Library, Denmark, pp 15-30, 1954.

Robinson, T. C. and Lele, P. P., An analysis of lesion development in the brain and in plastics by high-intensity focused ultrasound at low-megahertz frequencies, JASA, 51, pp 1333-1351, 1972.

Ruch, T. C. and Patton, H. D., Physiology and Biophysics, W. B. Saunders Co., Philadelphia, PA, 1966.

Sachs, T. D., Potential of TAST for measurement of perfusion, ultrasonic absorption and intensity at a point, in Proc. IEEE Ultrasonics Symposium, pp 52-59, November, 1973.

Sachs, T. D. and Janney, C. D., A two-beam acoustic system for tissue analysis, Phys. Med. Bio., 22, No. 2, pp 327-340, 1977.

Sachs, T. D., Welt, A. J., and Slayton, P. W., Thermo-acoustic sensing technique - TAST, in Proc. IEEE Ultrasonics Symposium, October, pp 54-58, 1972.

Schneider, F., Muller-Landau, F., and Mayer, A., Acoustical properties of aqueous solutions of oxygenated and deoxygenated hemoglobin, Biopolymers, 8, p 537, 1969.

Schwan, H. P. and Carstensen, E. L., Advantages and limitations of ultrasonics in medicine, J. Am. Med. Assoc., 149, pp 121-125, 1952.

Sehgal, C. M. and Greenleaf, J. F., Ultrasonic absorption and dispersion in biological media: a postulated model, JASA, 72, No. 6, pp 1711-1718, 1982.

Siedband, M. P. and Holden, J. E., Medical imaging systems, in Medical Instumentation, Application and Design, J. G. Webster, ed., Houghton Mifflin, Boston, 1978.

Slutsky, L. J., Ultrasonic chemical relaxation spectroscopy, in Methods of Experimental Physics, 19, P. D. Edmonds, ed., Academic Press, New York, 1981.

Spiegel, M. R., Theory and Problems of Statistics, Schuam's Outline Series in Mathematics, McGraw-Hill, New York, 1961.

Stuehr, J. and Yeager, E., The propagation of ultrasonic waves in electrolyte solutions, in Physical Acoustics, Principles and Methods, II-A, W. P. Mason, ed., Academic Press, New York, 1965.

Tschewnenko, A. A., Uber die ausbreitungsgeschwindigkeit des ultraschalls in den augengeweben, Wiss. Z. Humbolt Univ. Berlin Math. Naturwiss. Reihe, 14, pp 67-69, 1965.

van Heyningen, R., The lens, in The Eye: Vegetative Physiology and Biochemistry, H. Dawson, ed., Academic Press, New York, pp 213-287, 1962.

van Venrooij, G. E. P. M., Measurement of ultrasound velocity in human tissue, Ultrasonics, 9, pp 240-242, 1971.

Watt, B. K. and Merrill, A. L., Composition of foods, Agriculture Handbook No. 8, USDA, 1963.

Wells, P. N. T., Biomedical Ultrasonics, Academic Press, London, 1977.

White, A., Handler, P., and Smith, E. L., Principles of Biochemistry, McGraw Hill Book Co., New York, 1968.

Willard, G. W., Temperature coefficient of ultrasonic velocity in solutions, JASA, 19, No. 1, pp 235-241, 1947.

Wladimiroff, J. W., Craft, I. L., and Talbert, D. G., In vitro measurements of sound velocity in human fetal brain tissue, Ultrasound in Medicine and Biology, 1, pp 377-382, 1975.

Wolf, R. C. and Leathem, J. H., Hormonal and nutritional influences on the biochemical composition of the rat testis, Endocrinology, 57, pp 286-290, 1955.

Wolf, W. B., The body fluids, in Biological Foundations of Biomedical Engineering, J. Kline, ed., Little, Brown and Co., Boston, pp 391-411, 1976.

Yosioka, K., Oka, M., Omura, A., and Hasegawa, T., Absorption coefficient of ultrasound in soft tissues and their biological conditions, Mem. Inst. Scient. Ind. Res. Osaka U., 26, pp 55-59, 1969.

VITA

Michael John Haney was born April 8, 1955, in Evanston, Illinois. From 1973 to 1977, he attended the Massachusetts Institute of Technology. He was awarded simultaneous Bachelor of Science degrees in Physics and Mathematics in 1977, and produced a thesis titled "General Parameter Fitting Techniques Applied to X-Ray Burst Observations Using Rotating Modulation Collimators."

From 1977 to 1985, Mr. Haney attended the University of Illinois at Urbana-Champaign. For the first four years he worked as a teaching assistant, and was later promoted to Instructor in the Department of Electrical Engineering. He received the H. Oelson Award for Excellence in Teaching by a Graduate Student in 1979, and served as the Senior Member of the Student Advisory Committee from 1979 to 1981. From 1980 to 1981, Mr. Haney also participated in the development of hardware for the FASTBUS high speed data acquisition project with the High Energy Physics Group of the Department of Physics at the University of Illinois. He was awarded a Master of Science degree in 1981, and produced a thesis titled "Echolocation for Scene Interpretation."

From 1981 to 1985, Mr. Haney worked in the Bioacoustics Research Laboratory of the University of Illinois, funded by the Radiation Oncology Trainingship Program of the National Institutes of Health, and by Ultrasonix Research, Incorporated, while working on his doctoral disertation. His publications include:

Haney, M. J., Johnston, R. L., and O'Brien, W. D., Jr. "On standards for the storage of images and data," Picture Archiving and Communication Systems for Medical Applications, SPIE Proceedings, vol. 318, January 1982.

Downing, R. and Haney, M. J. "The FASTBUS segment interconnect," IEEE Transactions on Nuclear Science, vol. NS-29, pp 94-97, February 1982.

Haney, M. J. and O'Brien, W. D., Jr. "Ultrasound Tomgraphy for Differential Thermography," Acoustic Imaging, E. A. Ash and C. R. Hill, eds., Plenum Press, New York, pp 589-597, 1982.

Haney, M. J. and O'Brien, W. D., Jr. "Temperature dependency of ultrasonic propagation properties in biological materials," accepted for publication in Characterization of Tissue with Ultrasound, J. F. Greenleaf, ed., CRC Publishing, 1984 (in press).

Haney, M. J., Segal, L. A., Tervola, K. M. U., Grummer, M. A., Erdman, J. W., Jr., Frizzell, L. A. F., and O'Brien, W. D., Jr. "Comparison of ultrasonic properties measurements in fatty liver using several techniques," abstract presented at the AIUM/SDMS '84 conference in Kansas City, Mo., September, 1984.

At present, Mr. Haney is employed as a Computer Engineer with the Center for Supercomputing Research and Development at the University of Illinois, designing computer hardware for the Cedar supercomputer.